UNIVERSITY OF CALIFORNIA, SAN DIEGO

Material Synthesis and Properties for Functional Applications

A dissertation submitted in partial satisfaction of the

requirements for the degree Doctor of Philosophy

in

Materials Science and Engineering

by

Hyunsu Kim

Committee in Charge:

Professor Sungho Jin, Chair
Professor Renkun Chen
Professor Ratneshwar Lal
Professor Yu-Hwa Lo
Professor Yu Qiao

2013

The dissertation of Hyunsu Kim is approved, and it is acceptable in quality and form for publication on microfilm:

Chair

University of California, San Diego

2013

TABLE OF CONTENTS

LIST OF FIGURES

LIST OF TABLES

ACKNOWLEDGEMENTS

First and foremost, I wish to acknowledge and deeply thank my advisor, Professor Sungho Jin for his steadfast encouragement, guidance, and support during the course of this research here at University of California, San Diego. I sincerely thank to my dissertation committee members for their precious time and helpful suggestions: Professor Yu-Hwa Lo, Professor Renkun Chen, Professor Yu Qiao, and Professor Ratneshwar Lal. I also would like to thank Professor Byeong-Hyeok Sohn for implanting his tireless passion, enthusiasm, and endeavor for academic research in my mind while I was earning an M.S. degree in POSTECH in Korea.

I wish to express my gratefulness to the JIN Group members for their numerous help, stimulating discussions, and invaluable contributions, especially Dr. Chulmin Choi, Dr. Li-Han Chen, Jirapon Khamwannah, Duyoung Choi and Calvin Gardener. Also, I wish to thank the former JIN Group members, especially Dr. Kunbae Noh, Dr. Karla Brammer, Dr. Mariana Loya, Dr. Christine Frandsen for showing me the way of research. I appreciate all the helps from my collaborators. In retrospect, it was a hardship, hence pleasure, to face numerous tangled problems and unravel a complicated problem one by one. Priceless memories shared with each of you will be in my heart for the rest of my life.

I would like to recognize and thank Charlotte Lauve for the administrative paperwork, invaluable advice and informative seminar notices. I also wish to thank Korean seniors and juniors in UC, San Diego and their family for helping me in the aspects of not only various academic matters but also everyday life in San Diego. It was

my great pleasure to share memories with each of you, especially Hyunwoo Noh, Juhun Lee, Dae hoe Lee, Sun Young Noh, Jae-yun Moon, Jihye Baek, and Dr. Sungsik Hur.

Also, I wish to thank my dear family members for their cares, supports, and sacrifices shown not only through the course of this time but also the moment I am not recognized. Last but not least, I wish to express my infinite gratitude to my beloved wife, Seungah Yi and my lovely daughters, Minji and Minyoung for sharing all sorts of emotions. Their truly support and encouragement have been always fueled me up whenever I am tired, frustrated, and exhausted. Without their endless love and sacrifice, nothing would have been accomplished.

Chapter 3, in full, is a reprint of the material as it has been prepared for publication in Journal of Renewable and Sustainable Energy written by Hyunsu Kim, Chulmin Choi, Jirapon Khamwannah, Sun Young Noh, Yanyan Zhang, Tae-Yeon Seong, and Sungho Jin. The dissertation author was the primary investigator and author of this work.

Chapter 4, in full, is a reprint of the material as it has been prepared for publication in Nano Energy written by Hyunsu Kim, Jirapon Khamwannah, Chulmin Choi, Calvin J. Gardner, and Sungho Jin. The dissertation author was the primary investigator and author of this work.

Chapter 5, in full, is a reprint of the material as it appears in Angewandte Chemie International Edition, 50, 6771 (2011) written by Hyunsu Kim, Jongjin Park, Kunbae Noh, Calvin J. Gardner, Seong Deok Kong, Jongmin Kim, and Sungho Jin. The dissertation author was the primary investigator and author of this work.

Lastly, I would like to show appreciation to the financial support of this research by Iwama fund, Samsung Electronics, NSF-Nanomanufacturing Division (CMMI #0856674), CMRR (Center for Magnetic Recording Research) at UC San Diego, and especially Samsung Electronics Fellowship.

Hyunsu (Stanley) Kim

La Jolla, May 2013

VITA

1975	Born in Korea
1993 ~ 2000	B.S., Polymer Science, Kyungpook National University, Korea
2000 ~ 2002	M.S., Materials Science and Engineering, POSTECH, Korea
2002 ~ present	Samsung Electronics, Korea
2008 ~ 2013	Ph.D., Materials Science and Engineering, University of California, San Diego, U.S.A.

PUBLICATIONS

Journals Articles:

1. Hyunsu Kim, Jirapon Khamwannah, Chulmin Choi, Yang Shi, and Sungho Jin "Hydrothermally grown TiO_2 nanotubes on multi-layered Ti mesh photoelectrodes for enhanced photoelectrochemical reaction" MRS communications (in preparation)
2. Hyunsu Kim, Jirapon Khamwannah, Chulmin Choi, Calvin J. Gardner, and Sungho Jin "Formation of 8nm TiO_2 nanotubes on three dimensional electrode for enhanced photoelectrochemical reaction" Nano Energy (in preparation)
3. Jirapon Khamwannah, Hyunsu Kim, YanYan Zhang, Tae Kyoung Kim, and Sungho Jin, "Control of Nano geometry for Advanced Energy Applications", Journal of Nanoscience and Nanotechnology (in press).
4. Hyunsu Kim, Chulmin Choi, Jirapon Khamwannah, Sun Young Noh, Yanyan Zhang, Tae-Yeon Seong, and Sungho Jin "Plasmonic Au Nanoparticles on 8nm TiO_2 Nanotubes for Enhanced Photocatalytic Water Splitting" Journal of Renewable and Sustainable Energy (in revision)
5. Yanyan Zhang, Jirapon Khamwannah, Hyunsu Kim, Sun Young Noh, Haibin Yang, Sungho Jin, "Improved Dye Sensitized Solar Cell Performance in Larger Cell Size by Using TiO_2 Nanotubes", Nanotechnology 24, 045401 (2012)
6. Jirapon Khamwannah, Yanyan Zhang, Sun Young Noh, Hyunsu Kim, Christine Frandsen, Seong Deok Kong, and Sungho Jin "Enhancement of dye sensitized solar cell efficiency by composite TiO_2 nanoparticle/8nm TiO_2 nanotube paper-like photoelectrode" Nano Energy, 1, 411 (2012)
7. Jirapon Khamwannah, Sun Young Noh, Christine Frandsen, Yanyan Zhang, Hyunsu Kim, Seong Deok Kong, and Sungho Jin "Nanocomposites of TiO_2 and double-walled carbon Nanotubes for improved dye-sensitized solar cells" Journal of Renewable and Sustainable Energy, 4, 023116 (2012)
8. Kunbae Noh, Chulmin Choi, Hyunsu Kim, Young Oh, Jin-Yeol Kim, Se-Yeon Jung, Tae-Yeon Seong, and Sungho Jin "Di-block copolymer directed anodization of hexagonally ordered nanoporous aluminum oxide", Journal of Vacuum Science and Technology B 29, 06F207 (2011)
9. Kunbae Noh, Chulmin Choi, Hyunsu Kim, Young Oh, Jin-Yeol. Kim, Daehoon Hong, Li-han Chen, and Sungho Jin "Magnetic Properties of Anti-dot PatternedCo/Pd Multilayer Film", IEEE Transactions on Magnetics 47, 3478, (2011)
10. Hyunsu Kim, Jongjin Park, Kunbae Noh, Calvin J. Gardner, Seong Deok Kong, Jongmin Kim, and Sungho Jin "An X–Y Addressable Matrix Odor-Releasing System Using an On–Off Switchable Device" Angewandte Chemie International Edition 50, 6771 –6775 (2011)

11. Hyunsu Kim, Kunbae Noh, Chulmin Choi, Jirapon Khamwannah, Diana Villwock, and Sungho Jin "Extreme Superomniphobicity of Multiwalled 8 nm TiO_2 Nanotubes" Langmuir, 27, pp10191–10196 (2011)
12. Kunbae Noh, Karla S. Brammer, Hyunsu Kim, Se-Yeon Jung, Tae-Yeon Seong, and Sungho Jin "Highly self-assembled nanotubular aluminum oxide by hard Anodization" Journal of Materials Research, 26, pp186-193 (2011)
13. Karla S. Brammer, Hyunsu Kim, Kunbae Noh, Mariana Loya, Christine J. Frandsen, Li-han Chen, Laula S. Connelly, and Sungho Jin "Highly Bioactive 8 nm Hydrothermal TiO_2 Nanotubes Elicit Enhanced Bone Cell Response" Enhanced Bone Cell Response" Advanced Engineering Materials, 13, B88 (2011)

Conference proceedings:

1. Hyunsu Kim, Chulmin Choi, Jirapon Khamwannah, Li-han Chen, and Sungho Jin "Nitrogen-doping for Improved Photocatalytic Performance of Extremely Nanostructured TiO_2 Electrodes for Water Splitting" Materials Research Society, MRS Fall Meeting, San Francisco, CA. (April 2013)
2. Hyunsu Kim, Jirapon Khamwannah, Chulmin Choi, and Sungho Jin "Study of Extremely Nanostructured TiO_2 Electrode and Its Photocatalytic Performance for Water Splitting" Materials Research Society, MRS Fall Meeting, San Francisco, CA. (April 2012)
3. Kunbae Noh, Chulmin Choi, Hyunsu Kim, Young Oh, Jin-Yeol Kim, and Sungho Jin "Di-block Copolymer Directed Anodization of Hexagonally Ordered Porous Aluminum Oxide", International conference on Electron, Ion, and Photon BeamTechnology and Nanofabrication, Las Vegas, U.S.A. (Jun. 2011)
4. Kunbae Noh, Chulmin Choi, Hyunsu Kim, Young Oh, Jin-Yeol Kim, Li-han Chen, and Sungho Jin "Magnetic Properties of Anti-dot Patterned Co/Pd Multilayer Film", IEEE International Magnetics Conference, Taipei, Taiwan (April. 2011)

ABSTRACT OF THE DISSERTATION

Material Synthesis and Properties for Functional Applications

by

Hyunsu Kim

Doctor of Philosophy in Materials Science and Engineering

University of California, San Diego, 2013

Professor Sungho Jin, Chair

Titanium oxide is one of the most widely studied materials for photochemical electrodes because of its high photocatalytic activity. 8 nm diameter TiO_2 nanotubes formed by hydrothermal reaction have been fabricated for water splitting applications. To enhanced photoelectrochemical performance, plasmonic Au nanoparticles have been combined to the TiO_2 nanotubes.

First, successful distribution and attachment of fine Au nanoparticles on ~8 nm diameter TiO_2 nanotubes having significantly increased surface area have been demonstrated. Au thin film deposition onto hydrothermally grown TiO_2 nanotube arrays followed by thermal annealing breaks up the Au film into desired, uniformly distributed nanoparticles. Visible light absorption spectra of the gold nanoparticles on TiO_2 nanotubes indicate that the Au nanoparticles are photo-excited due to plasmon resonance, and charge separation is accomplished by the transfer of photoexcited electrons from the gold particle to the TiO_2 conduction band, thereby enhancing photoelectrochemical performance.

Second, a 3-D photoelectrode configuration having hydrothermally formed TiO_2 nanotubes on parallel Ti fins has been successfully fabricated. The Ti fin arrays were assembled by simple and facile spot welding of alternately tall and short Ti foil assembly, which provides significantly increased electrode surface area. A tangled forest of nanotubes of TiO_2 was produced on each of the Ti surface on all parallel and straight fin arrays. UV absorption spectra of the TiO_2 nanotubes indicate that the TiO_2 nanotubes are photo-excited due to their photocatalytic activities, and the charge separation is accomplished by the transfer of photoexcited electrons from the TiO_2 nanotubes to the Ti metallic substrate, thereby performing photoelectrochemical reaction.

Third, a novel X–Y matrix structured odor-releasing system with an elastomer-based device has been developed. Relatively low cost and compact design of the system may be achieved through the proposed switchable gas-release method. In addition, odor-release measurements with real time data-logging were also developed for model liquid/gas samples, such as ammonia, ethyl alcohol, and isopropyl alcohol, as well as two perfumes. The electrical actuation system enabled on–off switching of gas release.

CHAPTER 1: Introduction

Hydrogen is the ideal fuel for the future because it is clean, energy efficient, and abundant in nature. While various technologies can be used to generate hydrogen, only some of them can be considered environmentally friendly. Recently, solar hydrogen generated via photocatalytic water splitting has attracted tremendous attention and has been extensively studied because of its great potential for low-cost and clean hydrogen production. This thesis gives a comprehensive review of the development of photocatalytic water splitting for generating hydrogen, particularly under visible-light irradiation. The chapters covered include an introduction of hydrogen production technologies, a review of photocatalytic water splitting over titania and surface modified titania based photocatalysts, and a discussion of the current challenges. Based on the background reviewed here, the development of highly stable visible–light-active photocatalytic nanomaterials, and the design of efficient, low-cost 3D photoelectrodes are the key for the advancement of solar-hydrogen production via photocatalytic water splitting in the future. In this thesis work, thus, we have developed facile nanofabrication techniques for visible light sensitive photocatalyst structure using plasmomic Au nanoparticle. In addition, we have fabricated 3D photoelectrode having large surface area using spot welding. The photoelectrochemical performances of these advanced photoelectrodes have been investigated.

Chapter 1 gives a brief introduction on photocatalytic water splitting related to TiO_2 photoanode.

Chapter 2 gives broad background on alternative energies and solar hydrogen. Water splitting and photoelectrochemical reaction of TiO_2 photocatalysts are discussed

in detail. In addition, recent development on the surface modification of TiO_2 is discussed.

Chapter 3 contains fabrication of plasmonic Au nanoparticles on 8nm TiO_2 nanotubes for enhanced photocatalytic water splitting.

Chapter 4 contains fabrication and application of a 3-D photocatalytic electrode having nanoscale surface TiO_2 nanotubes for enhanced photoelectrochemical reaction.

Chapter 5 contains fabrication and a demonstration of an X–Y addressable matrix odor-releasing system using an on–off switchable device.

Chapter 6 gives a summary of the research results achieved, discusses the ongoing research, and makes suggestions as to what additional advances need to be made in the future.

CHAPTER 2: Background

2.1 Solar hydrogen

2.1.1 The problem with fossil fuels

Fossil fuels are widely used in the world, but there are a number of serious problems with burning these fuels to provide energy. They can cause significant damage to the natural and built environments, and to the health of the people who are exposed to the chemicals that are released when these fuels are burned. It is these types of problems that have made alternative, renewable sources of energy a more attractive option since they do not produce the same kinds of pollution and problems.

Fossil fuels such as gas, oil and coal can cause serious environmental problems. Burning fossil fuels for energy releases a number of chemicals into the air. These include carbon dioxide, nitrogen oxides, heavy metals, sulfur dioxide and volatile organic compounds.

2.1.2 Alternative energies and hydrogen

Human civilization is built by our energy system, which facilitates the development of technologies that provide us with a higher standard of living. Energy is an essential part of productivity and is as important as raw materials, capital, and labor. Today, most of the energy that we use comes from fossil fuels, which are not considered ideal due to the following reasons: First, the combustion of fossil fuels, such as coal and petroleum, will produce carbon dioxide (CO_2), which is one of the major greenhouse gases that causes climate change;[1] Second, the amount of fossil fuel on the Earth is limited and will be depleted someday. Nature has stored solar energy in the

form of mineral organic compounds or in fossil fuels such as coal, petroleum, and natural gas through millions of years of biological and non-biological processes.[2] However, the rate of global energy consumption has far exceeded the rate of energy storage, implying that fossil fuels will soon be exhausted;[3] Third, fossil fuels are generally controlled by certain nations in the world. As a result, a significant amount of time and money will be spent for the relocation and distribution of these fuels. To satisfy the energy demand, competition for resources among nations will continue to be seen. Therefore, it is imperative for us to search for a sustainable energy source that can be easily produced at low cost and that is friendly to the environment. To replace or reduce the use of fossil fuels, several alternative energies have been developed. Alternative energies are renewable and have lower carbon emissions when compared to conventional energy sources. These energy sources include wind, hydropower, solar, geothermal, etc. The term “wind energy” describes the process by which the wind is used to generate mechanical power or electricity.[4] Although wind energy is a free, renewable resource, its major challenge is that wind cannot be stored, and not all wind can be harnessed to meet the timing of the demand for electricity.

Hydropower is energy that is generated by water and converted to electricity.[5] The most common method of using energy from water is a hydroelectric dam in which water passes through turbines, causing them to rotate, and then the energy is captured to run a generator. The major disadvantage of hydropower is that dams are extremely expensive to build, which means that they must operate for many decades to become profitable. Moreover, the building of large dams can often cause serious geological and ecological damage.

Solar energy is a free, inexhaustible resource from the sun that can be converted to electricity (photovoltaic power) or heat using devices such as solar cells[6] or concentrators[7]. Electricity produced from solar energy has advantages over wind power and hydropower, since the latter two need turbines with moving parts that are both noisy and require much maintenance. However, the major disadvantage of solar energy is its intermittent nature. That is, the amount of sunlight a location receives varies greatly depending on the geographical location, time of day, season, and even clouds.

Geothermal energy is obtained by extracting heat from water or rocks deep underground[8]. Unlike wind and solar energy, geothermal energy is not intermittent, and hence it can be a reliable energy source for several years. However, heat typically is extracted from the rocks much more rapidly than it is restored from the environment. Therefore, geothermal plants have limited lifetimes and require periodic drilling of new holes for continued operation, which in turn increases the cost of electricity. In sum, the availability of energy from renewable sources is unstable with variability in location and time, and the energy may not be available to the end-users when it is needed. Therefore, it is necessary to identify a medium or container in which to store the energy.

Hydrogen is an ideal energy storage medium or carrier because of the following reasons; First, it is the most abundant element and it exists in both water and biomass; Second, it has a high energy yield (122 kJ/g) compared to other fuels such as gasoline (40 kJ/g); Third, it is environmentally friendly because its end use will not produce pollutants, greenhouse gases, nor any harmful effect on the environment. Last, but not least, hydrogen can be stored in gaseous, liquid or metal hydride form and can be distributed over large distances through pipelines or via tankers.

2.2 TiO_2 photocatalyst for hydrogen production

2.2.1 Historical background

TiO_2 powders have been commonly used as white pigments from ancient times. They are inexpensive, chemically stable and harm - less, and have no absorption in the visible region. Therefore, they have a white color. However, the chemical stability of TiO2 holds only in the dark. Instead, it is active under UV light irradiation, inducing some chemical reactions. Such activity under sunlight was known from the flaking of paints and the degradation of fabrics incorporating TiO_2.[9] Scientific studies on such photoactivity of TiO_2 have been reported since the early part of the 20th century.[10] It was reported that UV absorption produces active oxygen species on the TiO_2 surface, causing the photobleaching of dyes. It was also known that TiO_2 itself does not change through the photoreaction, although the ``photocatalyst'' terminology was not used for TiO_2 in the report, but called a photosensitizer. It is equivocal when and who started utilizing first such a photochemical power of TiO_2 to induce chemical reactions actively, but at least in Japan, there were a series of reports by Mashio et al., from 1956, entitled ``Autooxidation by TiO_2 as a photocatalyst''.[11] They dispersed TiO_2 powders into various organic solvents such as alcohols and hydrocarbons followed by the UV irradiation with an Hg lamp. They observed the autooxidation of solvents and the simultaneous formation of H_2O_2 under ambient conditions.

In those days, however, the photocatalytic power of TiO_2 might have attracted only partially limited scientists' attention in the field of either catalysis or photochemistry, and the study of TiO_2 photocatalysis had not developed widely in either academic or industrial society.

2.2.2 Water photolysis with TiO_2 (1970s)

In the late 1960s, one of the present authors (AF) began to investigate the photoelectrolysis of water, using a single crystal n-type TiO_2(rutile) semiconductor electrode, because it has a sufficiently positive valence band edge to oxidize water to oxygen. It is also an extremely stable material even in the presence of aqueous electrolyte solutions, much more so than other types of semiconductor that have been tried. The possibility of solar photoelectrolysis was demonstrated for the first time in 1969 and reported in Nature by analogy with a natural photosynthesis in 1972.[12] In those days, crude oil prices ballooned suddenly, and the future lack of crude oil was a serious concern. Thus, this became known as the time of ``oil crisis''. Therefore, this report attracted the attention not only of electrochemists but also of many scientists in a broad area, and numerous related studies were reported in the 1970s.

2.2.3 Powdered TiO_2 (1980s)

The problem of light-assisted water splitting has also been focused in the late 1970s with the photocatalytic approach, i.e., essentially with photoelectrochemistry but without an external circuit. Photocatalytic water splitting has been studied intensively with powdered anatase TiO_2 suspensions, with Pt deposited on TiO_2 as a cathodic catalyst. Although there were several experiments for the simultaneous production of H_2 and O_2 in the powder systems, either such experiments could not be reproduced or the reaction efficiency was very low.[13] Kawai and Sakata examined, in 1980, the reasons why the water photolysis could not proceed in the powder system, although it could in the electrode one. They concluded that the produced H_2 and O_2 gases might recombine to regenerate water molecules through the back reaction in the powder system, because

the production sites of each gas are located close to each other. To solve this problem, they added organic compounds to the aqueous suspension of platinized TiO_2. In this case, water is reduced, producing H_2 at the Pt sites and the organic compounds are oxidized instead of water by photogenerated holes at the TiO_2 sites. In general, anatase (EG=3.2eV) gives better results than rutile (EG=3.0eV) for hydrogen production in powder photocatalysis. One of the main reasons for the higher efficiency is probably the higher reduction potential of photogenerated electrons in the former than in the latter, i.e., the bottom of the conduction band of anatase is located 0.1V more negative than that of rutile.[14]

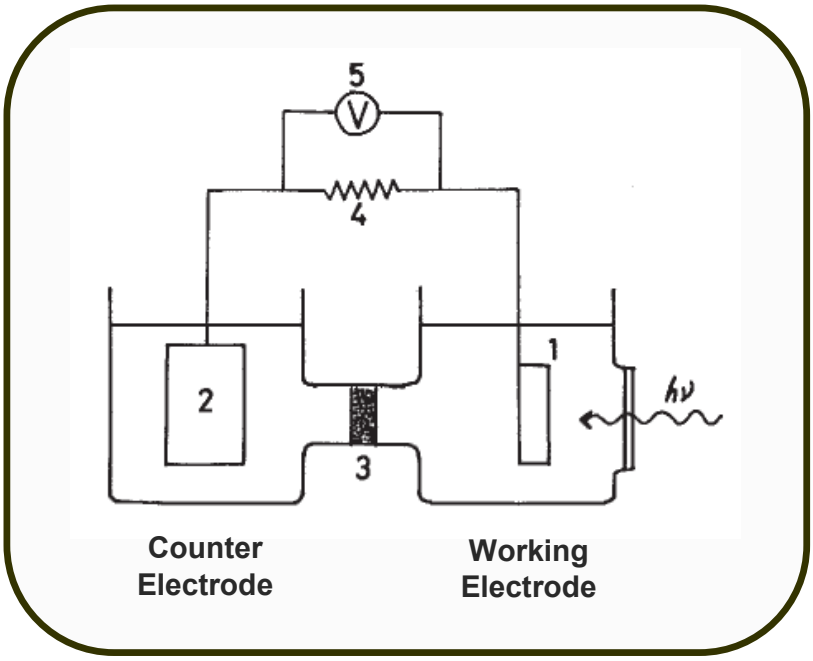

Figure 2.1: Electrochemical photolysis of water.

For the purpose of easy handling of photocatalysts, the immobilization of TiO_2 powders on supports was carried out in the late 1980s.[15] Although many research studies were on the purification of wastewater and polluted air, TiO_2 photocatalysis could not be developed to the stage of a real industrial technology in the 1980s.

2.3 Properties and characteristics of TiO_2

An ideal photocatalyst for photocatalytic oxidation is characterized by the following attributes [16]:

(1) Photo-stability.

(2) Chemically and biologically inert nature.

(3) Availability and low cost.

(4) Capability to adsorb reactants under efficient photonic activation ($h\upsilon \geq Eg$).

Titania is the most widely employed (nano)material in photocatalytic processes, although there are several (nano)materials currently considered as photocatalysts and/or supports for photocatalysis aside from titania. These include related metal oxides, metal chalcogenides, zeolites (as supports), etc. The schematic diagram of band gaps for various semiconductors is shown in Figure 2.2.

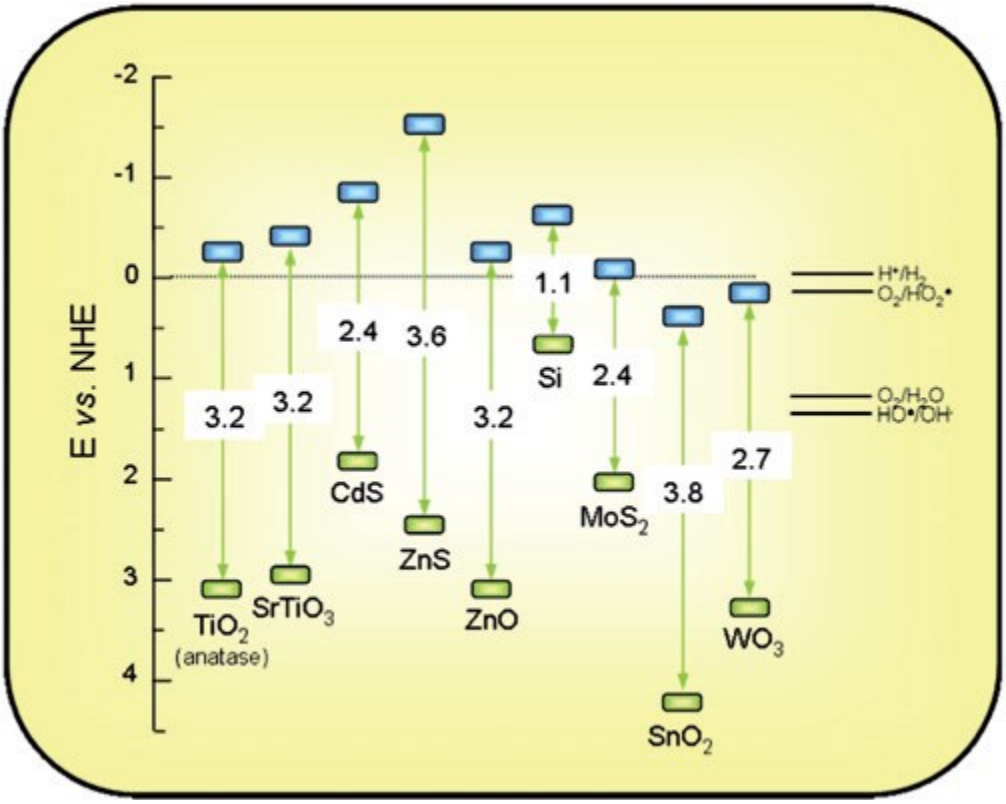

Figure 2.2: Band gaps (eV) and redox potentials for various semiconductors.[17]

2.3.1 Photocatalytic properties

The relatively high quantum yield and elevated stability of TiO_2 are the key reasons for the preponderance of this semiconductor, which has become a virtual synonym for photocatalyst. Nowadays, the market for photochemical applications of TiO_2 is thriving, especially in Asian countries such as Japan, South Korea and China. [18-20] Photocatalytic coatings deposited on external building elements, like windows, along with air purifiers are the main products of this emerging business, but dozens of other commercial uses have been proposed and some experimental devices are already on the market.[18-20] Despite these achievements and remarkable advantages,

heterogeneous photocatalysis with TiO_2 has to cope with significant limitations. The most important drawback of photocatalysis is derived from the mismatch between the TiO_2 band gap energy and the sunlight spectra, which overlap only in the UVA (400–320 nm) and UVB (320–290 nm) ranges. As a consequence, this technology can only take advantage of less than 5% of the solar energy impinging on the Earth's surface, and its potential as a sustainable technology cannot be entirely fulfilled.[21] This fact has profoundly influenced research in photocatalysis, so that modification of TiO_2 to achieve efficient photoactivation in the visible spectrum is an active field of research.[22]

2.3.2 Optical properties of TiO_2

The dielectric functions of anatase and rutile single crystals for the electric field perpendicular and parallel to the c-axis show that in the IR to visible spectral range, anatase is less anisotropic than rutile, whereas in the band-gap region, anatase shows important anisotropy.[23] It has been found that depending on the degree of reduction of rutile TiO2, a blue color arises from the visible tail of an IR absorption band peaking at about 0.75–1.18 eV.[24] Similarly, in anatase too, the blue color has been observed,[25] which is caused by a wide absorption band with its maximum in the IR. In addition, a color center at 3 eV due to an oxygen vacancy has been identified giving rise to a yellow color.[26]

2.3.3 Electrical/electronic properties of TiO_2

The valence band (VB) of wide-gap rutile and anatase consist of O 2p states, whereas the conduction band (CB) is formed by Ti 3d states.[27] As a wide band-gap

semiconductor, TiO_2 crystals have a high resistivity (~1015 cm),[28] and bulk oxygen vacancies, titanium interstitials, and reduced crystal surfaces are considered to generate shallow electron donor levels that contribute to the electric conductivity of TiO_2.[29] TiO_2 is an n-type semiconductor, and the n-type conductivity increases with the extent of oxygen loss within the crystal lattice. Point defects in terms of doubly charged oxygen vacancies and interstitial titanium ions with three or four charges affect the conductivity and ionization energy of the rutile crystal.[30] The ionization energies have been reported to be around 0.007–0.08 eV (depending on temperature) for titanium interstitials,[31,32] whereas oxygen vacancies contribute to the electronic conduction as double donors with a shallow donor level (0–200 meV) and a deep donor level (600–750 meV).[33] In general, oxygen vacancies are observed to be the dominant phenomenon under weakly reducing conditions or low annealing temperatures (below 870 K in vacuum), whereas in the more reducing conditions and higher annealing temperatures (above 1070 K in vacuum), titanium interstitials become more predominant in effect.[34]

2.3.4 Safety and availability of TiO_2

Titanium dioxide is a material with a great number of technological applications (such as pigments, sensors, photovoltaic cells, catalysts.) and its annual production for whitening products as diverse as paper, plastics or paints was more than 5.28 millions tons per year.[35] In spite of this high consumption, a shortage of TiO_2 is not foreseen in the near future. Titanium is the ninth most abundant element and constitutes about 0.63% in weight of the Earth's crust. Minerals rutile and ilmenite, $FeTiO_3$, are the main ores of this element and they are found in large deposits in Norway, Australia, China,

Canada and many other countries.[16] The toxicity of TiO_2 is low and it has been approved as a food colorant.[16] In fact many everyday products such as toothpaste, pill coatings and chewing gum contain TiO_2.[16] Nevertheless, new concerns have arisen recently as a consequence of the extensive research on TiO_2 particles of nanometric size. Nanomaterials present risks associated with their small size which greatly facilitates intake by inhalation. In the case of TiO_2, oral administration of a high dose of nanoparticles (5g Kg^{-1}) does not cause acute toxicity, although evidence of hepatic damage was found.[36]

2.4 Influence on TiO_2 photoactivity

2.4.1 Structural and electronic characteristics

Four TiO_2 polymorphs were prepared using conventional synthesis conditions: anatase (tetragonal), rutile (tetragonal), brookite (orthorhombic) and TiO_2 (B) (monoclinic).[37] However, these last two phases have been scarcely used as photocatalysts, and consequently we will focus exclusively on anatase and rutile. All TiO2 forms can be described as arrangement of slightly elongated TiO_6 octahedra connected in different ways by vertices and edges.[16,34,38] Although rutile is generally considered the most stable polymorph, differences in the Gibbs free energy of formation between rutile and anatase are small (lower than 15 KJ mol^{-1}).[39] Consequently, anatase can be easily obtained by synthesis at low temperature treatments (below 400 ^{o}C), but rutile frequently starts to appear at moderate temperatures (400–600 ^{o}C) and it becomes the predominant phase after annealing at higher temperatures.8,39 Due to the presence of a small amount of oxygen vacancies, which are compensated by the presence of Ti^{3+} centers, TiO_2 is an n-type semiconductor.

The band gaps are 3.2 and 3.0 eV for anatase and rutile, respectively.8–13,39 Interband transitions of TiO_2 are indirect[34] (i.e. implying both electronic levels and lattice phonons) but factors like the crystalline size or the presence of dopants can modify the type of transition and somewhat conflicting reports are found in the literature.[40,41] This characteristic directly affects the photonic efficiency because indirect semiconductors present a reduced photon absorption and consequently require a higher mass of photocatalyst to obtain the same effect. In any case, it is worth emphasizing that as much as a 90% of the electron–hole pairs recombine in less than 10 ns and consequently photogenerated carriers available for surface reactions are quite limited.[34] Values of quantum yield vary broadly with the process considered, for TiO_2 reactions in solution they are typically lower than 1%,[42] but they can exceed 25% for some gas phase reactions.[43] These values depend, among other factors, on electronic transferences in the interface and surface characteristics, but considering exclusively the photoactivation process, TiO_2 shows a limited performance. Thus, in contrast with silicon, which presents internal quantum efficiency (IQE) close to 100% under illumination at 600 nm,[44] with TiO_2 the absorbed photon-to-current efficiency (APCE, parameter equivalent to quantum yield) is about 30% at 360 nm.[45] The chemical potentials of photogenerated electrons and holes depend on the position of the energy levels in the semiconductor.

More specifically, the redox potential of a donor species adsorbed on the surface of the photocatalyst needs to be more negative (higher in energy) than the valence band position of the semiconductor in order to replenish the electron vacancies. Similarly, acceptor molecules must have a redox potential more positive (lower in energy) than the conduction band.[46] In view of this, one of the key advantages of TiO_2 among other

semiconductors is that its electronic structure is such that it allows both the reduction of protons ($E_{NHE}(H^+/H_2)$ = 0.0 eV) and the oxidation of water ($E_{NHE}(O_2/H_2O)$ = 1.2 eV), which are key processes for water splitting.[47] Therefore, in contrast to other semiconductors, which are efficient for either water reduction like Si, or for water oxidation like SnO_2, TiO_2 is suitable for activating both reactions simultaneously. Surface OH^- groups can act as donor species, reacting with a valence band holes to yield hydroxyl radicals, $OH^\bullet$. These species have a very high oxidation potential ($E_{NHE}(OH^\bullet/H_2O)$ = 2.27 eV) and are considered the key intermediate in the photooxidation reactions with TiO_2.[46,47]

Several reasons are proposed to explain differences in photoactivity between anatase and rutile structures, including variations in electronic (e.g. Fermi level position,electron mobility.) or surface (e.g. hydroxyl concentration.).[16] In addition, rutile generally presents lower surface area than anatase, due to the larger crystalline size imposed by thermodynamic constraints,[39] and this fact may also contribute to the lower photoactivity of this phase. In any case, numerous studies have also shown that elevated rates for organic pollutants degradation are achieved with anatase–rutile mixtures, such as the benchmark photocatalyst Degussa P25.[48] Corrosion of semiconductors can be induced by irradiation, if the photogenerated charge carriers attack the solid constituents. This phenomenon is known as photo-corrosion, but it does not affect to TiO_2 because water oxidation, is thermodynamically more favoured than the formation of molecular oxygen from oxide anions. This stability, which is maintained over a large pH range, is a crucial feature which explains the widespread use of TiO_2 in solution.

2.4.2 Surface properties

Water molecules dissociate on the surface of TiO_2 to yield hydroxyls groups, which saturate the coordination sphere of Ti^{4+}, and protons, which bind to the bridging oxygen.[49] This process reduces the excess energy caused by the abrupt discontinuity of the solid structure at the edge of the crystal and it occurs even with air moisture. Consequently, adsorption of reagent molecules is determined, to a great extent, by the density and specific characteristics of hydroxyl groups. Many organic substances like aromatic compounds are attached to the TiO_2 surface by hydrogen bonding,50 but stronger interactions with formation of new bonds can be observed for other molecules such as alcohols vapors or acidic gases.[50] In aqueous solution, it is necessary to consider the amphoteric character of the >Ti–OH species, because the surface charge depends on the pH. Thus, at low pH values the TiO_2 surface is positively charged, while in alkaline conditions it is negatively charged. In the case of photocatalytic reactions with ionic species, this parameter is crucial, because it defines the pH interval at which adsorption is facilitated or hindered by electrostatic interactions.[51]

As in any heterogeneous catalytic process, surface area is also a relevant parameter for photocatalysis, because adsorption capacity is related to its magnitude. Nevertheless, the extensive literature on this subject indicates that photoactivity is relatively insensitive to the increment of specific surface, and consequently its effect on reaction rates is modest.[52] The reasons for this behaviour are not entirely clear and most likely are diverse, but a possible explanation is that the rate limiting step of the photocatalysis corresponds to electronic processes rather than surface reactions. In this regard, it is worth emphasizing that any increment of surface area is often associated

with a reduction of crystallinity which may increase the density of recombination centers.

2.5 Water splitting

2.5.1 Types of TiO_2 catalysts

The most frequently used TiO_2 photocatalyst is the Degussa P25 material [68–71]. Its particle size is about 25 nm and its surface area is very small (50 m^2/g). Reducing the particle size, up to a few nanometres, has the benefit of increasing the external surface area. These small particles tend to agglomerate by strong interparticle forces when the nanometric size region is reached. Further decrease of the particle size to a few nanometers reaches one point below which quantum size effects also start to operate and the band gap of the semiconductor increases, blue-shifting the light absorption.

Titania in the form of photocatalyst titania materials of 1D dimensionality such as nanotubes, nanorodrs and nanowires have also attracted attention for their use in photocatalysis.[54–56] In particular titania nanotubes with 10–100 nm in diameter and micrometric length have been the subject of intensive investigations. Compared to spherical particles, one-dimensional TiO_2 nanostructures could provide a high surface area and a high interfacial charge transfer rate. The carriers are free to move throughout the length of these nanostructures, which is expected to reduce the e^-/h^+ recombination probability. Titania nanotubes have a relatively high surface area compared to nonporous titania and time-resolved diffuse-reflectance spectroscopy has shown that charge recombination is disfavored by the tubular morphology of the titania. These titania nanotubes can be conveniently obtained starting from titania nanoparticles as, for

instance P25, that are digested under strong basic conditions in an autoclave at about 150 °C for several hours.[57] Annealing of these nanotube-TiO_2 at 400 °C for 3 h rendered nanotubes that are composed by anatase.

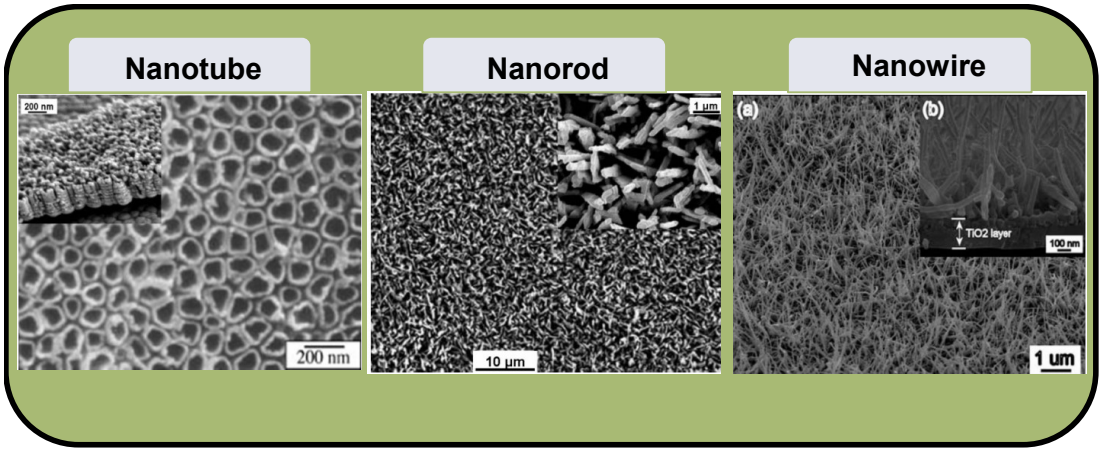

Figure 2.3: 1D nanostructures of TiO_2[54–56]

Despite the research efforts in the search for novel photocatalysts over the last two decades, titania (in its anatase form) has remained a benchmark to compare with any emerging material candidate [58]. Zhang and Maggard also reported the preparation of hydrated form of amorphous titania with wider band energy gap than anatase and significant photocatalytic activity [59].

2.5.2 Photocatalytic water splitting reaction

Photocatalysis is defined as the chemical reaction induced by photoirradiation in the presence of a catalyst, or more specifically, a photocatalyst. Such material will

facilitate chemical reactions without being consumed or transformed. The basic working principle of photocatalysis is simple. First, irradiation of light with energy greater than the bandgap of photocatalyst, separating the vacant conduction band (CB) and filled valence band (VB), excites an electron in VB into CB to result in the formation of an electron (e^-) - hole (h^+) pair. These e^- and h^+ reduce and oxidize respectively chemical species on the surface of photocatalyst, unless they recombine to give no net chemical reaction. The original structure (or chemical composition) of photocatalyst remains unchanged if an equal number of $e^-$and h^+ are consumed for chemical reaction and/or recombination.

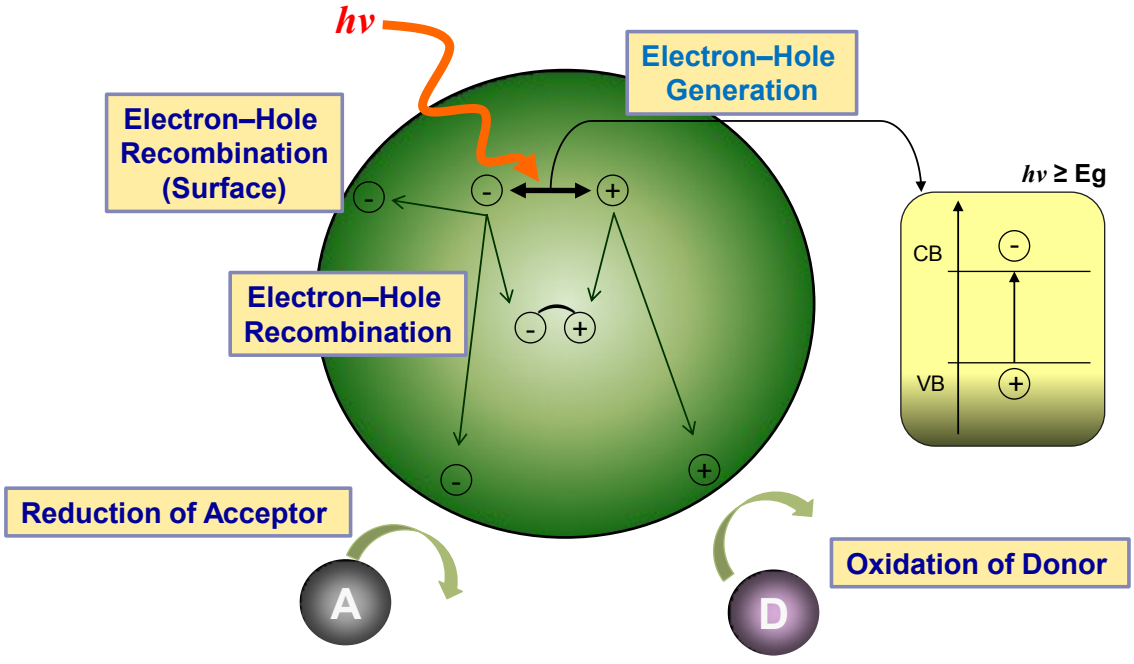

Figure. 2.4: Major processes occurring on a semiconductor particle.

In a photocatalytic water splitting reaction, photocatalyst plays a crucial role. Until now, titania (TiO_2) has been a widely used photocatalyst for photocatalytic water splitting because it is stable, non-corrosive, environmentally friendly, abundant, and cost-effective. More importantly, its energy levels are appropriate to initiate the water-splitting reaction.[60] In other words, the CB of TiO_2 is more negative than the reduction energy level of water ($E_{H+/H2} = 0$ V), while the VB is more positive than the oxidation energy level of water ($E_{O2/H2O} = +1.23$ V), as shown in Figure 2. 5.

Despite the many advantages of TiO_2, its photocatalytic water-splitting efficiency under solar energy is still quite low, mainly due to the following reasons; First, the photo-generated electrons in the CB of TiO_2 may recombine with the VB holes quickly to release energy in the form of unproductive heat or photons; Second, the decomposition of water into hydrogen and oxygen is a chemical reaction with large positive Gibbs free energy (ΔG = 237 kJ/mol), thus the backward reaction (recombination of hydrogen and oxygen into water) easily proceeds; Third, the bandgap of TiO_2 is about 3.2 eV, and therefore, only UV light can be utilized to activate the photocatalyst.

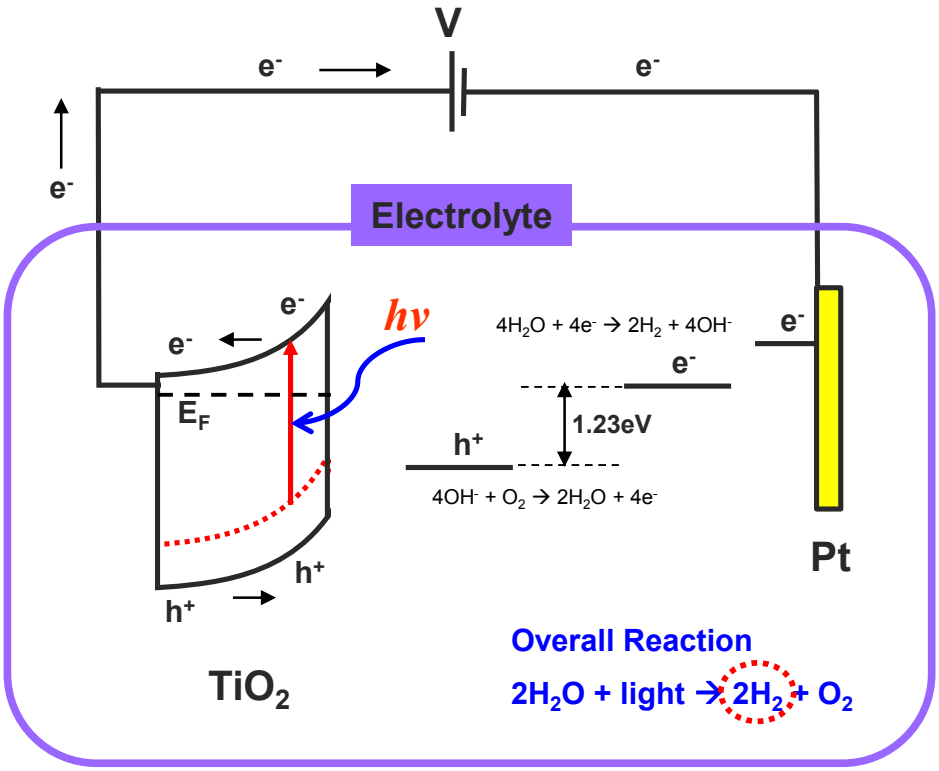

Figure 2.5: Schematic diagram of Photoelectrochemical Reaction

In general, the literature on hydrogen production via photocatalytic water splitting can be classified into 2 types: (1) photochemical-cell reaction; and (2) photoelectrochemical-cell reaction. In a photochemical cell, powder photocatalyst as suspended particles in solution is used to perform the water-splitting reaction. Most of the photocatalytic water-splitting reactions that we have introduced so far are examples of photochemical-cell reaction. In a photoelectrochemical cell, on the other hand, photocatalyst is deposited as a thin film on a substrate to form a photo-anode (or photoelectrode) for carrying out the water-splitting reaction in solution. An external circuit is required to direct the photo-generated electrons from photo-anode to a cathode where hydrogen is evolved. An example of photocatalytic water splitting performed in a

photoelectrochemical cell (PEC) was first demonstrated by Fujishima and Honda in 1972 [12]. Figure 2.5 is a schematic diagram of the photoelectrochemical cell (PEC) used to carry out the reaction. The mechanism basically involves 4 major steps: (1) generation of electron-hole pairs upon light irradiation on the photo-anode; (2) oxidation of water by photo-generated holes on the photo-anode surface to give O_2 and H^+; (3) transfer of photo-generated electrons through an external circuit to the cathode; and (4) reduction of H^+ by photo-generated electrons on the cathode surface to give H_2.

Usually, photochemical cells have the advantage of a simple process because additional film deposition or coating equipment is not required. Another advantage is that suspended photocatalyst tends to have a larger surface area per unit weight available for photocatalytic reaction, which means more active sites for photocatalytic reaction. The advantage of photoelectrochemical cell is that an internal bias can be easily achieved by the photo-anode with a combination of different materials. The bias formed will facilitate electron-hole separation and result in higher photocatalytic activity. Other than the internal bias, an external bias can also be applied between the electrodes for further enhancement.

2.6 Typical strategies to improve the photoactivity of TiO_2

2.6.1 Surface modification of TiO_2

Various ways of modifying TiO_2 have been reported, such as metal ion or anion doping, metal ion implantation, dye sensitization, addition of sacrificial or other components to the electrolyte, and so on. However, all these processes produce a very

low rate of water splitting.[61] Various measures have been taken to increase the rate of hydrogen evolution over TiO_2 surfaces such as using artificial high-power UV light sources and/or nanostructured materials.[62] However, the energy conversion efficiency on TiO_2 was rather low and the reasons for this are

1) fast recombination of photogenerated electrons and holes
2) fast backward reaction
3) inability to harvest visible and IR light at longer wavelengths than ~400 nm
4) less effective surface area

Photocatalysis being a surface phenomenon, surface area is very important in determining the amount of reaction sites, and charge carriers have to be utilized properly to improve their ability to initiate surface reactions. On the other hand, TiO_2 crystallinity should be high to prevent the recombination of e^- and h^+. Highly crystalline TiO_2 prevents the recombination of charge carriers relative to amorphous and less crystalline TiO_2. As mentioned earlier, because the energy conversion efficiency on TiO_2 depends on several factors such as surface area, e^- h^+ recombination rates, solar energy spectrum, and so on, as a working hypothesis, surface area, and crystallinity of the TiO_2 powder have to be improved for efficient photocatalysis.

Modification of the surface area of TiO_2 is performed by using nanostructured materials. Nanoparticulate electrodes are commonly used for these purposes, which consist of a several micrometer-thick film consisting of a random 3-dimensional network of interconnected 15–20 nm particles. While these electrodes possess a high

surface-to-volume ratio, the structural disorder at the contact between two crystalline particles leads to an enhanced scattering of free electrons, thus reducing the electron mobility. On the other hand, the nanotube array architecture, being ordered and strongly interconnected, eliminates randomization of the grain network and increases contact points for good electrical connection. The nanotube arrays have a large surface area enabling higher contact with electrolytes. Details of the fabrication processes of various nanostructured TiO_2 have been discussed previously.

2.6.2 Doping or metal loading methods

In order to solve the problems mentioned above and to make solar photocatalytic water splitting of TiO_2 feasible, continuous efforts have been made to promote the photocatalytic activity of TiO_2 and enhance its visible-light response. The techniques that have been investigated in the past include the addition of sacrificial agent/carbonate salts, metal loading, dye sensitization, ion (cation, and anion) doping, etc. Some of them have been proven to be useful for improving the photocatalytic activity of TiO_2.

Doping with carbon, nitrogen, sulfur and other non-metallic elements has been recently reported to introduce visible light absorption on titanium dioxide [63]. Asahi et al. were the first to show an absorption increase in the visible region upon nitrogen doping [64]. This opened the way to study titania doping with non-metallic elements [65]. However, due to corrosion and instability of doped materials, it remains to be seen whether non-metallic element doping can be regarded as a general and valid approach to increase the photocatalytic efficiency of titania.

Due to rapid recombination of photo-generated CB electrons and VB holes, it is difficult to achieve water splitting for hydrogen production using TiO_2 photocatalyst in

pure water. Adding electron donors or sacrificial reagents to react with the photo-generated VB holes is an effective measure to enhance the electron-hole separation, resulting in higher quantum efficiency. However, the drawback of this technique is the need to continuously add electron donors in order to sustain the reaction since they will be consumed during photocatalytic reaction. Li et al.[66] reported enhanced photocatalytic hydrogen production when organic pollutants acting as electron donors, such as oxalic acid, formic acid, and formaldehyde, were added into the reaction system. Decomposition of the organic pollutants was reported to be consistent with hydrogen production. Besides the use of sacrificial agents, the addition of carbonate salts was found to improve photocatalytic hydrogen production by suppressing its backward reaction to form water. Sayama et al. [67] reported that adding carbonate salts to Pt-loaded TiO_2 suspensions led to highly efficient stoichiometric photocatalytic decomposition of water into H_2 and O_2. It was found that Pt-loaded TiO_2 photocatalyst during reaction was covered with several types of carbonate species. These carbonate species can effectively suppress the back reaction of water splitting to form water and alleviate the photoabsorption of oxygen on the TiO_2.

Usually, loading of metals that act as co-catalysts on the surface of photocatalyst, such as Pt, Pd, or Rh, is essential for enhancing its performance. Loading of metals, including Pt, Au, Pd, Rh, Ni, Cu, and Ag, have been reported to be very effective for improving TiO2's activity in photocatalysis. As the Fermi levels of these metals are lower than the CB of TiO_2,[68] photo-excited electrons can be transferred from the CB of TiO_2 to metal particles deposited on its surface, while photo-generated VB holes remain on the photocatalyst. Accumulated electrons on metal particles can then be used to carry out a reduction reaction, while holes on the photocatalyst can be used to carry

out the oxidation reaction. Therefore, metals with suitable work-function can help prevent electron-hole recombination, leading to higher photocatalytic activity of TiO_2. Bamwenda et al.[69] prepared Au and Pt loaded TiO_2 photocatalysts by deposition precipitation, impregnation, photodeposition, and colloidal mixing methods for hydrogen production. It was found that synthesis methods and metal loadings affect H_2 production significantly.

The roles of Au and Pt on TiO_2 include the trapping of photogenerated electrons, the reduction of protons, and the formation/desorption of hydrogen. Murdoch and co-workers studied the effect of Au loading and particle size on photocatalytic hydrogen production over Au/TiO_2 nanoparticles[70]. It was concluded that the increase in the hydrogen production rate is simply due to the greater availability of Au particles at the interface with TiO_2, trapping electrons to reduce hydrogen ions into hydrogen molecules. Anpo and Takeuchi[71] employed ESR signals to investigate electron transfer from TiO_2 to Pt particles.

Besides the role of electron traps to improve the photo electron-hole separation, loading of metal, such as Au or Ag, may also promote the activity of photocatalyst by the surface plasmon resonance (SPR) effect. SPR is defined as the collective motions of the conduction electrons induced by light irradiation, which is associated with a considerable enhancement of the electric near-field.[72] The resonance wavelength strongly depends on the size and shape of the nanoparticles, the inter-particle distance, and the dielectric property of the surrounding medium.[73] As for Au loaded TiO_2, electrons from the valence band of photocatalyst are excited to the conduction band by UV light irradiation, and then transferred to the gold particles on TiO_2. The SPR effect induced by appropriate visible-light irradiation (~560 nm for Au) can then boost the

energy intensity of the trapped electrons, resulting in enhancement of photocatalytic activity[74]. Kowalska and co-workers have examined a series of Au/TiO_2 samples prepared by photodeposition for the degradation of carboxylic acids. It was observed that the position of the surface plasmon band varies from 520 to 570 nm depending on the average particle size of the TiO_2 support.[75] It was also observed that gold deposition significantly enhanced the activity of photocatalyst due to the surface plasmon resonance effect. Silva et al. reported the investigation of Au/TiO_2 nanoparticles for the generation of hydrogen and oxygen from water.[76] They demonstrated that gold nanoparticles exhibit a dual role as light harvesters, injecting electrons into TiO_2's conduction band, and also as catalytic sites for gas generation, depending on the excitation light source used. For instance, when using excitation wavelengths corresponding to gold plasmon band, gold nanoparticles will absorb photons and inject electrons to the conduction band of TiO_2 to perform water reduction.

The surface or bulk modification of TiO_2 by noble metal ions, as reported by Kisch et al.[77], can also produce a visible-active center for the degradation of organic pollutants, such as 4-chlorophenol. Similarly, Li et al.[78] have also reported the photo-degradation of methylene blue in aqueous solutions under visible light irradiation over Au^- or Au^{3+}-modified TiO_2 powder.

Some reports have shown noble metals deposited on TiO_2 to effectively depress recombination of electron–hole pairs although they may have little effect on extending light absorption into the visible region;[79] thus, the photoactivity can be improved under UV instead of visible light illumination.

2.6.3 Origin of surface plasmon resonance in noble metal nanoparticles

The free electrons in the metal (d electrons in silver and gold) are free to travel through the material. The mean free path in gold and silver is ~50 nm, therefore in particles smaller than this, no scattering is expected from the bulk. Thus, all interactions are expected to be with the surface. When the wavelength of light is much larger than the nanoparticle size it can set up standing resonance conditions as represented in Fig. 3. Light in resonance with the surface plasmon oscillation causes the free-electrons in the metal to oscillate. As the wave front of the light passes, the electron density in the particle is polarized to one surface and oscillates in resonance with the light's frequency causing a standing oscillation. The resonance condition is determined from absorption and scattering spectroscopy and is found to depend on the shape, size, and dielectric constants of both the metal and the surrounding material. This is referred to as the surface plasmon resonance, since it is located at the surface. As the shape or size of the nanoparticle changes, the surface geometry changes causing a shift in the electric field density on the surface. This causes a change in the oscillation frequency of the electrons, generating different cross-sections for the optical properties including absorption and scattering.

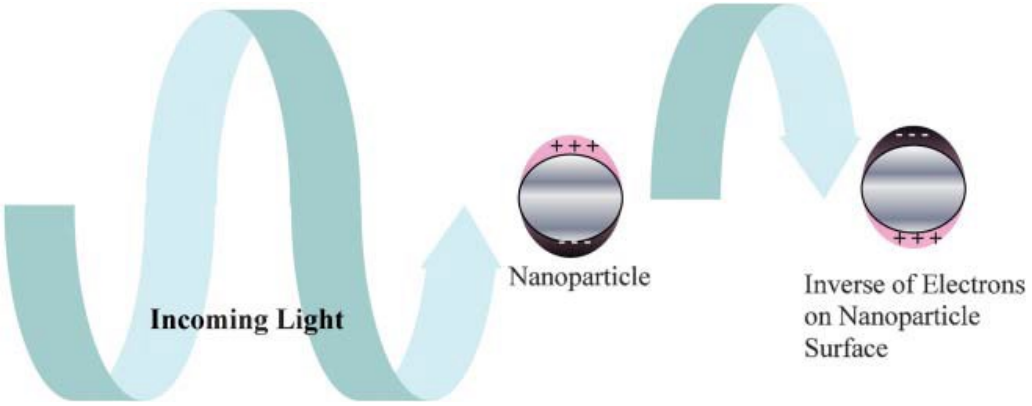

Figure 2.6: Origin of surface plasmon resonance due to coherent interaction of the electrons in the conduction band with light.[80]

2.7 Hydrothemal synthesis of TiO_2 nanotubes

2.7.1 Hydrothermal synthesis: A process definition

The first publications on hydrothermal synthesis of ceramics started appearing in the scientific literature in the middle of the 19th century.[81]. Hydrothermal synthesis is a process that utilizes single or heterogeneous phase reactions in aqueous media at elevated temperature ($T > 25\ ^{o}C$) and pressure ($p > 100MPa$) to crystallize ceramic materials directly form solution. However, researchers also use this term to describe process above the solution at the specified temperature and composition of the hydrothermal solution. However, in the case of hydrothermal growth of single crystals, pressure adjustment is done to control solubility and growth rate, usually by increasing solution fill level in the vessel are generally called precursors, which are administered in the form solutions, gels, and suspensions. Mineralizers are either inorganic or organic additives that are often used to control PH but are used at excessively high

concentrations (e.g., 10 molal) to also promote solubility. Other additives, also organic or inorganic, are used to serve other functions such as promote particle dispersion or control crystal morphology.

Upper limits of hydrothermal synthesis extend to over 1000 ^{o}C and 500MPa pressure. Nevertheless, from the point of view of large-scale materials production, practical temperature and pressure restrictions fall around 350 ^{o}C and 100 MPa, below which reaction conditions are considered mild and above which conditions are considered severe. This transition from mild to severe conditions is determined mostly by corrosion and strength limits of the materials of construction that comprise the hydrothermal reaction vessel. Intensive research has led to a better understanding of the hydrothermal chemistry, which has significantly reduced the reaction time, temperature, and pressure for hydrothermal crystallization of materials. A significant number of chemical systems in the form of powders and films can be synthesized in the range between that of ambient conditions and temperatures and pressure of 200 ^{o}C and < 1.5 MPa, respectively. This breakthrough has made hydrothermal synthesis more economical since processes can be engineered using cost-effective and proven pressure reactor technology and methodologies already established by the chemical process industry. In addition, the maintenance and safety procedures are far less involved with reactions performed under mild conditions as opposed to severe ones, which are considerations that influence productivity and cost.

2.7.2 The merit of hydrothermal synthesis

Hydrothermal synthesis offers many advantages over conventional and nonconventional ceramic synthetic methods. All forms of ceramics can be prepared

with hydrothermal synthesis, namely powders, fibers, and single crystals, monolithic ceramic bodies, and coatings on metal, polymers, and ceramics. Unlike many advanced methods that can prepare a large variety of forms, such as chemical vapor-based methods, the respective costs for instrumentation, energy and precursors are for less for hydrothermal methods. From the environmental perspective, hydrothermal methods are more environmentally benign than many other synthesis methods. This can be attributed in part to energy convenient disposal of waste that cannot be recycled. The low reaction temperatures also avoid other problems encountered with high temperature processes such as poor stoichiometry control due to volatilization of components and stress-induced defects caused by phase transformations that occur as the ceramic is cooled to room temperature. From the standpoint of ceramic powder production, there are far fewer time- and energy-consuming processing steps since mixing and milling steps are not necessary. Moreover, the ability to precipitate the powders directly from solution regulates the rate and uniformity of nucleation, growth and aging, which affords size, morphology and aggregation control that is not possible with many synthesis processes. From the standpoint of thin films (coatings), other methods such as physical vapor deposition, chemical vapor deposition and sol-gel suffer from the disadvantage that they all require high-temperature processing to crystallize the ceramic phase. Thermally induced defects result, such as cracking, peeling, undesired reactions between the substrate and coating and decomposition of the substrate material. In contrast, hydrothermal synthesis can be used to directly crystallize films on to substrate surfaces at low temperatures.

2.7.3 TiO_2 nanostructures synthesized via a hydrothermal treatment

Nanosize materials with peculiar properties are not expected in bulk phase and have already led to a breakthrough in various fields of science and technology. Over the past decades, nanosize materials derived from TiO_2 have extensively been investigated for vast applications, including solar cells/batteries, electroluminescent hybrid devices, and photocatalysis, owing to their peculiar chemical and physical behaviors. Currently developed methods of fabricating TiO_2-based nanotubes comprise the assisted–template method,[82] the sol–gel process,[83] electrochemical anodic oxidation,[84] and hydrothermal treatment.[85]. TiO_2-based nanotubes were first reported by Hoyer[82] via the template–assisted method. Thereafter, electrochemical anodic oxidation and hydrothermal treatment succeeded in fabricating TiO_2 nanotubes. Regarding the template–assisted method, anodic aluminum oxide (AAO) nanoporous membrane, which consists of an array of parallel straight nanopores with uniform diameter and length, is usually used as template. The scale of TiO_2 nanotubes can be moderately controlled by applied templates. However, the template–assisted method often encounters difficulties of pre-fabrication and post-removal of the templates and usually results in impurities. Among the aforementioned fabrication approaches, both electrochemical anodic oxidation and hydrothermal treatment received wide investigations, owing to their cost-effective, easy route to obtain nanotubes, and the feasibility/availability of widespread applications. Figure 2.7 shows various applications of vertically aligned TiO_2 nanotube arrays formed by hydrothermal reaction. Concerning electrochemical anodic oxidation, the self-assembled TiO_2 nanotubes with highly ordered arrays was discovered by Grimes' group,[86] and the method is based on

the anodization of Ti foil to obtain nanoporous titanium oxide film. They also demonstrated the crystallization and structure stability of TiO_2. The comprehensive reviews associated with the fabrication factors, characterizations, formation mechanism, and the corresponding applications of TiO_2-based nanotubes arrays have been also conducted by Grimes' group.[62]. These methods, other than the hydrothermal process, are either not suitable for large scale production or not able to yield very low dimensional, well separated, crystallized nanotubes.[87] The demonstrated architecture of TiO_2-based nanotubes constructed via the hydrothermal treatment is capable of good crystalline formation and establishment of a pure-phase structure in one step in a tightly closed vessel.

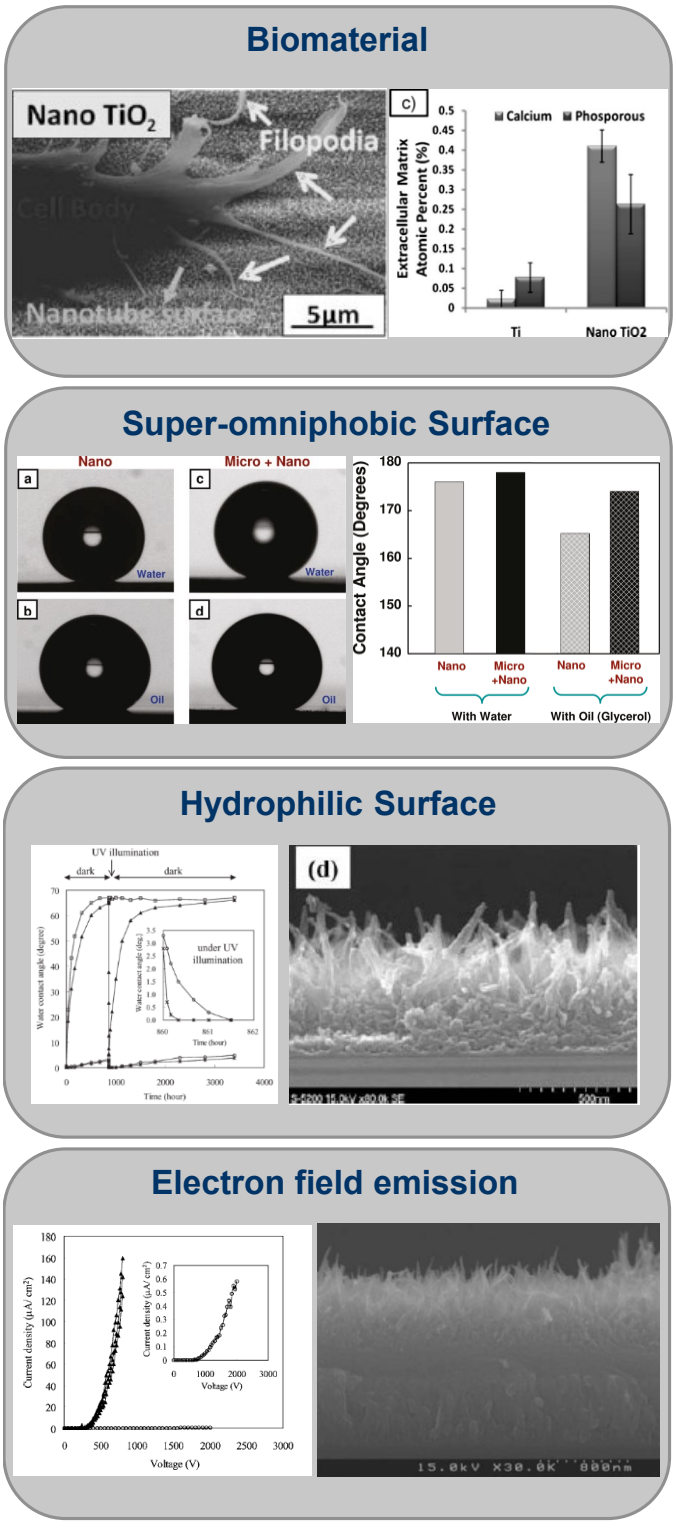

Figure 2.7: Applications of vertically aligned TiO_2 nanotube arrays

Chapter 3:
Plasmonic Au nanoparticles on 8nm TiO_2 nanotubes for enhanced photocatalytic water splitting

3.1 Introduction

Titanium dioxide (TiO_2) is one of the most widely studied photocatalysts for energy applications. It is also a promising candidate for the development of photochemical electrodes for water splitting and solar hydrogen production[12] as well as dye sensitized solar cells.[88] For energy applications, nanostructured TiO_2 is a very attractive material due to its large surface area and high electrochemical catalytic activity. In addition, TiO_2 is generally inexpensive compared to other photosensitive materials and has also outstanding resistance to photocorrosion in aqueous solutions over a long period of time.[89] Recently, one-dimensional TiO_2 nanostructures such as nanorods, nanotubes, and nanowires have emerged as promising building blocks for a new generation of nanoscale devices.[90,91] In particular, Miyauchi has reported the vertically aligned TiO_2 nanotube films by hydrothermal reaction of metal titanium and various functions derived from aligned structures of these films.[92] The hydrothermal processing technique is a simple and economic approach for creating one-dimensional nanotube architecture, which can produce nanostructures with significantly smaller dimensions and larger surface areas.[93] Also, the integrated electrode (e.g., with TiO_2 nanotubes vertically standing on the Ti surface) gives lower contact resistance, better stability, and enhanced geometrical exposure to react/connect better with the electrolytes or substrates compared to other TiO_2 architectures.

Although one-dimensional TiO_2 nanostructures provide larger surface areas,[94-96] there are still fundamental problems concerning the efficiency of photocatalysis that need to be solved. One of the biggest problems intrinsic to TiO_2 is its relatively large band gap of 3.2 eV (anatase),[17] that requires high energy UV light. Since UV light only accounts for about 5% of the solar radiation that reaches Earth's surface, the inability to utilize visible and infrared light limits the efficiency of solar photocatalytic activity. Thus, different strategies have been adopted in order to resolve this problem. Among various approaches, the deposition of foreign metal nanoparticles on TiO_2 surface has been widely studied[97] to reduce the limitations caused by the wide band gap and the high percentage of recombination of excited electron and hole, which decreases photocatalytic activity.[98]

Recently, improved photocatalytic activities by introducing Au nanoparticles to TiO_2 materials have been reported.[99-102] Gold nanoparticles on semiconductors are known to have excellent properties suitable for photocatalytic applications such as water splitting and CO oxidation. Au nanoparticles can be synthesized using different methods.[103-105] For large scale adoption and fabrication, the method has to be economically viable and compatible with the fabrication process of thin film photovoltaic modules.[106] For this reason, Catchpole and Pillai added Au nanoparticles to Si through solid-state dewetting of Au films for enhanced photocatalytic properties. They showed that a thin metal layer deposited on a Si surface, followed by thermal annealing, can be transformed into a layer of metallic nanoparticles.[107] This method is simple and can be easily integrated into the thin film fabrication process. They also investigated surface plasma resonance properties of Au nanoparticles formed by thermal annealing of Au films deposited on the Si substrate.

In this paper, we investigated the effect of thermally dewetted Au nanoparticles on the surface of extremely fine, 8 nm diameter, hydrothermally grown TiO_2 nanotubes having a very large substrate surface area on photoelectrochemical behavior. Also, the structure of the thermally dewetted metal particles on 8 nm diameter TiO_2 nanotubes was not previously reported.

3.2 Experimental procedures

3.2.1 Synthesis of TiO_2 nanotubes.

A titanium foil (0.25 mm thickness, Alfa Aesar, purity 99.5%) was ultrasonically cleaned using acetone, ethanol, and deionized (DI) water for 5 min in each step, followed by N_2 blow drying. The cleaned Ti foil was hydrothermally oxidized to produce the extremely fine TiO_2 nanotube arrays on the top surface of the microstructure of Ti by immersing into 10 M aqueous NaOH solution, heated at 120 °C for 30 minutes in a PTFE-lined autoclave, and subsequently washed with 0.1 M HNO_3 aqueous solution and deionized water. After drying in air, the samples were annealed in air at 500 °C for 1 hour in order to transform the as-fabricate amorphous TiO_2 nanotubes to the anatase TiO_2 phase.[93,108] For the purpose of measuring absorption spectra of Au nanoparticles, TiO_2 nanotube array was also synthesized on optically transparent sapphire substrates (0.432mm thickness, Alfa Aesar) by similar hydrothermal treatment. For this, a polycrystalline titanium film was first deposited on sapphire substrates by DC-magnetron sputtering (Discovery 18 Sputter System, Denton). The film sputtering was conducted under an argon gas pressure of 3×10^{-3} Torr at room temperature with a DC-power of 200 W. The Ti films were ~200 nm thick.

3.2.2 Preparation of Au nanoparticle decorated TiO_2 nanotubes.

Cleaned substrates were loaded into a Denton sputtering chamber to deposit Au films having thicknesses of 3, 5 and 7 nm. The sputtering deposition chamber was evacuated to a base pressure of better than 10^{-6} millitorr before the deposition process was started. Typical vacuum deposition techniques such as the evaporation process (and to a less degree the sputtering process) are line-of-sight deposition processes, and hence the Au deposition on 8 nm diameter TiO_2 nanotubes, especially in the core of the nanotube forest, is likely to be nonuniform. Therefore, we have utilized a high pressure sputtering at ~25 millitorr argon for deeper penetration of the plasma and increased scattering of the Au atoms/molecules for more uniform Au deposition on the nanotube surface.[109] The sample was also rotated during sputtering for uniform coating on TiO_2 nanotube surface. The sputtering rate was controlled and the deposition was stopped when the film thickness reached the target value. The deposited samples were annealed at 400 °C for 1 hour in vacuum so as to break up the Au film into nanoparticles. The TiO_2 nanotubes containing a Au film with a thickness of 3, 5 and 7 nm are hereafter referred to as '3 nm-sample', '5 nm-sample', and '7 nm-sample', respectively.

3.2.3 Characterization

Field-emission scanning electron microscope (FESEM, XL30, FEI) was used to analyze the morphology of the titanium nanotubes and Au nanoparticles. Typically, the images were acquired at low accelerating voltages (less than 5 kV) using short exposure

times. Transmission electron microscopy (FEI Tecnai Sphera 200 kV TEM) was also used in order to image the structure of the TiO_2 nanotubes. The UV absorption spectra of the films were measured using a UV spectrophotometer (SQ4802, UNICO). A standard three-electrode configuration (with platinum foil as a counter electrode and a saturated Ag/AgCl reference electrode) was used for the photoelectrochemical measurements. All three electrodes were immersed in a glass cell on which a quartz window was installed for light illumination. The photocurrent was measured in a 1M KOH solution using a scanning potentiostat (DY2311, Digi-Ivy) at a scan rate of 10 mV s^{-1}. Photovoltaic properties were measured under an AM 1.5 solar condition using a Xenon lamp (Oriel 66986, Newport) having a 300 W power capacity. The incident light intensity was measured to be 100 mW cm^{-2}. Measurements were performed using a full-spectrum solar simulator with and without a glass filter (FSQ-GG400, Newport) that blocks light at wavelength shorter than 400 nm. A standard Si photodiode (PIN-10DP/SB, OSI optoelectronics) was used as a reference to calibrate the power density of the light source. N_2 gas was purged through the cell during the measurement to instantaneously flush away O_2 from the working electrode and H_2 from the counter electrode. Electrical contacts were made from the Ti substrate using an insulated copper wire after removing the oxide layer on the surface of the Ti foil. The sample size exposed to the incident light was 1 cm^2.

3.3 Results and discussion

3.3.1 Size and morphology of gold nanoparticles

Shown in Figure 3.1a and 1b are the scanning electron microscopy (SEM) images of a typical array of hydrothermally grown TiO_2 nanotubes. In our previous work, we reported characterization of the hydrothermally grown TiO_2 nanotubes for osteoblast adhesion and bone growth.[110] Figure 3.1c shows a cross-sectional view at 45^o tilted angle of the TiO_2 layer grown on a Ti foil. The nanotubes grow mostly perpendicular but at somewhat tilted angles, and give an appearance of tangled network. This image displays an example nanotubes layer with a thickness of about 150 nm. The TEM micrograph, Figure 3.1d, reveals the multiwalled nature of the TiO_2 nanotubes having ~8 nm average diameter. The adhesion of the nanotubes on Ti substrate appears to be good as the nanotubes remain strongly attached during various handling processes. This is anticipated since the nanotube film is formed by etching of the Ti metal substrate itself, with the film and substrate sharing the same element, Ti.

3.3.2 Morphological characteristics of the Au nanoparticles

For enhanced photocatalytic properties, we have added Au nanoparticles on the prepared TiO_2 nanotubes. We have chosen gold in this work as a typical plasmonic material for visible light absorption enhancement. Au films having different thicknesses of 3, 5 and 7 nm were deposited on the TiO_2 nanotubes by sputtering and subsequently annealed at 400 °C for 1 hour in vacuum to produce the Au nanoparticles. An experimental flowchart of the procedures used is illustrated in Figure 3.2.

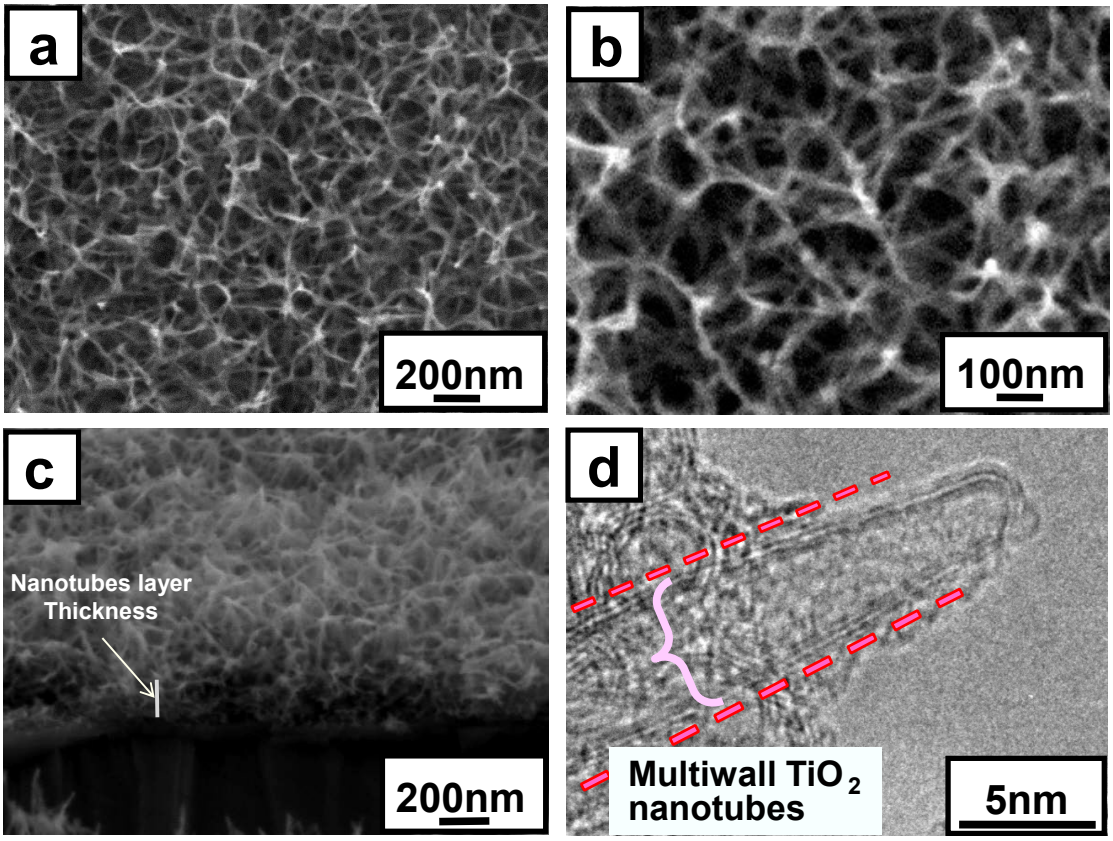

Figure 3.1: SEM images showing (a) top view, (b) magnified top view (c) cross-sectional view for near-vertically aligned but somewhat tangled TiO_2 nanotube arrays, (c) TEM micrograph showing the multiwall nature of the ~8 nm diameter TiO_2 nanotubes.

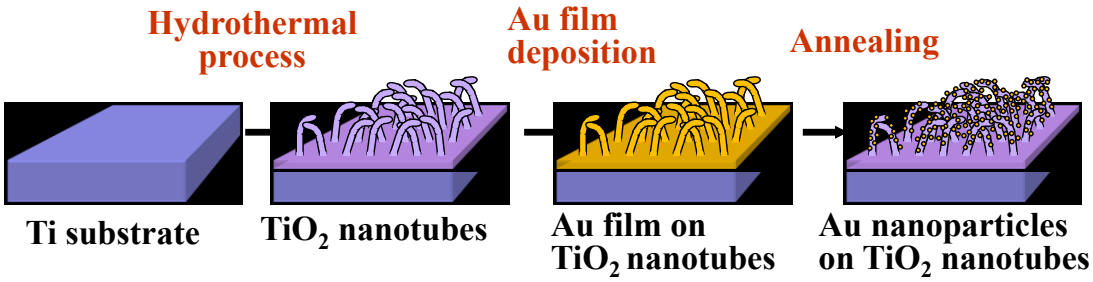

Figure 3.2: Schematic illustration of the experimental steps to fabricate Au nanoparticles dispersed on TiO_2 nanotube surface.

The 8 nm diameter nanotubes are formed almost vertically, with some contacting of neighboring nanotubes seen if a supercritical drying is not used after the hydrothermal process. Figure 3.3 compares the SEM images for the bare TiO_2 nanotubes, 3 nm thick Au coated TiO_2 nanotubes, and Au nanoparticle decorated TiO_2 nanotubes. It is seen that all the individual nanotubes appear to have been coated well by Au film and the one-dimensional nanotube array structure is preserved in the as-deposited state, as well as after break-up of the Au film into discrete nanoparticles by annealing. Figure 3.4 shows the effect of the initial deposited Au layer thickness (varying from 3 to 7 nm) on the final morphology of the Au nanoparticles after identical annealing steps (at 400 °C/1 hr). The observed bright contrast is related to the Au nanoparticles on the nanotube surface due to the high electrical conductivity of gold. A generally uniform distribution of Au nanoparticles with a nearly spherical shape can be seen on all three types of the samples. The SEM images clearly indicate that the increased initial deposited film layer thickness results in a corresponding increase of the averaged nanoparticle size. The averaged particle size of the Au nanoparticles in the 3 nm-sample is estimated to be ~10 nm, while that for the 7 nm-sample is about 40 nm. As the thickness of the Au films increases, the density of the nanoparticles decreases due to a coalescence of the nanoparticles and thereby their sizes increase. The number of nanoparticles can be estimated by dividing the total volume of Au film with the average particle volume. Corresponding to the decreased density, the calculated numbers of nanoparticles in the 3 nm-sample, 5nm-sample, and 7nm-sample are 5732, 1638, and 209, respectively for the identical unit substrate area of 1 μm x 1 μm. Also, total surface areas of Au nanoparticles in these samples are 1.8 μm^2, 1.6 μm^2, and 1.0 μm^2, respectively. Thus, well-distributed nanoparticles having sufficient total surface

area can be obtained avoiding from agglomeration of nanoparticles in other deposition methods using chemical solution or suspension of Au precursor. This suggests that a careful selection of the initial Au film thickness is desirable to optimize the size and density of the final Au nanoparticles on TiO_2 nanotubes. Solid-state dewetting of a metallic film on a substrate is driven by reducing the surface energy of the thin film and the interface energy between film and substrate.[111,112] The Au nanoparticle dimension can be controlled by either by altering of the initial Au layer thickness. Various experimental results that we obtained indicate that the control of Au layer thicknesses might be a more robust and easier approach in obtaining reproducible Au nanoparticle, in agreement with previous reports.[113] In this work, we have demonstrated the benefit of distributing adherent plasmonic noble metal nanoparticles onto the large-surface-area TiO_2 nanotubes having extremely small diameter. A less expensive noble metal or alloy-diluted Au could later be introduced for more practical purposes.

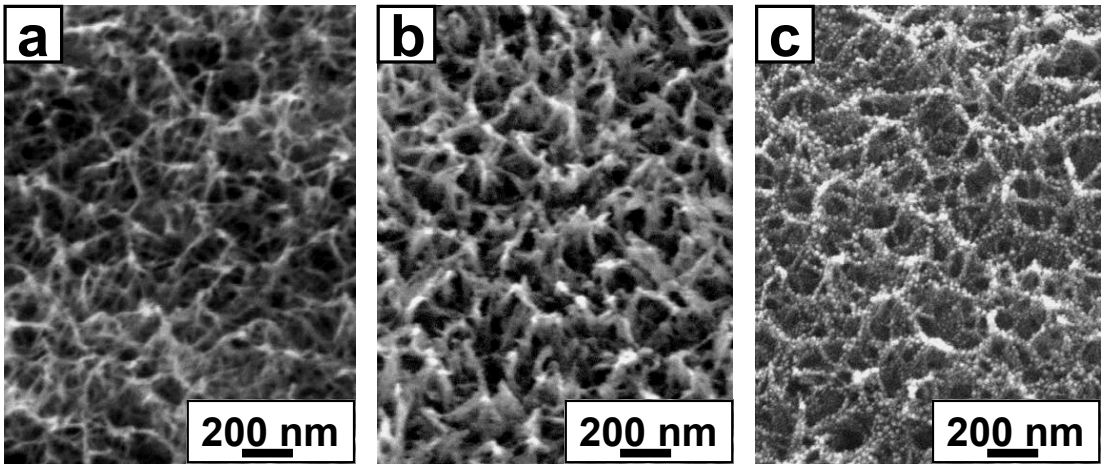

Figure 3.3: SEM images (tilt view) showing (a) bare TiO_2 nanotube array, (b) Au film deposited TiO_2 nanotubes array, and (c) Au nanoparticle attached TiO_2 nanotube array after annealing.

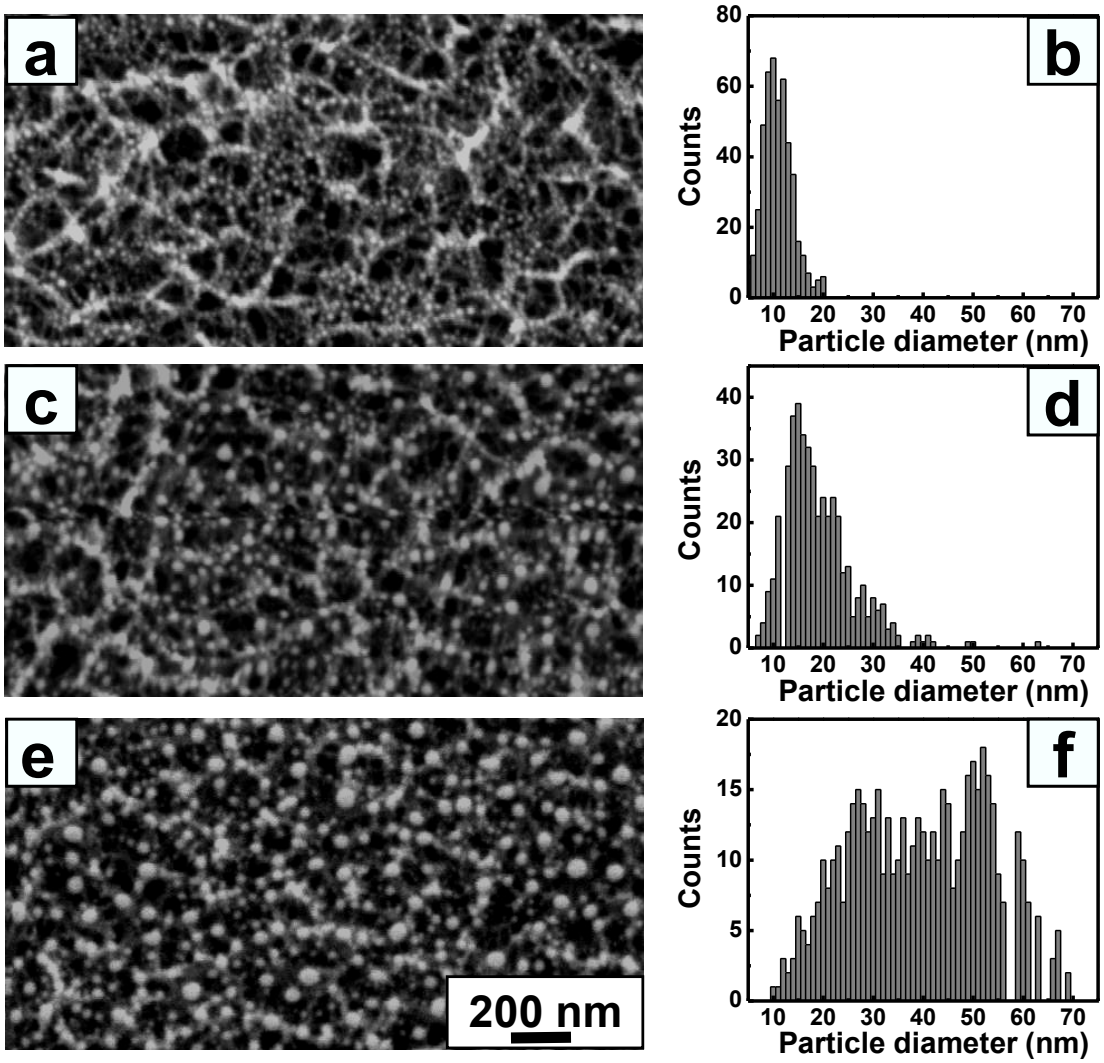

Figure 3.4: SEM images and the corresponding histograms of particle size distribution of the Au nanoparticles on TiO_2 nanotubes after 400°C anneal (a, b) TiO_2 nanotubes with average ~10 nm diameter Au nanoparticles from 3nm Au layer deposit (initial Au layer thickness), (c, d) ~18 nm diameter from 5nm Au layer, and (e, f) ~40 nm diameter from 7nm Au layer.

3.3.3 Absorption spectra of Au-modified TiO_2 electrode

Figure 3.5 shows the UV-visible absorption spectra of TiO_2 nanotubes with and without Au nanoparticles. The spectrum of the TiO_2 nanotubes (solid black curve) shows the absorption below 390 nm in wavelength. Unlike the bare TiO_2 nanotube sample, all the TiO_2 nanotubes containing the Au nanoparticles (solid color curves) absorbed more visible light, exhibiting absorbance maxima in the 500–600 nm wavelength region well beyond the UV regime. Such a spectrum shift in the visible spectrum region is believed to be caused by excitation of localized surface plasmons.[114] The results indicate that all TiO_2 nanotubes decorated with Au nanoparticles exhibit desirably broader optical absorption spectra in the general range from 300 to 800 nm, instead of the UV dominated behavior seen by bare TiO_2 nanotubes without Au nanoparticles. This might be meaningful and useful for the enhancement of photocatalytic behavior in solar energy application. The broader absorption of the Au nanoparticle decorated TiO_2 nanotube samples may be the results of some distribution in, shape, and separation of these plasmonic Au nanoparticles, as is noticeable in the SEM images of Figure 3.4.

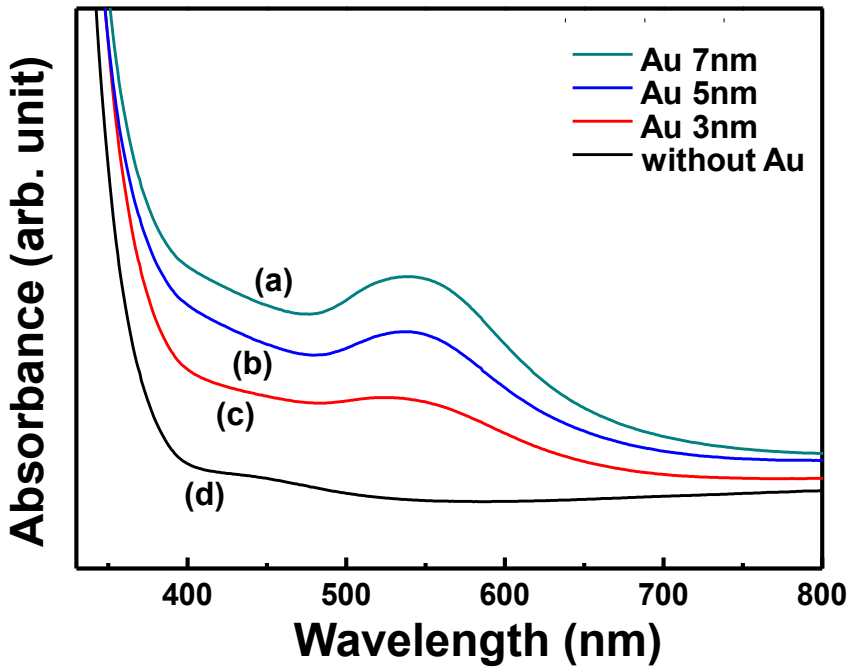

Figure 3.5: UV-visible absorption spectra of (a) TiO_2 nanotubes with gold nanoparticles from 3nm initial thickness Au layer, (b) from 5nm Au layer, (c) from 7nm Au layer (all annealed at 400 ^oC), and (d) bare TiO_2 nanotubes.

3.3.4 Photoelectrochemical performance

Figure 3.6 shows the current–potential response of a TiO_2 nanotube sample and Au nanoparticle decorated TiO_2 nanotube samples in aqueous solution with the potential measured relative to a Ag/AgCl standard electrode in the AM 1.5 simulated solar illumination. This photoelectrochemical measurement in aqueous solution is a well acknowledged general method for evaluating the performance of water splitting. In the photoelectrochemical measurements, the unreacted part of the metallic titanium foil underneath the nanotube array also serves as the conducting substrate to transport the photogenerated electrons.[115-117] The photocurrent density at 0.5 V of the hydrothermally formed TiO_2 nanotubes (without Au nanoparticles) was 122 $\mu A/cm^2$. In

comparison, the 3 nm Au-sample with very fine Au nanoparticles exhibited a significant enhancement in photoresponse with a photocurrent density of 153 $\mu A/cm^2$ under the identical illumination conditions, which is 25% higher than that of the TiO_2 nanotubse alone. Previously, Kamat and co-workers have reported the TiO_2 nanostructured electrodes with gold nanoparticles. They obtained the photocurrent density of 400 $\mu A/cm^2$ with 10 µm thick Au-TiO_2 film.[118] Also, Gomez and Villarreal have also reported the photocurrent density of 220 $\mu A/cm^2$ with 3 µm thick Au-TiO_2 film.[119] Compared with these results, the current densities in this study are not significant. However, the thickness of TiO_2 nanotube layer used in this study is only about 150 nm. Since it has been reported that 2 µm is the maximum penetration depth of the incident light in TiO_2, further increase in the nanotube length toward ~2 µm regime would increase the photocurrent density due to the enhanced light capture.

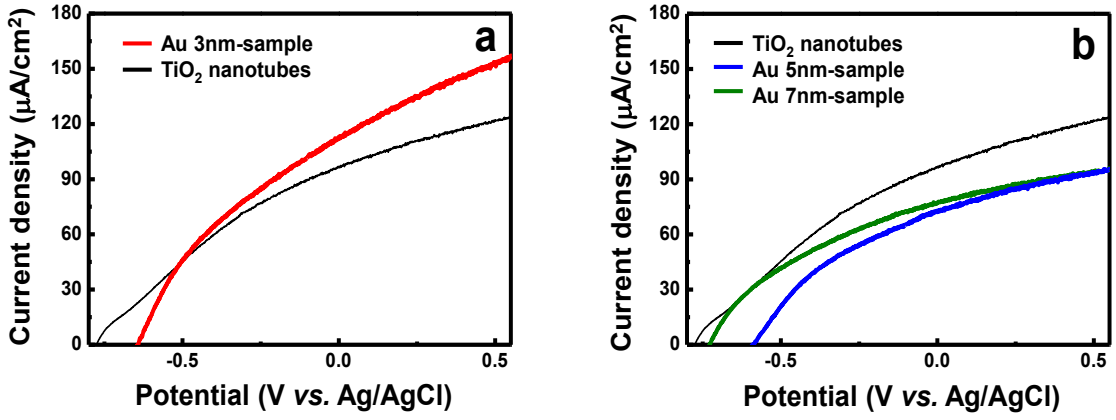

Figure 3.6: Photocurrent versus bias voltage of TiO_2 nanotube with various amounts of Au nanoparticles in aqueous solution.

3.3.5 Beneficial Role of Au Nanoparticles

A possible mechanism of this enhanced photoelectrochemical response is plasmon-induced charge separation. Since TiO_2 is mostly operative in the UV region, the visible light plasmonic effect can be obtained by subtracting the TiO_2-only photocurrent from the total photocurrent. Therefore, the increased photo-induced current in Figure 3.6 due to the presence of Au nanoparticles is attributed to the enhanced visible light absorption as demonstrated with the UV-visible absorption spectra in Figure 3.5. At the Au nanoparticle surface, collective oscillation of electrons is induced by incident light. In the Au–TiO_2 interfacial region, where energy bands of TiO_2 may bend in the space charge layer,[120] the oscillating electrons may be influenced by the electric field of the layer. This should cause the transport of the electron(s) to TiO_2 bulk. After the measurement of the 3 nm Au-sample, other samples were also measured as shown in Figure 3.6b. Interestingly, the larger diameter Au nanoparticles produced from the thicker deposited Au layers (5 nm and 7 nm thickness) having the resultant dewetted Au nanoparticle size much larger than ~10 nm (from the 3 nm layer Au deposit) show even lower photocurrent densities than the bare TiO_2 nanotube sample. Haruta has also shown that the catalytic activity of Au particles is derived from the nanometric dimensions of the metal particles. It is generally accepted that the optimum size of gold particles is smaller than 10nm for catalytic applications.[121] Also, an excessive amount of metal particle deposition would cause a shadow effect to partially block the sunlight and reduce photon absorption by TiO_2. The surface area of TiO_2 in direct contact with the aqueous solution might also become electron-hole recombination centers resulting in lower efficiency.[122] Therefore, our results indicate that a careful control of the Au particle size as well as the amount is

desired. The photoelectrochemical performance under AM 1.5 illumination was remarkably improved after introducing Au nanoparticles, most likely due to the enhanced charge separation.[123-125]

To understand the role of Au nanoparticles, we performed the photoelectrochemical measurements with mostly visible light using a high-pass filter with a "cut on" wavelength of 400 nm (FSQ-GG400, Newport Corp.) to remove the UV component of sunlight. Figure 3.7 shows the photocurrent densities of TiO_2 nanotubes with various amounts of Au nanoparticles, irradiated with visible light only without the UV light portion. The 3 nm Au-sample with very fine Au nanoparticles exhibited a significant enhancement in photoresponse with a photocurrent density of 11 $\mu A/cm^2$ under visible illumination, which is ~3.5 times higher than that of the TiO_2 nanotubes alone. Pure Au nanoparticles also show light absorption in UV-region due to interband transition.[126,127] The UV-excitation of Au nanoparticles can also contribute to the photocurrent density. An IPCE (incident photon to current conversion efficiency) measurement would be useful for advanced characterization and understanding of the mechanisms, which we will be carried out in future experiments. A thinner Au layer deposited than 3 nm thickness can also be investigated for further experiments. In this case, more enhanced catalytic activity of smaller nanoparticles obtained from this layer is anticipated due to the improved plasmonic effect.

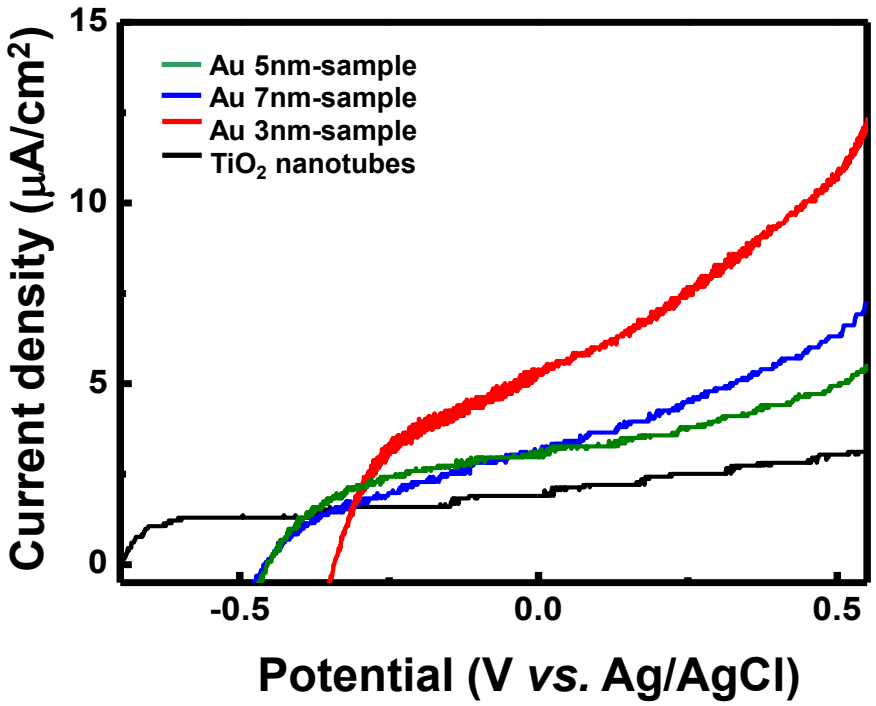

Figure 3.7: Photocurrent versus bias voltage of TiO_2 nanotubes with various amounts of Au nanoparticles irradiated with visible light.

The TiO_2 nanotubular structure provided a larger surface area with further reaction sites and much more rapid reaction rate. The hydrothermally grown TiO_2 nanotubes are extremely fine (8 nm in diameter). The distance between the neighboring nanotubes is roughly about 50 nm. Correspondingly, the calculated total surface areas of the plain (flat) TiO_2 layer sample vs that of the TiO_2 nanotube sample having 150 nm thick TiO_2 nanotube layer (assuming a square array of 8 nm diameter and 50 nm spaced apart vertical nanotubes for the latter) are estimated to be 1 μm^2 and 2.13 μm^2, respectively for the identical unit substrate area of 1 μm x 1 μm. Therefore, the hydrothermally grown TiO_2 nanotube array sample exhibits ~2 times more surface area than the plain TiO_2 layer. Being able to produce large surface area in catalytic structure

is highly desirable. As the 8 nm TiO_2 nanotubes can be grown taller (e.g., 1.5 μm tall nanotube array has been observed in our preliminary experiments), a further increased surface area and enhanced catalytic activity are anticipated. For an example of 1.5 μm tall nanotube array, the calculated total surface area is increased by a factor of ~12 with a comparable anticipated increase of the number of Au catalyst nanoparticles, which should lead to a substantially higher photocurrent density. A preparation of such a thicker TiO_2 nanotube layer for enhanced photocurrent behavior is in progress, which will be reported in future publications. In addition, a 3D construction of Ti foil can be used to make the overall surface area larger. The 8nm TiO_2 nanotubes can be introduced by growing on this 3D photoelectrode.

The TiO_2 nanotubes containing the Au nanoparticles exhibit increased and extended light absorbance from the UV regime to the visible spectrum region, presumably caused by excitation of localized surface plasmons. The photoelectrochemical current density was remarkably improved after introducing Au plasmonic nanoparticles on the TiO_2 nanotube surface. The photoactivity seems to be related to not only the size of gold particles but also the structural properties of the TiO_2 nanostructure support. Therefore, the 8 nm diameter TiO_2 nanotubes can be utilized as a convenient, large-surface-area support for finely distributed plasmonic Au–nanoparticles to help electron injection and transport[128] as illustrated in Figure 3.8.

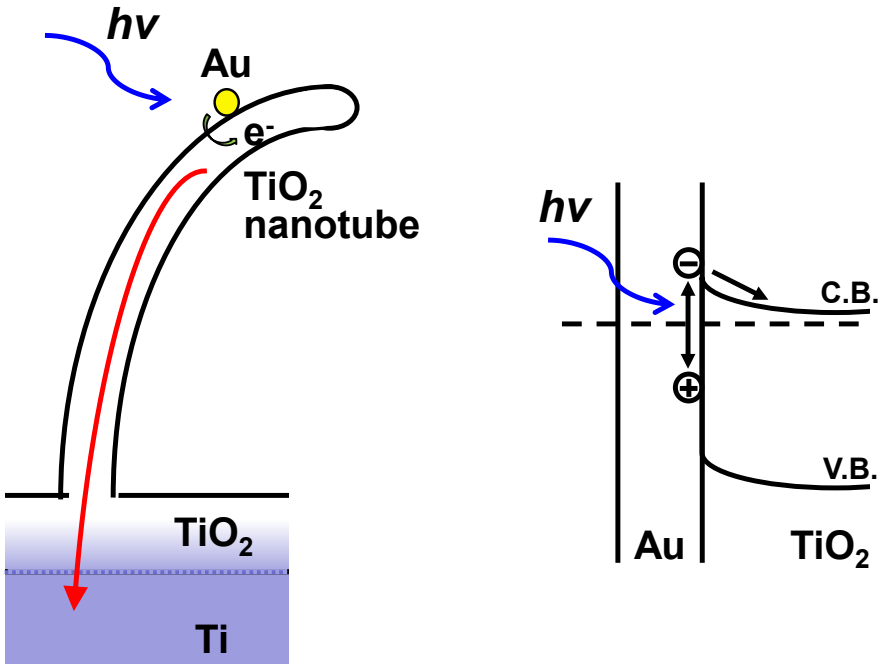

Figure 3.8: Schematic diagram of a gold nanoparticle attaching on a TiO_2 nanotube and a band diagram indicating the electron injection process.

3.4 Summary

We have successfully fabricated the plasmonic-metal/semiconductor photocatalysts composed of extremely fine hydrothermally grown titania nanotubes and near-spherical Au nanoparticles formed by thermal annealing. We have demonstrated that the 8 nm TiO_2 nanotubes can be employed as large-surface-area building blocks to support increased number of plasmonic Au nanoparticles. By virtue of substantially increased surface area with the 8 nm TiO_2 nanotube substrate in combination with the plasmonic effect of distributed gold nanoparticles, significantly increased photocurrent density was obtained with extended light absorbance from the UV regime to the visible

spectrum region, more notably in the visible light regime. Such gold nanoparticle decorated, extremely fine TiO_2 nanostructures fabricated by a simple and versatile method can be useful for hydrogen generation by water splitting, CO oxidation and various other types of photocatalysts and photovoltaic fuel cells.

Chapter 3, in full, is a reprint of the material as it has been prepared for publication in Journal of Renewable and Sustainable Energy written by Hyunsu Kim, Chulmin Choi, Jirapon Khamwannah, Sun Young Noh, Yanyan Zhang, Tae-Yeon Seong, and Sungho Jin. The dissertation author was the primary investigator and author of this work.

CHAPTER 4:
Formation of 8nm TiO_2 nanotubes on a three dimensional electrode for enhanced photoelectrochemical reaction

4.1 Introduction

Alternative sources of energy have received are important for sustainability of human civilization as the fossil fuels and nuclear energy have a number of serious long-term availability, environmental impacts, and safety issues.[129,130] Hydrogen, in particular, is considered an ideal fuel for the future because it is clean, energy efficient, with the desirable source of hydrogen, i.e., water, being abundant in nature.[131] While various techniques can be used to generate hydrogen including electrolysis, decomposition of fossil fuels, and others, only some of them can be considered environmentally friendly. Recently, solar hydrogen generated via photocatalytic water splitting has attracted tremendous attention and has been extensively studied because of its great potential for low-cost, clean hydrogen production.[132,133] Photocatalysis is defined as the chemical reaction induced by photoirradiation in the presence of a photocatalyst. In water splitting, photocatalysts have the ability to convert sunlight energy into chemical energy through a series of electronic processes and surface reactions without being consumed or transformed. Therefore, a robust and efficient photocatalytic electrodes are essential to the success of water splitting. These electrodes consist of a photocatalytic surface material that performs charge separation to generate electrons, and an underlying conducting material that transports the electrons. Electron-hole pairs can be generated and separated in this photocatalytic material by the

absorption of light when the energy of the light is greater than that of the material band gap.[134] The underlying conducting material in the electrode also provides mechanically supporting structure on which photocatalytic material are securely attached. While there are many parameters that influence the photocatalytic efficiency, the surface area of the employed photocatalytic material is one of the essential factors for high efficiency reactions. Therefore, an optimized structure of underlying substrate is also substantially important to maximize utilization of photocatalytic material. For efficient solar-to-chemical energy conversion, a photocatalytic electrode should be developed and optimized on both nano-dimensional photocatalyst geometrical structures and micro/macro substrate geometrical structures.

In the past few years, low-cost, efficient, stable, and nontoxic photocatalytic materials hae been studied for high efficient light absorption. In particular, one-dimensional nanostructures such as nanorods, nanotubes, and nanowires have emerged as promising forms for the new generation of photocatalytic devices due to their large surface area.[54,135,136] Unlike the studies on photocatalytic material itself, however, there have been relatively few reports on improving the performance by engineering the structure of the conducting substrate. For improved light conversion efficiency, one of the approaches to increase surface area is to employ three-dimensionality of substrate architectures.[137] A three-dimensional photocatalytic structure possesses an increased surface area and also exhibit less light reflection, and hence can absorb more light to generate increased number of separated charges (electrons) than a flat panel of the same overall-area footprint, which could prove useful in circumstances where the available space is limited. The large surface area of a 3-D electrode is expected to contribute to

the higher photocurrent since it increases the interface area with the electrolyte solution as well as the overall amount of photocatalytic material.

With such a structural design in mind, we have constructed a parallel straight-fin assembly made of double-sided Ti foil surfaces which can serve as a 3-D highly conductive electrode. Such an arrangement intuitively enables light trapping while allowing a smooth water flow through the microchannels between adjacent parallel fins during continuous-flow water splitting operations. In some ways one might think that this assembly may be viewed as a parallel line or groove patterned substrate. Typical fabrication methods for line patterned structure include lithography, plasma etching and vacuum deposition.[138] However, these methods generally are expensive, have limited manufacturing capacity, and limited aspect ratio of a micrometer scale protrusions in height.

As an alternative, industrially more viable approach, we have employed an assembly of alternately tall and short Ti foils, which is then rapidly spot welded in seconds to produce the desired 3-D electrode structures. Spot welding is one of the most practical methods for the fabrication of sheet metal assemblies since it is very simple, fast, effective and of low-cost.[139] In particular, spot welding process is used extensively for joining steel components such as high-strength low-alloy steel, stainless steel, nickel, aluminum, titanium and copper alloys.[140] Among these engineering nanomaterials, titanium can be considered as one of the suitable substrates for use in energy applications because it is abundant, stable in aqueous and conducting.[141] Also, the oxide form of titanium (TiO_2) is well known as an efficient photocatalyst, albeit more in the UV regime. TiO_2 nanostructures are useful for the energy-related applications, such as hydrogen generation by water splitting[12] or dye-sensitized solar

cell.[88] Furthermore, TiO_2 has its unique advantages of being inexpensive, nontoxic, and having a relatively high chemical stability.

Recently, Miyauchi has reported the vertically aligned TiO_2 nanotube films by hydrothermal reaction of metal titanium and various functions derived from aligned structures of these films.[92,93] These vertically oriented titania nanotubes are widely used in the photoelectrolysis[142], hydrogen storage,[143] and biomedical applications[110] because of their high surface area, good charge-transport properties, and ease of use. In the hydrothermal process, TiO_2 nanotube film can be formed directly onto Ti substrate surface by chemical reaction process without other precursors.[93] An additional advantage of TiO_2 nanotubes is that these nanostructures are not grown or separately produced and attached onto the substrate, but are rather formed by etching of the Ti substrate, therefore there is a natural mechanical and electrical connection at the interface between the nanostructure and the underlying substrate.

In this study, we produced a 3-D photocatalytic electrode having nanoscale surface TiO_2 nanotubes. The fabrication of such 3-D structured Ti substrate was done by alternate stacking of tall vs short Ti foils and a quick spot welding assembly, followed by, the formation of conformal 8 nm diameter TiO_2 nanotube array layer by hydrothermal process. The photocatalytic activity of the TiO_2 nanotube array on the vertically aligned Ti fins was evaluated in aqueous solution and compared with that of the planar TiO2 nanotube film. The 3-D photocatalytic electrode provided further reaction sites and much rapid reaction rate via increased surface area. As a result, a ~300% improved photocatalytic effect has been obtained.

4.2 Experimental procedures

4.2.1 3-D structured Ti fin assembly electrode.

The 3-D structured Ti substrates were prepared by joining sheet metal using a spot welding machine (CEA, ZT-11). The Ti foils (0.25 mm thickness, Alfa Aesar, purity 99.5%) were cut two sets of widths using a standard metal foil shear machine, to the dimension of 10 x 10 mm (tall Ti foil) and 10 x 7 mm (short Ti foil), respectively. Their surfaces were chemically cleaned by acetone before resistance spot welding to eliminate surface contamination. The tall foils and short foils were alternately assembled and gravity aligned into a 3-D structure having the tall foils (fins) protruding upward with a ~3 mm height difference. This assembly was maintained by clamping using paper binder clips during the spot welding. (See Figure 4.1.) The welding was carried out using a current and time controlled electric resistance spot welding machine. The machine employed pure copper electrodes with 6 mm end diameter. After the welding, the welded Ti substrate was removed from the machine and left cooling in open air. Prior to the next process, the welded Ti substrate was dipped in 20% HF solution for 20 seconds to remove the thermal oxide during welding.

4.2.2 Synthesis of TiO_2 nanotubes.

The 3D structured Ti substrate was hydrothermally oxidized to obtain the TiO_2 nanotube arrays on the surface of the Ti fins by immersing into 10 M aqueous NaOH solution, heated at 120°C for 2 hours in a PTFE-lined autoclave, and subsequently washed with 0.1 M HNO_3 aqueous solution and deionized water. After drying in air, the

samples were annealed at 500°C for 1 hour in air in order to transform the as fabricated 8 nm diameter TiO_2 nanotubes to the anatase TiO_2 phase.[93]

4.2.3 Structural and optical characterization

Field-emission scanning electron microscope (FESEM, XL30, FEI Co., USA) was used to analyze the morphology of the titanium nanotubes. Typically, the images were acquired at low accelerating voltages (less than 5 kV) using short exposure times. Transmission electron microscopy (FEI Tecnai Sphera 200 kV TEM) was also used in order to image the structure of the TiO_2 nanotubes. The UV absorption spectra of the films were measured using a UV spectrophotometer (SQ4802, UNICO).

4.2.4 Photoelectrochemical characterization

A standard three-electrode configuration (with platinum foil as a counter electrode and a saturated Ag/AgCl reference electrode) was used for the photoelectrochemical measurements. All three electrodes were immersed in a glass cell on which a quartz window was installed for light illumination. The photocurrent was measured in a 1M KOH solution using a scanning potentiostat (DY2311, Digi-Ivy) at a scan rate of 10 mV s^{-1}. Photovoltaic properties were measured under an AM 1.5 solar condition using a Xenon lamp (Oriel 66986, Newport) having a 300 W power capacity. The incident light intensity was measured to be 100 mW cm^{-2}. A standard Si photodiode (PIN-10DP/SB, OSI optoelectronics) was used as a reference to calibrate the power density of the light source. N_2 gas was purged through the cell during the measurement to instantaneously flush away O_2 from the working electrode and H_2 from the counter electrode. Electrical contacts were made from the Ti substrate using an

insulated copper wire after removing the oxide layer on the surface of the Ti foil. The backside and edges of samples were protected using epoxy so that only the sample front side could be in contact with the electrolyte. The footprint area exposed to the incident light was 1 cm^2.

4.3 Results and discussion

4.3.1 Morphological characteristics of the 3D photoelectrode

Spot welding process was carried out in a fixture illustrated schematically in Figure 4.1. Ti foil pieces cut to two sets of dimensions (10 x 10 mm (tall Ti foil) and 10 x 7 mm (short Ti foil)), and alternately assembled and gravity-aligned into a 3-D structure having the tall foils (fins) protruding upward with a ~3 mm height difference beyond the short Ti foils. This assembly was maintained by clamping using paper binder clips during the spot welding.

As shown by the cross-sectional view and oblique incident view pictures in Figure 4.2, a three-dimensional Ti layer assembly was constructed easily that consisted of linearly aligned, parallel thin foils (Ti fins), on the surface of which a high-density, 8 nm diameter TiO_2 nanotubes were synthesized by hydrothermal process. A reasonably well arranged periodic, linear patterned Ti structure was formed by assembling two sets of sheared Ti foils (each 250 μm thick) having different heights (~3 mm different). The protruding Ti fins are arranged in parallel very regularly, with a length of about 3 mm above the base line Ti structure. Subsequent spot welding resulted in a 3D structured substrate, in contrast to a regular planar Ti foil substrate. In this 3-D profile having the protruding portion of Ti substrate at an aspect ratio of ~12, the vertical walls increase the overall electrode surface area by that much. Different geometrical designs can be

used for obtaining higher aspect ratio if desired. This 3-D assembled Ti fin substrate was then used to form the 8 nm diameter TiO_2 nanotubes to further increase the active surface area. A flow chart of the procedures used in this experiment is presented in Figure 4.3. The spacing between the Ti fins of 250 μm with an aspect ratio of ~12 seems to be adequate for the subsequent hydrothermal process to form the TiO_2 nanotubes in a conformal manner on most of the surfaces of each fin including the valley area. Furthermore, this 250 μm level spacing between adjacent active fins could well provide sufficient gap spacing for smooth water flow through the gap during a continuous-mode water splitting operation in large-scale solar fuel manufacturing environments.

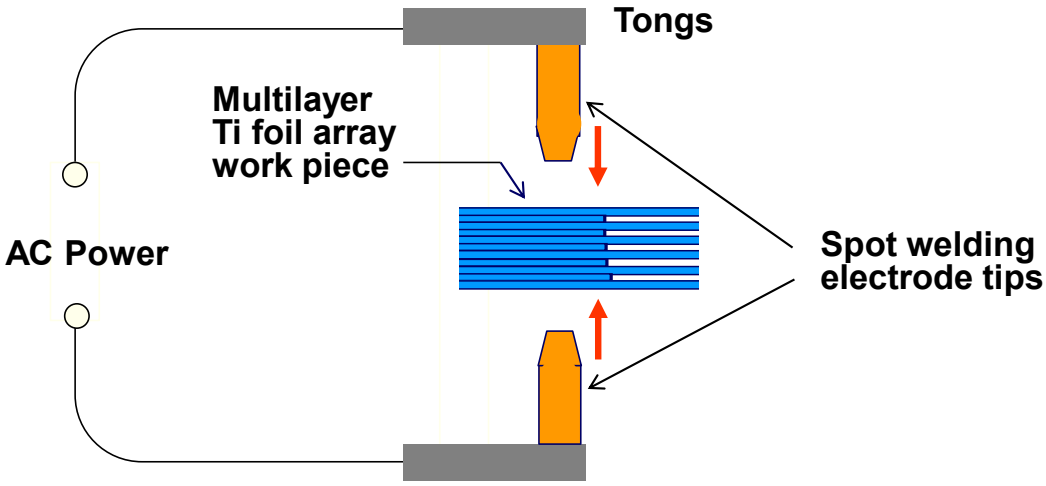

Figure 4.1: Basic configuration of resistance welding of short and tall Ti foil multilayer assembly.

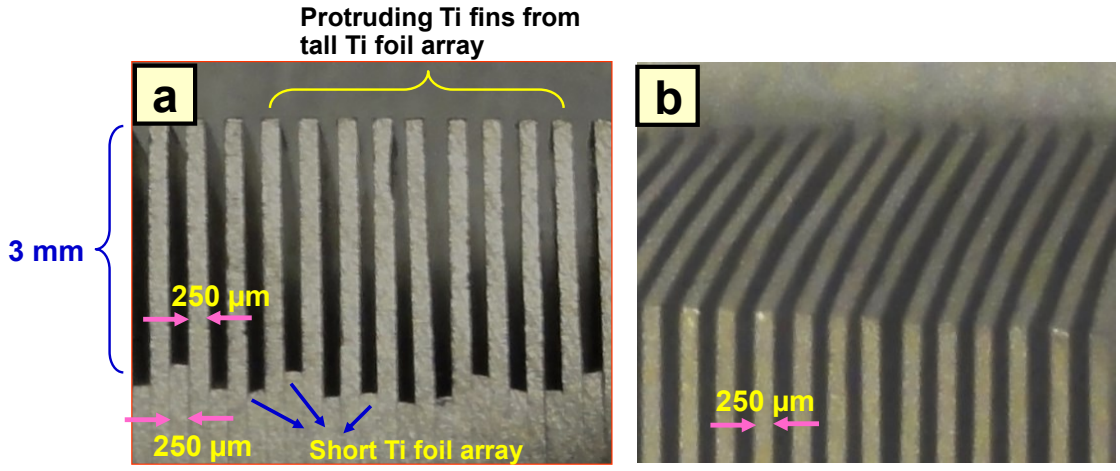

Figure 4.2: Photographs of a three-dimensional Ti layer assembly consisting of parallel thin foils and protruding fin array. High density, 8 nm diameter TiO_2 nanotubes are added onto each of the Ti layer surfaces. (a) cross-sectional view, (b) oblique incident view. The spot welded region is located below the photographed regions in the figure and is not shown.

Figure 4.4 shows the scanning electron microscopy (SEM) image of a typical array of hydrothermally grown TiO_2 nanotubes. The nanotubes form in a conformal manner on the entire 3D Ti surfaces (exposed surfaces) as determined by SEM analysis. The large amount of 8 nm diameter TiO_2 nanotubes produces a nanoscaled roughness and substantially increased surface area on the Ti substrate. Assuming the 8 nm diameter nanotubes are separated by 18 nm spacing and their height is 0,5 micrometer tall, the total surface area of all the nanotubes on 1 $(\mu m)^2$ substrate area is estimated to be roughly 3 x 107 nm^2, which is ~30 times larger than a planar Ti foil having an identical flat surface of 1 $(\mu m)^2$ area. With the protruding fin structure having 250 µm width, 3 mm height and 1 cm assumed depth along the axis perpendicular to the plane of the photograph Figure 4.2(a) or (b), there will be 40 fins per linear cm in the Figure

4.2 horizontal axis. With both surfaces of each fin contributing to the water-splitting reaction, the surface area increase by the fin structure is estimated to be by a factor of ~24, as compared to a planar foil surface, which is significant.

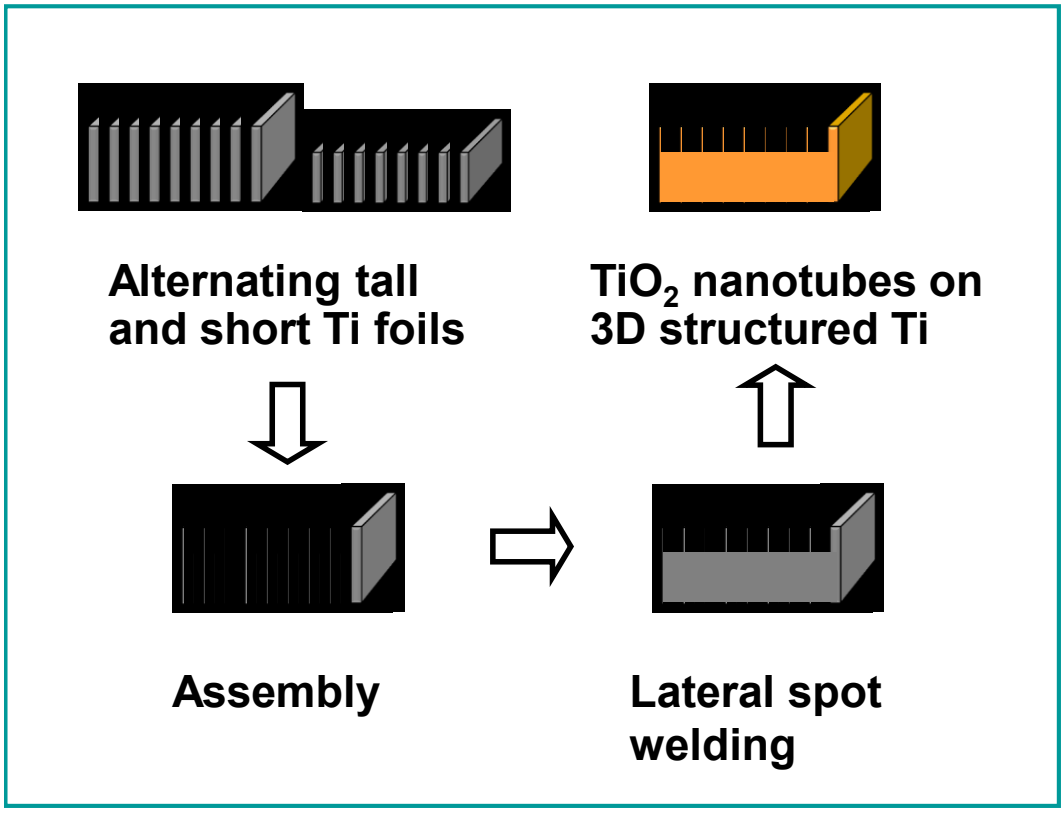

Figure 4.3: Schematic illustration of the experimental steps to fabricate TiO_2 nanotubes formed on 3-D titanium structure.

The profile of the substrate structure is retained during the hydrothermal process for TiO_2 nanotube formation. Figure 4.4a and b show that well aligned TiO_2 nanotube arrays were formed on the surface of the Ti substrates, representing the morphologies on the top surface, the walls of the fins, and the bottom of the fins, all appearing to be somewhat similar. The nanotubes of TiO_2 grow more or less perpendicular to the local surface and the growth rate of the nanotubes is constant. Figure 4.4c shows the tilted view of the TiO_2 nanotube arrays. In our previous work, we have reported characterization of the hydrothermally grown TiO_2 nanotubes.[110] The adhesion of the 8 nm nanotubes on the Ti substrate surface appears to be good as indicated by preliminary shear deformation experiments after which the nanotubes remained intact. This is anticipated since the nanotube film is formed by etching of the Ti metal itself, with the film and substrate sharing the same element, Ti. TEM micrograph, Figure 4.4d, reveals the multiwalled nature of the hydrothermally formed TiO_2 nanotubes having ~8 nm average diameter. Thus the hydrothermal processing technique is a simple approach for creating one-dimensional nanotube architecture, and provides additional larger surface area, e.g., ~8 nm diameter TiO_2 nanotubes on the 3-D structured surface.

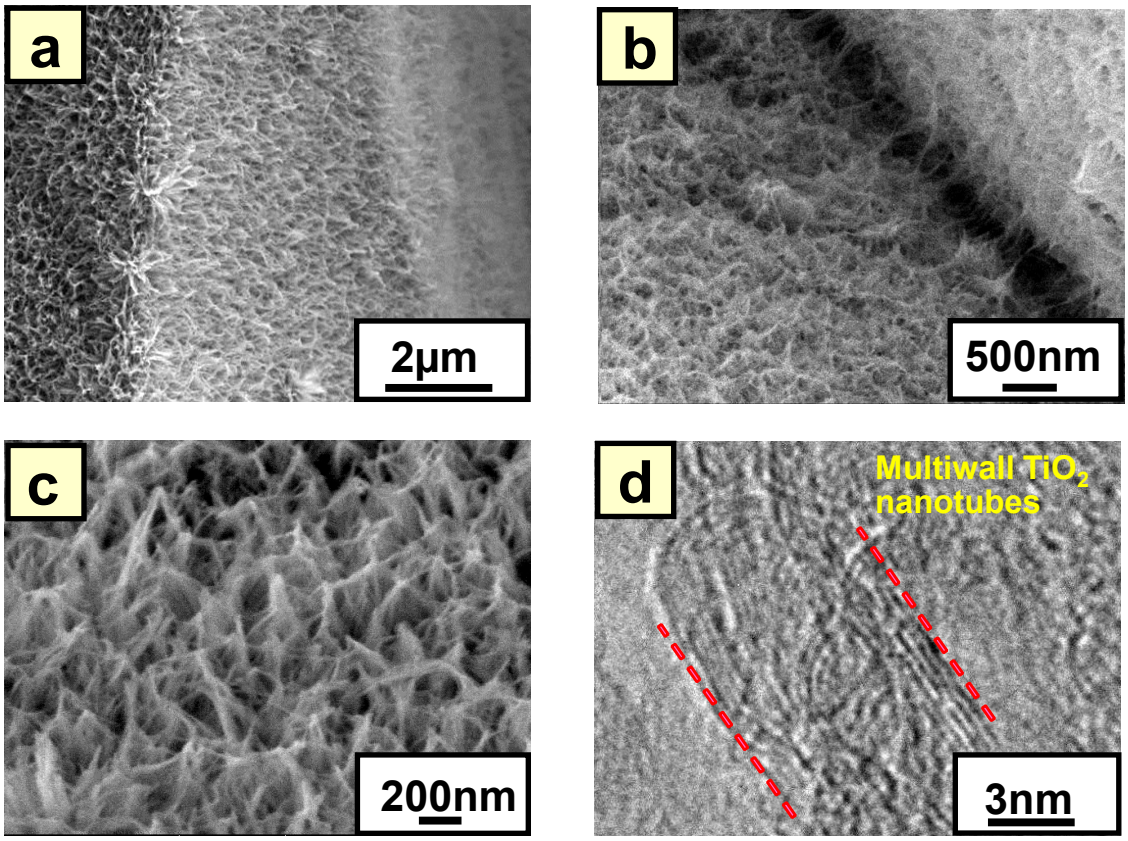

Figure 4.4: SEM images showing conformal TiO_2 nanotubes on (a) the wall of each Ti fin, (b) TiO_2 nanotubes present near the recessed bottom of the Ti fin, (c) tilted view of somewhat tangled TiO_2 nanotube arrays, and (d) TEM micrograph showing the multiwall nature of the ~8 nm diameter TiO_2 nanotubes.

4.3.2 Absorption spectra of TiO_2 nanotubes

Figure 4.5 shows the UV-visible absorption spectra of TiO_2 nanotubes (placed on sapphire as a transparent substrate for optical measurement purpose). The spectrum of the TiO2 nanotubes shows the UV light absorption below 390 nm in wavelength. TiO_2 is mostly operative in the UV region since its band gap of 3.2 eV, and hence requires high energy UV light.[16] Figure 4.6 shows the current–potential response of the 3D structured TiO_2 electrode in aqueous solution with the potential measured relative to the Ag/AgCl standard electrode in the AM 1.5 simulated solar illumination. This photoelectrochemical measurement in aqueous solution is a well acknowledged general method for evaluating the performance of water splitting. In the photoelectrochemical measurements, the unreacted part of the metallic titanium foil underneath the nanotube array also serves as the conducting substrate to transport the photogenerated electrons.[115-117] In this structure, This integrated electrode (with TiO_2 nanotubes vertically and conformally standing on most of the Ti surface) gives better stability and geometrical exposure to react better with the substrate compared to other TiO_2 architectures using a binder or buffer material. The photocurrent density at 0.5 V of the hydrothermally formed 8 nm TiO_2 nanotubes on planar Ti electrode was 122 $\mu A/cm^2$. In comparison, the TiO_2 nanotubes on 3D structured electrode exhibited a significant enhancement in photoresponse with a photocurrent density of 364 $\mu A/cm^2$ under the identical illumination conditions, which is ~300% higher than that of the planar electrode. Therefore, the increased photo-induced current in Figure 4.6 due to the increased surface area of 3-D structure is attributed to the enhanced light absorption, as is noticeable in the photographs of Figure 4.2.

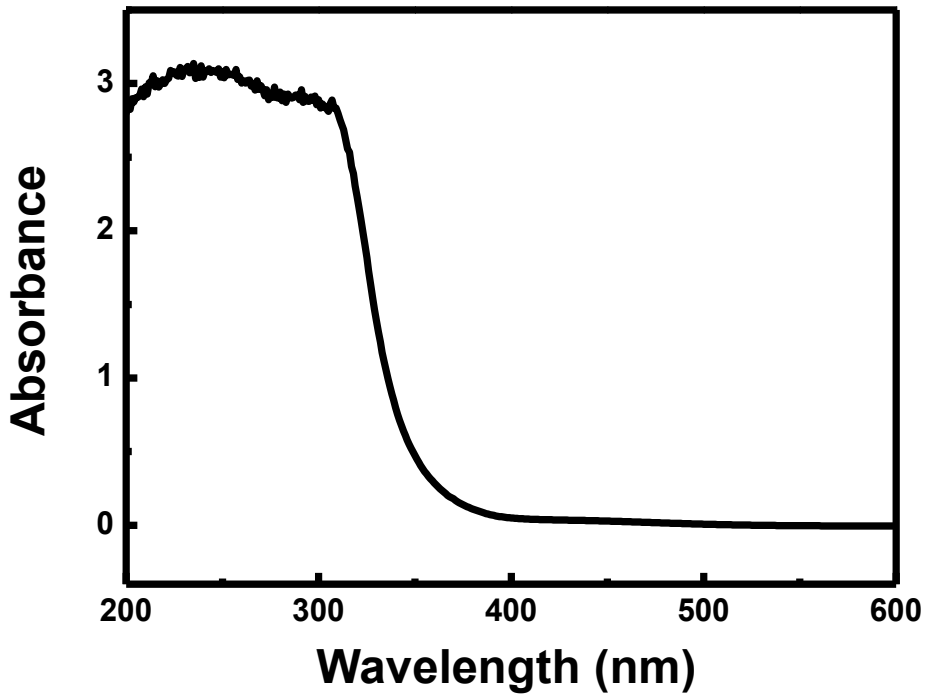

Figure 4.5: UV-visible absorption spectra of TiO_2 nanotubes showing a predominant UV absorption.

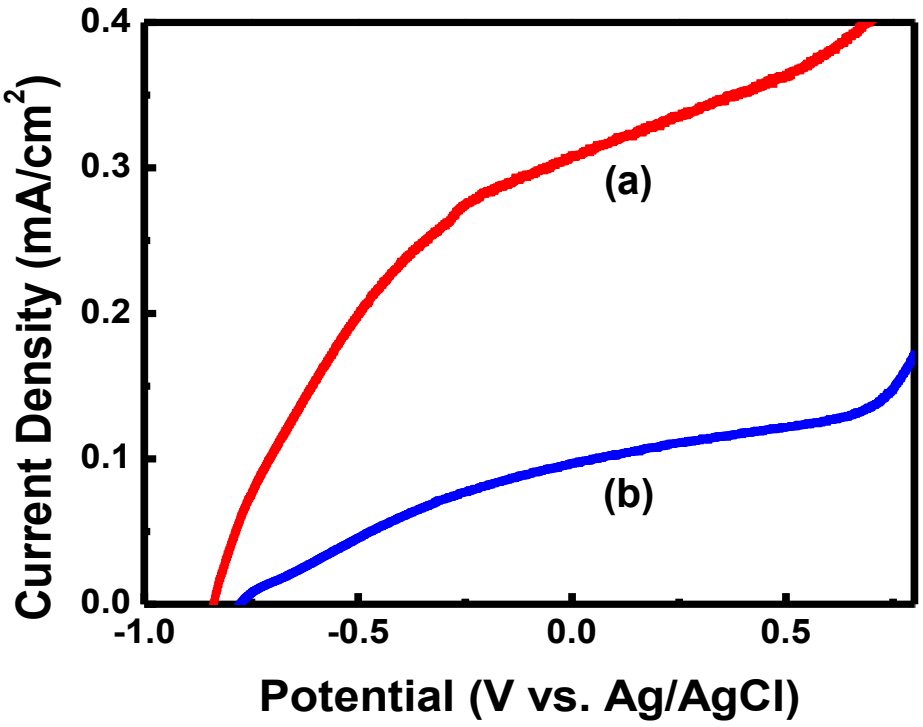

Figure 4.6: Comparative photocurrent versus bias voltage curves of TiO_2 nanotube layers on (a) a 3-D structured Ti electrode and (b) a single layer planar electrode.

4.3.3 Photoelectrochemical performance

3-D architecture by spot welding is indeed an effective structure to enhance the areal amount of nanotubes so as to substantially improve the performance of the photocatalytic nanomaterial in a simple and viable way for scale-up water splitting applications. Moreover, the better catalytic performance can also be ascribed to an increased effective contact area between the photocatalytic material and electrolyte solution. Therefore, the 3-D structured electrode provides a desirably much larger surface area with further reaction sites. The photoactivity is related not only to the photosensitivity of photocatalytic material but also the structural configuration of the conducting substrate supporting the photocatalytic material. Compared with the planar

electrode, the 3-D structured electrode can be utilized as a convenient, large-surface-area support for photocatalytic nanotube array to help electron transport as illustrated in Figure 4.7.

The large surface area of the 3-D substrate can be used to support photocatalytic nanomaterials for light harvesting. The combination of spot welding and hydrothermal process creates more structural surface and expands the application of TiO_2 in relevant areas with dramatically enhanced performance. The geometric effect of the fins faced each other may have a positive effect on photocatalytic activity. In this structure, vertically aligned walls of the fins could repeatedly reflect light down toward the bottom of the fins (to the valleys), so that there are more opportunities to absorb light. Therefore, the catalytic performance would be further optimized by carefully designed feature size, density, recessed depth, and so on, which are some of the possible ways to further enhance the photocatalytic activity.

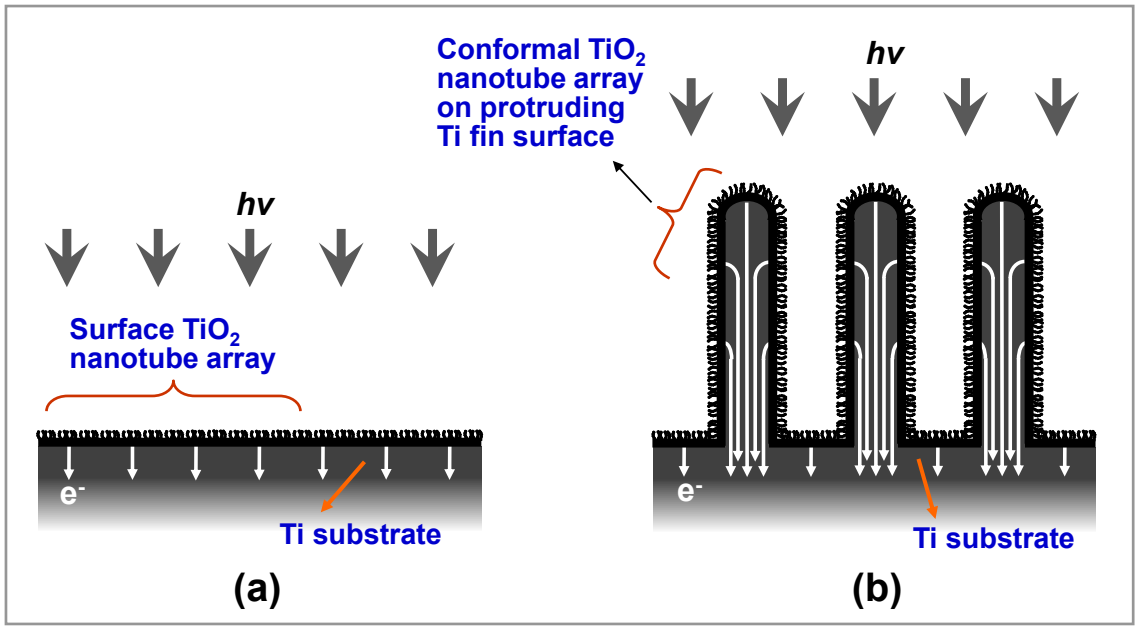

Figure 4.7: Schematic diagram of TiO_2 nanotube layers adhered on the surface of (a) a planar electrode and (b) a 3-D structured electrode, also indicating the electron injection process (white arrows).

4.4 Summary

We have successfully demonstrated a simple method to fabricate a 3-D water splitting electrode assembly containing 8 nm diameter TiO_2 photocatalytic nanotubes. The 3-D photoelectrode configuration having hydrothermally formed conformally placed TiO_2 nanotubes on parallel Ti fins, was assembled by simple and facile spot welding of alternately tall and short Ti foil assembly, which provided ~24 times increased electrode surface area. By virtue of substantially increased surface area with the 3-D photoelectrode, significantly increased (by ~300%) photocurrent density was obtained with the photocatalysis of TiO_2 nanotubes in combination with enhanced electrical current path between conducting Ti fin substrates and the photocatalytic TiO_2 on the fin surface. Such 3-D straight fin array structures fabricated by a simple and versatile method can be useful as a robust photocatalytic electrode for hydrogen generation by water splitting, solar cells, CO oxidation and various other types of photocatalytic or photovoltaic cells.

Chapter 4, in full, is a reprint of the material as it has been prepared for publication in Nano Energy written by Hyunsu Kim, Jirapon Khamwannah, Chulmin Choi, Calvin J. Gardner, and Sungho Jin. The dissertation author was the primary investigator and author of this work.

CHAPTER 5:
An X–Y Addressable Matrix Odor-Releasing System Using an On–Off Switchable Device

5.1 Introduction

In recent decades, much research has been dedicated to the development of virtual reality for entertainment,[144] engineering,[145] and medical application.[146] Virtual reality can be made more realistic with an artificial three-dimensional visual or other sensory environment using the experience of moving seats,[147] odors of explosives or flowers,[148] sprinkling water, laser lights, and wind blowing. Odor-releasing devices that allow repeatable, remote, and reliable switching of odor flux, in particular, could have a significant impact on the effectiveness of virtual reality. However, although various devices for the added sense experience have been developed recently, very few odor-generating devices with practical and useful control of induced sense of smell have been reported. The development of an odor-releasing system that can provide specific odor selectively began in the early days as a crude device. The oldest system is “Sensorama”,[149] a game machine, wherein odor is presented according to the scene on the display and the chair or steering wheel vibrates. After Sensorama, there were discussions about which movie needs odor presentation, referring to some experiments on providing odors synchronously as the movie scenes evolve. In the AMLUX theatre, there was an attempt to add odor information to visual media. Also, there have been some tests to induce the relaxation effect through odor presentation in art objects. Furthermore, there were some approaches to utilize odor information for the fire-fighter training system,[150] and the soldier training system by

using a scent collar.[151] These systems present odor information by evaporating bulk smelly material or by spraying it using propellant gas or inkjet technology. However, these well-known technologies are coarse and crude in nature, and it is hard to apply them to delicate home electronics or personal devices owing to their bulkiness, their lack of reproducible release over multiple cycles, their slow response times to stimuli, as well as their inability to dynamically adjust the amount/intensity of odor according to the recipient's needs. Therefore, the development of odor releasing or transferring systems for the electronic device virtual reality has been difficult. Moreover, televisions, home theatre, or video-game devices are getting thinner and smaller, requiring faster and more accurate control. Indeed, no existing device could overcome all of these limitations at the moment. For example, an automatic aerosol dispenser containing odor-filled reservoirs can achieve rapid on-demand odor delivery but the odor-storing cans are filled with compressed gas or flammable solvents used as propellants and require a complicated valve system which is difficult to scale down. The desirable odor-generating systems should not depend on a mechanical switching system and should be thin enough to insert into small devices. For these reasons, innovative technologies are needed. The primary requirement to the development of a gas-release device for odor generation is an accurate control capability. From this perspective, an ideal device for odor generation should safely contain a suitable quantity of odor-releasable solution, can release little or no odor in the "off" state, and be repeatedly switched to the "on" state without mechanically disrupting the device.

In recent years, many researchers have been trying to develop on–off switchable devices for drug release using polymers,[152–154] because some polymers have good reversible switching properties. We have employed in our new odorgenerating system, a

stable polymer, polydimethylsiloxane (PDMS), a representative silicone elastomer. PDMS is optically clear and, in general, is considered to be inert, non-toxic, and non-flammable. One of the primary fields of applications for PDMS is the embedding or encapsulation of electronic components by casting, which prolongs the life span of the circuit chips. A silicone elastomer such as PDMS, exhibits mechanical elasticity, acts as a dielectric isolator, and protects the components from environmental factors and mechanical shock over a relatively large temperature span (e.g., 50–2008C).[155] In addition, the inertness and stability of PDMS has been traditionally utilized as a biomaterial in implants, catheters, drainage tubing, and membrane oxygenators.[156] We have therefore utilized the desirable properties of PDMS for the development of our on–off switchable odor releasing system. Cross-linked (cured) PDMS elastomer does not allow aqueous solvents to infiltrate and swell the polymer,[157] so that it can be used as a container which can store a water-based liquid. Although elastomers are not usually completely impermeable to most gases, the gas permeability decreases with increasing cross-linking.[158,159] As will be discussed below, we utilized X–Y matrix addressable localized heating from an x–y grid electrical resistance heating wires, which induces a local reversible shrinkage/expansion of PDMS and this thermally induced volume change can open a tiny exit hole on the top of the specific odor-container element to release gas as described in Figure 5.1a.

5.2 Experimental procedures

5.2.1 Preparation of gas releasing device

The odor-generating system is composed of heating elements and containers which are used for containing the odor materials. The experimental setup had the

advantage of being more comparable to a real odor releasing process. Odor generating systems were prepared by curing of PDMS with a cavity so that the ammonium hydroxide solution was filled in PDMS containers without vaporization. Sylgard-184 elastomer from Dow Corning was made according to instructions. The mixing ratio A(monomer) : B(hardener) was 10:1. The elastomer properties are listed in Table 1. After being weighed, the compound was mixed for 5 min with a wooden stick and then left for 10 min to let air bubbles diffuse out of the liquid. The mass was then poured into the mold and degassed, in order to prevent micro-bubbles at the bottom of the mold.

A plastic Petri dish (Falcon, 35mm in diameter) was used as a mold. The filled form was carefully sealed with a plastic lid which had a corn shaped polytetrafluoroethylene (PTFE) for making the corn shaped cavity in the PDMS, and then hardened in the oven (Thermolyne, OV12900) for 30min at 80 °C. After the hardening process, the PTFE was removed from the PDMS and the formed PDMS was placed on the mixed PDMS liquid for the second hardening process. The bottom diameter of the cone shaped empty space in the PDMS is 7 mm and the height of that was 6 mm.

Nichrome resistance wires (Jelliff Corporation, 0.01 inch in diameter) for the internal heating system were attached on the bottom of the PDMS container with third PDMS liquid hardening. Aqueous Ammonium hydroxide (Fisher, 14.8N), isopropyl alcohol (Fisher), and ethyl alcohol (Rossville Gold Shield) were used as solutions for gas detection. Each solution was injected into the PDMS container by using the syringe (BD, 10ml in volume) and the syringe needle (BD, 0.31mm in diameter). After removing the needle for the syringe injection of the ammonium hydroxide solution, the puncture site was restored immediately. A gas outlet, which is pointing upward, is

located below the cover of measurement apparatus. The liquid can leave the system from the top end of the PDMS container.

For heating the PDMS container, constant current was applied to the Nichrome wires by a DC power supply (BK precision, 1627A). The generated gas was measured by a gas monitor (RAE systems, VRAE) with data logging. The sealed Petri dish and the gas monitor were connected by the flexible tubing (Tygon, 0.125 inch in diameter).

One of the PDMS samples was prepared for leakage measurement. A simple-to-use color changing tubes (RAE systems, Gas Detection Tube) were used for visualization of gas release. The perfumes, "Live by Jennifer Lopez" and "Passion by Elizabeth Taylor", were used as solutions for odor generation. The distance between the odor generation system and the detecting human nose was fixed at 30 cm.

Table 5.1: Material parameters of Sylgard 184[160]

Material	**Sylgard 184**
Color	**Transparent**
Viscosity (mPa s)	**3900**
Shore-A hardness	**50**
Elastic modulus (MPa)	**1.8**
Thermal conductivity ($W\ m^{-1}\ K^{-1}$)	**0.18**
Thermal expansion coefficient ($\mu m\ m^{-1}\ K^{-1}$)	**310**
Dielectric breakdown strength ($kV\ mm^{-1}$)	**21.2**
Dielectric constant	**2.65**
Resistivity (Ω cm)	**1.2×10^{14}**

5.2.2 Measurement of gases

A Sealed Petri dish (Fisherbrand, 60mm in diameter) was used for the measurement of the generated gas. When using ammonia, ammonia is injected in first. After the measurement apparatus is closed, the current applies along the heating wires. For heating the PDMS container, constant current was applied to the Nichrome wires by a DC power supply (BK precision, 1627A). The internal heating system using the Nichrome wires of the PDMS gas releasing device was attached on the bottom of PDMS container and tested by evaluating the volume concentration of ammonia gas as a function of time. The odorant solution is released using a resistance wire that heats the odorant. The measured concentration of the odor is controlled by applying current to heating wire. The generated gas was measured by a gas monitor (RAE systems, VRAE) with data logging. The sealed Petri dish and the gas monitor were connected by the flexible tubing (Tygon, 0.125 inch in diameter). Pumps for odor airflow are connected to the odor cells with different solutions, and the gas monitor is connected directly to the odor-presenting unit. One of the PDMS samples was prepared for leakage measurement.

5.2.3 Visualization of gas release

A simple-to-use color changing tubes (RAE systems, Gas Detection Tube) are used for visualization of gas release. A gas enters through one hole via Tygon tubing connected to the measuring apparatus. The second hole connected to the gas monitor which has an internal sampling pump. Ammonia and ethyl alcohol are then tested with their respective detector tubes.

5.2.4 Interference test of adjacent gas container

We installed two containers which contains isopropyl alcohol and ethyl alcohol, respectively. These containers are connected to each other in the matrix structure with row Nichrome wires. Crossed Nichrome wires were insulated by PDMS layer avoid being short-circuited. When the gas releasing device for isopropyl alcohol turned on, ethyl alcohol was not detected, and vice versa. Therefore, the gas release of each device can be controlled by certain combination of row and column switches without any interference. Figure 5.7 shows that there was no difference in response between single cell operation and multi cell operation connected with column heating wires.

5.3 Results and discussion

5.3.1 Elastomeric container for odor releasing

Herein, we report a gas/odor release system based on a gated PDMS chamber array which is employed as a rapid, repeatable, and reliable gas/odor release upon electrical actuation. A novel two-dimensional (2D) cell-chamber array capable of selective odor generation is proposed as described in Figure 5.1b,c. The proposed X–Y matrix structured odor-release system has an array of gas/odor containers with rows and columns of electrical heating lines, in which only the intersecting cell (and no other cells) from many arrayed cells is allowed to pass beyond the threshold accumulation of gas/odor pressure to force-open the cell gate for gas/odor release.

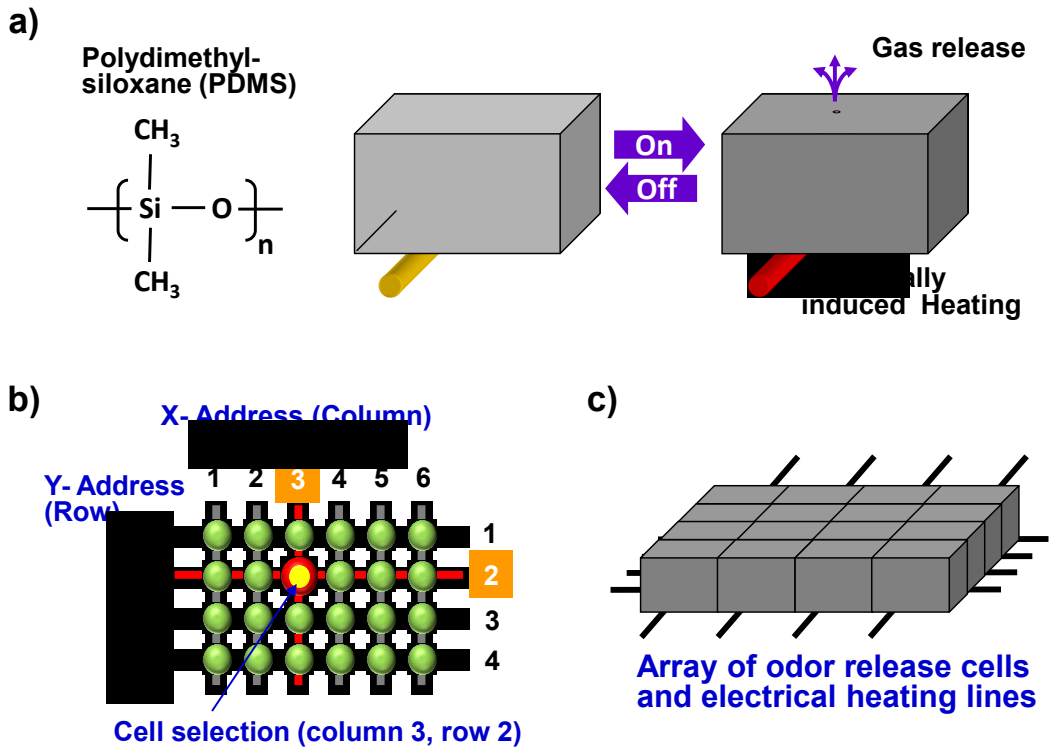

Figure 5.1: a) Proposed action of a gas/odor-release device based on an elastic chamber material. b) a diagram illustrating the x–y coordinate cell-selection method, and c) a X–Y matrix structured odor-releasing system with 4x 4 cells.

We have demonstrated the single-cell operation of a PDMS gas/odor-release device. The fabrication process for the device and the configuration of the measurement apparatus for this experimental setup are illustrated in the Supporting Information Figures 5.2 and 5.3. The size (volume) of a cone-shaped cell is 0.077 mL. Each of the PDMS cells has a gate at the top made of a puncture hole (but without actually removing any of the PDMS material), which elastically keeps the hole tightly closed if unactivated, but opens allowing the gas/odor release when activated by electrical heater lines.

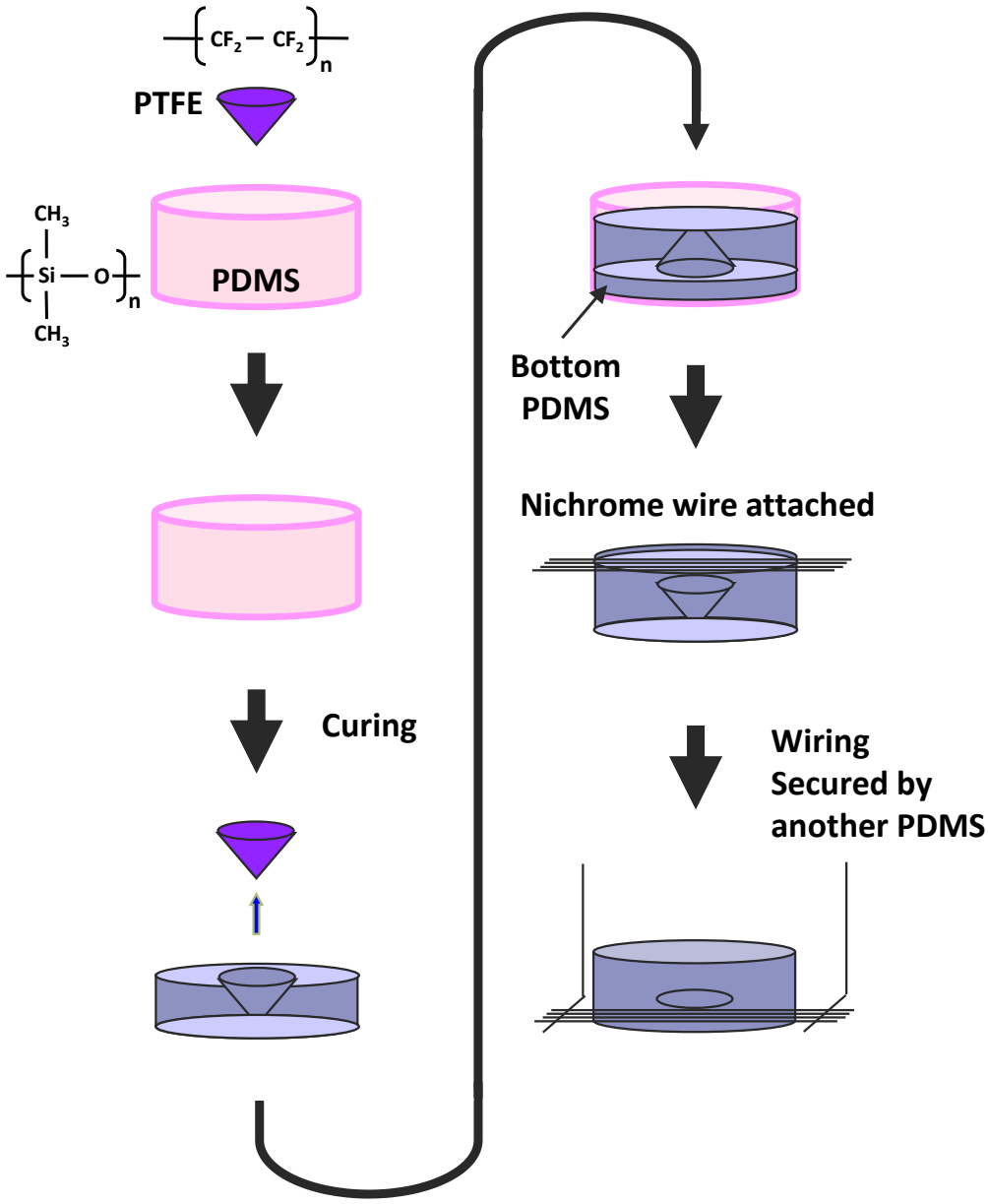

Figure 5.2: Sketch illustrating the process flow to fabricate a PDMS odor generating device.

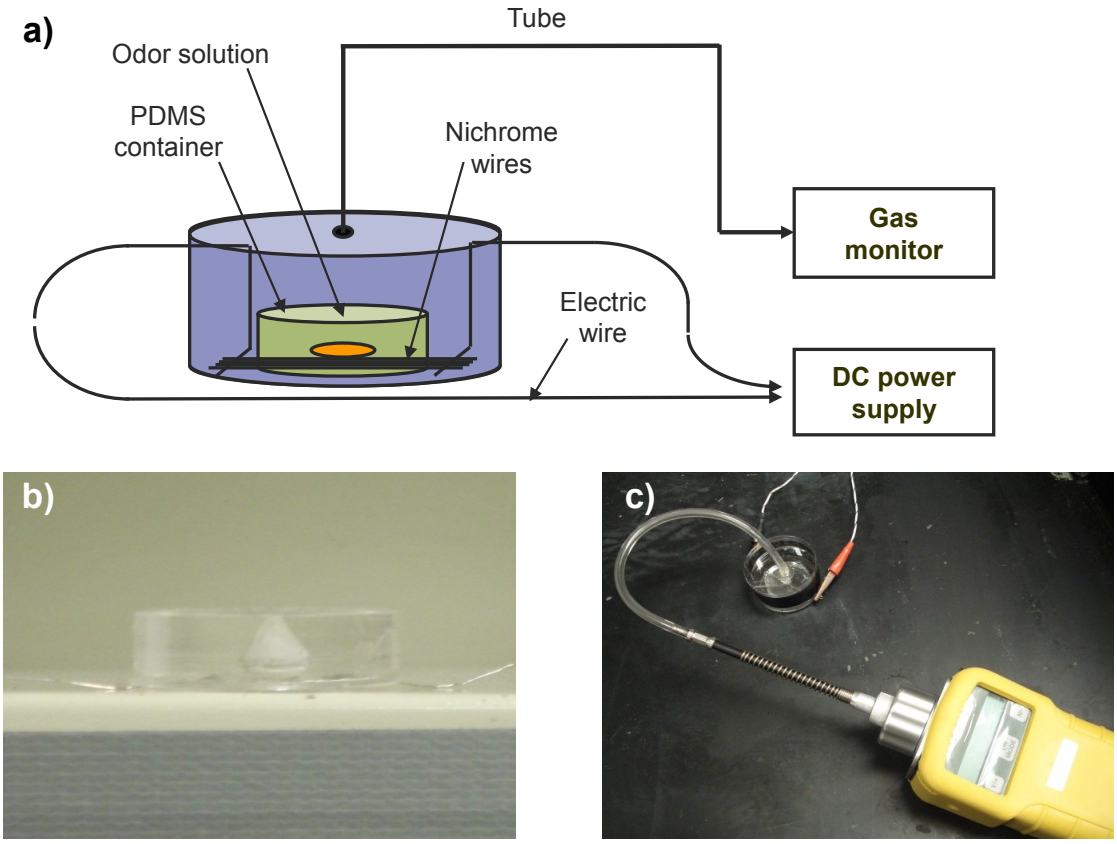

Figure 5.3: a) Diagram of the gas measuring apparatus, b) the photographs of a PDMS gas release device and c) the configuration of gas measurement tools.

Ammonia was injected into the cell cavity through the puncture hole. The system was designed in such a way that a certain threshold pressure is required to overcome the elastic closure force of the gate. This threshold pressure is made to occur only when the specific targeted chamber is heated simultaneously by two crossing lines (both x-line and y-line), thus providing X–Y matrix selectivity for any one chamber cell. The detector setup has the capability to monitor real time data change as a gas detector. This provides a better control for the assessment of the amount of gas released during

operation because traditional gas measurement techniques using gas chromatography and photo-acoustic spectroscopy suffer from the major drawbacks of being slow, being operationally impractical, and do not allow for real-time measurements.[161]

5.3.2 Detection of controlled gas release

One of the compounds that we have chosen as the source of an odor is aqueous ammonia. The aqueous ammonia can easily be filled into the chamber cell regardless of container shape and easily generates odor from the solution on electrical actuation in the form of ammonia gas. It is believed that the primary mechanism for gas/odor release is the pressure-buildup beyond the threshold to open the elastic gate, but a contribution from the thermal expansion mechanism that geometrically alters the pore dimension may also play a role. Further research is needed to elucidate the exact mechanism of gas/odor release in our device system. The electric current for heating the Nichrome electrical heating wires positioned underneath the chamber cell array was kept at 1.5 A for the sample. The Nichrome alloy is a well known commercially available electrical heating element made of 80% Ni and 20% Cr in weight, having a high electrical resistivity of approximately 150 mW-cm. Liquid NH_4OH was injected with a hypodermal syringe to the chamber. Figure 5.4 shows the detected ammonia gas during the “on” state. Continuous release of odor was performed by continuous passage of electrical current to the heating wire. Real-time monitoring has been conducted instantaneously in percentage by volume for the sampled gas in the air. The maximum volume concentration of ammonia gas was approximately 0.6 vol% of all gases involved (ammonia + oxygen + nitrogen). The area under the gas concentration curve was integrated and used to calculate the total amount of released gas. Since the gas flow

rate in the gas monitor is 6.7 mLs^{-1}, the concentration can easily be converted into volume. Figure 5.4b shows the accumulated amount of ammonia. Total amount of ammonia gas released is estimated to be 9 mL.

Another PDMS device was constructed and used for a leakage test. When the device filled with ammonia was kept in the "off" state (without applied current) for 24 h, no noticeable signal of ammonia was detected. This implies that the elastically closed "gate" is very tight and can hold the gas in place without leakage. As gas molecules can escape through even extremely small nanopores, this leakage test data is quite encouraging. Thus, the PDMS container with electrical actuation system could be used as a reversible/repeatable gas/odor-releasing device.

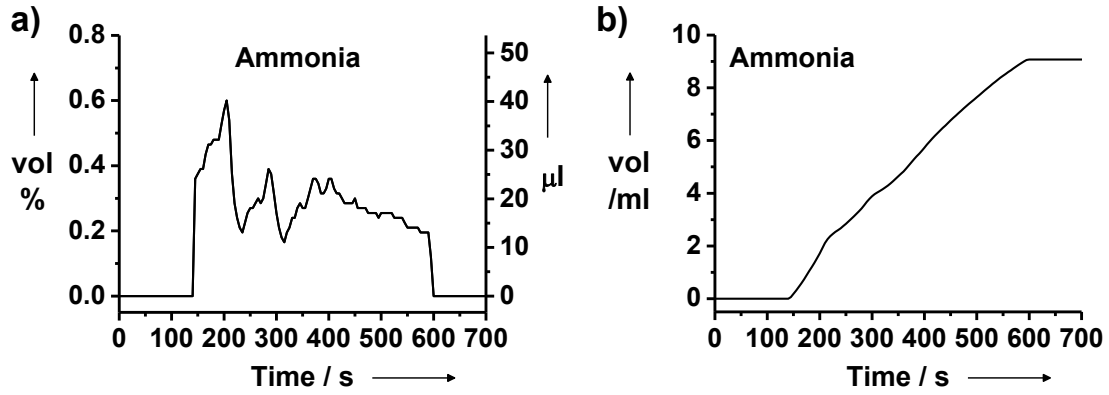

Figure 5.4: a) The concentration of gas (ammonia) release detected versus actuation time (vol% on the left axis, released volume in mL on the right axis), and b) total accumulated amount of released ammonia as a function of actuation time.

5.3.3 On–off switching of the PDMS gas/odor-release system

Shown in Figure 5.5 are the results of the on–off switching of the PDMS gas/odor-release system. When the system is in the "on" state, that is, an electrical current of 1.5 A is applied to the heating wires, the maximum concentration of measured ammonia is about 0.4 vol% (of the total gas detected) for each cycle. The abrupt increase of concentration in the "on" state could allow the gas/odor to be detected by a human nose (see below). During the "off" state (no electrical current), the temperature of the PDMS decreased and the gate shut so that no ammonia flux was detected (Figure 5.5). The ammonia flux could be switched on and off over multiple thermal cycles with high reproducibility, suggesting that the system is fully reversible. It is conceivable that the thermal expansion near the base of the PDMS container causes the PDMS container near the puncture hole to shrink and reduce the compressive stress on the elastomer gate thus assisting in the release of gas.

The gas/odor release device was turned "on" with approximately 40 second time lag after the current was applied and turned "off" with approximately 40–50 second lag (Figure 5.5), which is presumably due to some delay in heat propagation and the time it takes to clear the previously released gas from the chamber. We have observed a very similar on–off switching behavior when the model gas was switched to other gases, such as isopropyl alcohol, a typical anhydrous volatile liquid unlike aqueous ammonia (Figure 5.5b,d).

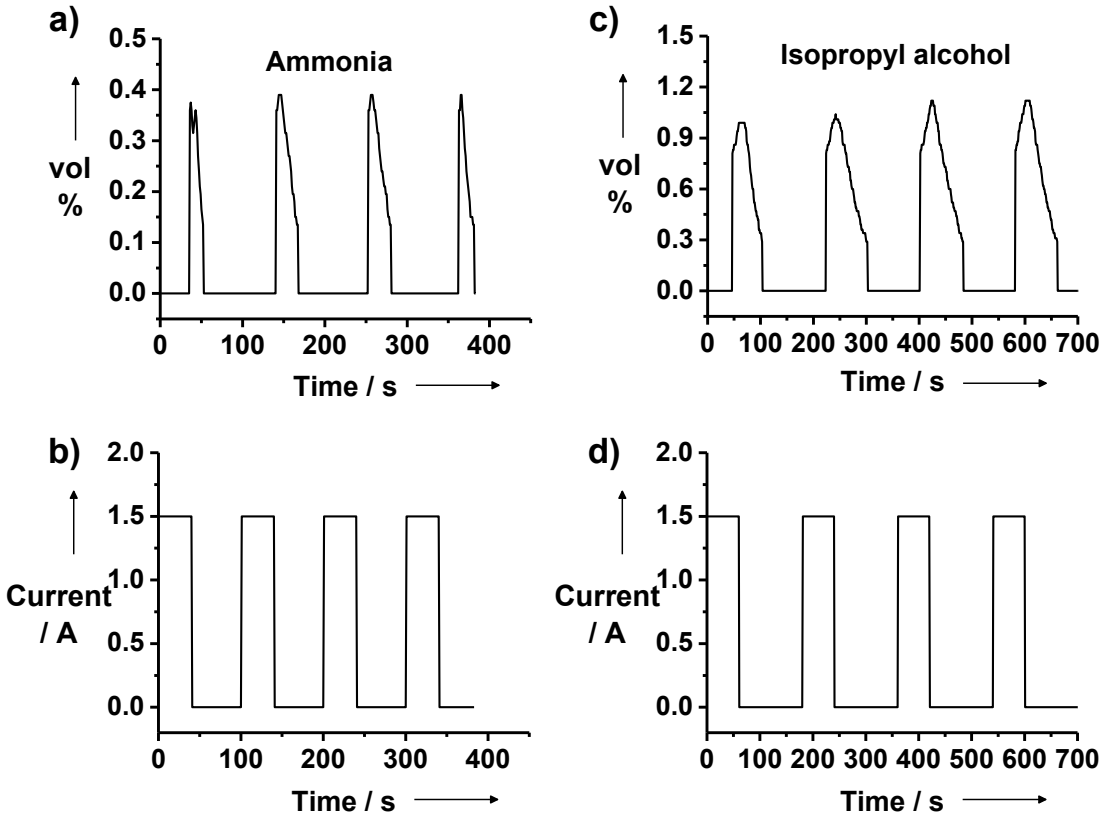

Figure 5.5: On–off switchable gas release (a,c) and applied current intensity (b,d) for ammonia (a,b), and isopropyl alcohol (c,d).

We have shown reproducibility over four thermally induced cycles (Figure 5.5), although many more cycles can be performed with essentially a similar fidelity. For industrial application, a similar amount of gas flux should be switched on and off over many cycles. Therefore, the engineering performance of the odor generating device on multiple cycles will be investigated with the focus on duration in more detail in the future. While the on–off switchable release of ammonia gas over multiple thermal cycles has been successfully demonstrated using PDMS-based devices without leakage in the "off" state, an important aspect to consider in using the odor-releasing device in

virtual-reality applications is how to control the odor releasing system containing multiple odors.

Although all the individual cells can be separately actuated by individual actuation/control system, this would require too many actuation control devices: N_2 for a X–Y matrix array of odor/gas chambers (where N is the number of the rows or columns in a square matrix). Therefore, we have created an X–Y coordinate system (Figure 5.1b,c) and attempted to operate the PDMS gas-releasing system with crossed heating wires on the bottom of the release chambers, so that we need only 2N controllers instead of N_2 controllers. For 10 000 odor chambers, 200 controllers instead of 10000 controllers would be sufficient.

We chose isopropyl alcohol as a gas to test the odorrelease function and controllability for the X–Y matrix system (Figure 5.6a,b) When 1.6 A current was applied to the row wires, no gas release was detected. However When 1.6 A was applied to the row wires and 1 A was applied to the column wires together, the cell at the intersection was activated for gas release. (The column electrical wires were placed/attached closer to the chambers, they require less current than for the row wires to reach the same temperature). The measured maximum concentration of isopropyl alcohol was about 1 vol% for each on–off release cycle (Figure 5.6a). When the electric current of the column wires was off, the concentration of isopropyl alcohol released decreased down to the "off" state even though the row wires remained activated. We have found a similar on–off switchable release performance using ethyl alcohol (Figure 5.6c,d). When we tested gas release from a cell adjacent to the selected cell, no interference was observed between the two cells (Fig. 5.7). Since the 2D cell array was designed to allow individual cells to maintain a set distance apart, the continuous "on"

state of one cell should not affect the operation of adjacent cells. However, if the neighboring cells were too close to each other, leakage heat to cause the neighboring cell to reach the operating temperature for gas release.

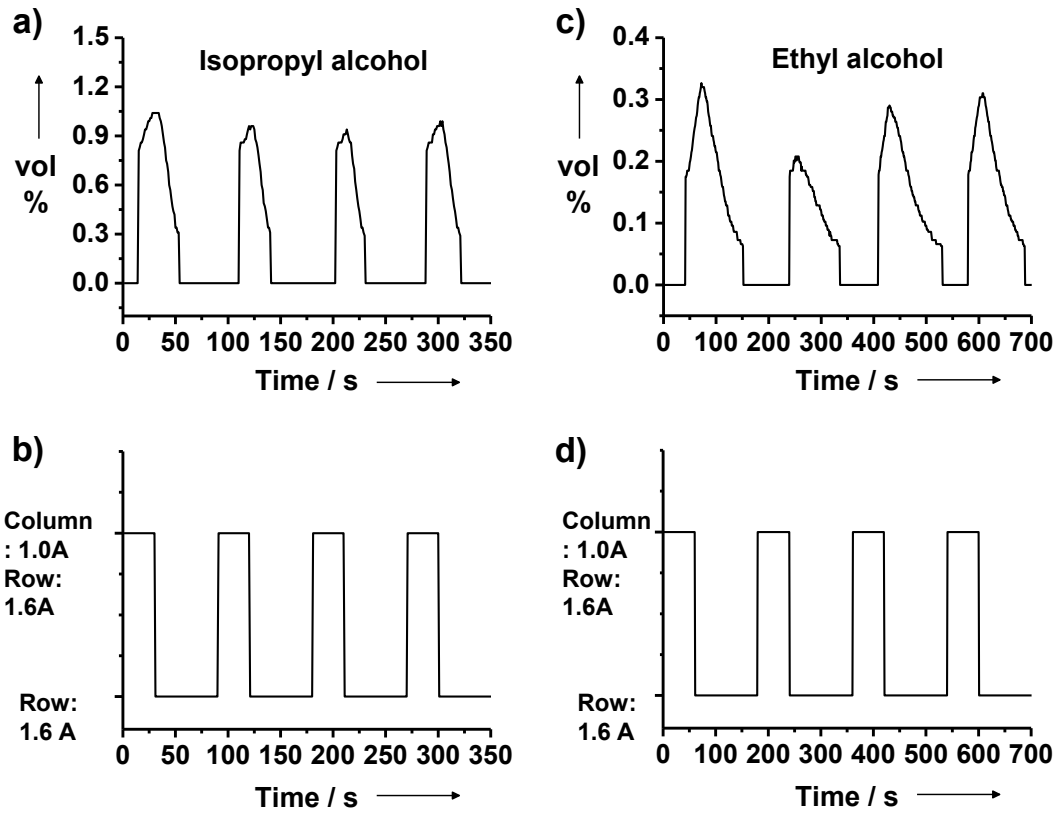

Figure 5.6: Gas concentration released and applied current for a),b) isopropyl alcohol, and c),d) ethyl alcohol during the on–off control of the PDMS gas-release device with crossed heating wires.

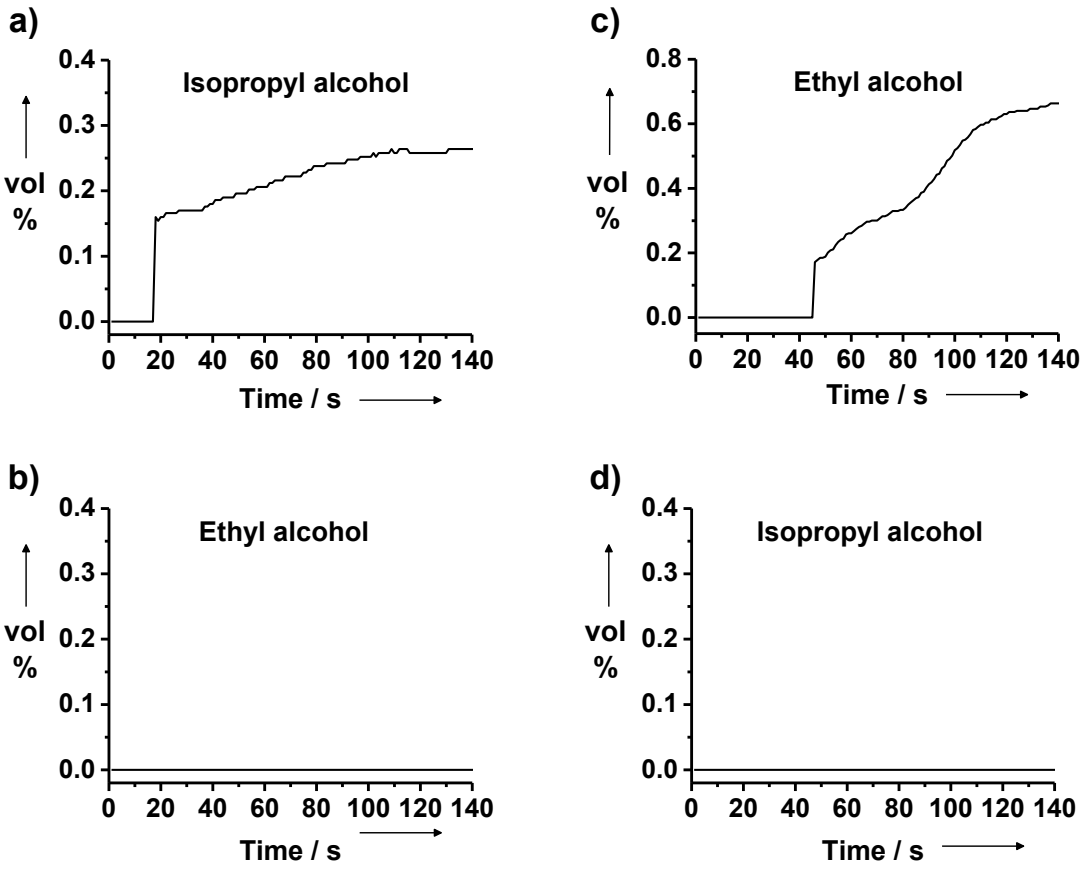

Figure 5.7: Gas concentration of a) isopropyl alcohol and b) ethyl alcohol during the "on" state of the isopropyl alcohol container. Gas concentration of c) ethyl alcohol and d) isopropyl alcohol during the "on" state of the ethyl alcohol container.

Sometimes, visualization using various colorimetric methods including gas-sensor arrays[162–165] can be utilized, instead of gas-detection electronic systems, to indicate the release of gas/odor in a simple manner. These colorimetric gas tubes are conveniently connectable to the Tygon tubing in the gas measurement apparatus without changing the configuration and the gas enters through one end of gas detection tube. Figure 5.8, shows two released gases being detected by using gas detection tubes. The color of the gas detector tube is changed by a reaction of the reagent in the tube and the incoming gas [Eq. (1), Eq. (2)]. Gas detector tubes were successfully used for the quick measurement of present gases.

$$3NH_3 + H_3PO_4 \rightarrow (NH_4)_3PO_4 \quad (1)$$

$$C_2H_5OH + Cr(IV) + H_2SO_4 \rightarrow Cr(III) + \text{Oxidation products} \quad (2)$$

The results show that the X–Y matrix gas-release system offers controllable gas release. Since the final potential applications would be aimed at odor sensing by the human nose, we utilized human olfaction as a detector for two types of distinctively different perfumes as model odors (see the Supporting Information). Traditional sensing systems have insufficient sensitivity towards perfumes which consist of a mixture of various ingredients and additives. We used the “Live by Jennifer Lopez” and the “Passion by Elizabeth Taylor” as perfume odor materials instead of isopropyl alcohol and ethyl alcohol. Figure 5.9 shows the experimental data for the on–off switchable release of these two different perfumes. Similar to isopropyl alcohol and ethyl alcohol, two perfumes were detected in turn by on–off switching processes for each cell. The type of X–Y matrix vapor/odor-releasing system reported herein has the potential to

improve the quality of virtual reality system for 3D TVs, cell phones, and other portable devices, and could also be useful for various entertainment, chemical engineering, and medical applications, such as combinatorial studies of multiple gas reactions and vapor-based drug development.

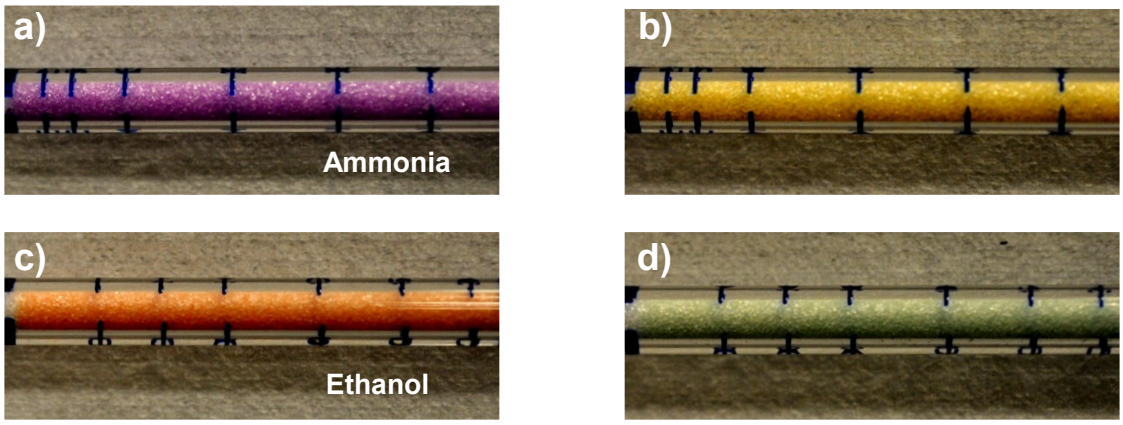

Figure 5.8: Color visualization photographs from ammonia and ethyl alcohol gas detection tubes. a),b) for ammonia gas before and after gas sampling, respectively. c),d) for ethyl alcohol gas before and after sampling, respectively.

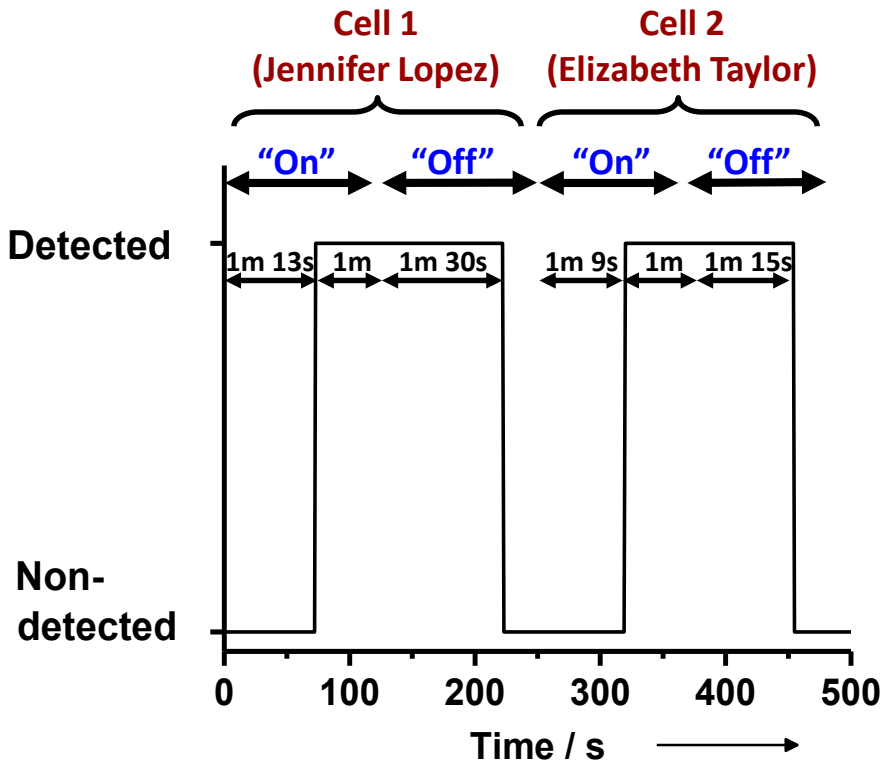

Figure 5.9: Real-time responses of human olfaction measured for the smell of two perfumes, "Live by Jennifer Lopez" (Cell 1) and "Passion by Elizabeth Taylor" (Cell 2).

5.4 Summary

In conclusion, we have demonstrated a novel X–Y matrix structured odor-releasing system with an elastomer-based device. Relatively low cost and compact design of the system may be achieved through the proposed switchable gas-release method. In addition, odor-release measurements with real time data-logging were also developed for model liquid/gas samples, such as ammonia, ethyl alcohol, and isopropyl alcohol, as well as two perfumes. The electrical actuation system enabled on–off switching of gas release. The main advantage of the proposed system is that the individual cells can be filled with different odorants which can be released on demand without interference. Thus, this X–Y matrix odor-releasing system has the potential to greatly improve the quality of virtual reality systems. Further improvements in fabrication, the use of advanced materials, and device structures for storing a large amount of odor, for example, in high-aspect-ratio chambers, or in solid form rather than liquid form, would make the capacity and duration of odor release much larger. Enhanced odor release kinetics may also be explored using nanostructured, large surface area materials and distributed 3D networked actuators. These advances are being investigated to develop a more robust and reproducible odor generating system, which will be reported in future publications.

Chapter 5, in full, is a reprint of the material as it appears in Angewandte Chemie International Edition, 50, 6771 (2011) written by Hyunsu Kim, Jongjin Park, Kunbae Noh, Calvin J. Gardner, Seong Deok Kong, Jongmin Kim, and Sungho Jin. The dissertation author was the primary investigator and author of this work.

CHAPTER 6:
Overall Summary, Conclusions, and Future Work

In this thesis, improved photoelectrodes having nanostructured photocatalysts have been discussed including their preparations, properties and applications. Also, a novel X–Y matrix structured odor-releasing system with an elastomer-based device has been introduced.

First, a successful distribution and attachment of fine Au nanoparticles on ~8 nm diameter TiO_2 nanotubes having significantly increased surface area have been demonstrated. Au thin film deposition onto hydrothermally grown TiO_2 nanotube arrays followed by thermal annealing breaks up the Au film into desired, uniformly distributed nanoparticles. Visible light absorption spectra of the gold nanoparticles on TiO2 nanotubes indicate that the Au nanoparticles are photo-excited due to plasmon resonance, and charge separation is accomplished by the transfer of photoexcited electrons from the gold particle to the TiO_2 conduction band, thereby enhancing photoelectrochemical performance. By virtue of substantially increased surface area with the 8 nm TiO_2 nanotube substrate in combination with the plasmonic effect of distributed Au nanoparticles, significantly increased photocurrent density was obtained with extended light absorbance from the UV regime to the visible spectrum region. Such gold nanoparticle decorated, fine TiO_2 nanostructures fabricated by a simple and versatile method can be useful for hydrogen generation by water splitting, CO oxidation and various other types of photocatalysts and photovoltaic fuel cells.

Second, a 3D photoelectrode having hydrothermally formed TiO_2 nanotubes on straight Ti fin arrays assembled by spot welding, with increased surface area has been successfully fabricated. A tangled forest of nanotubes of TiO_2 was produced on the Ti surface of the straight fin arrays. UV absorption spectra of the TiO_2 nanotubes indicate that the TiO_2 nanotubes are photo-excited due to their photocatalytic activities, and charge separation is accomplished by the transfer of photoexcited electrons from the TiO_2 nanotubes to the Ti substrate, thereby performing photoelectrochemical reaction. By virtue of substantially increased surface area with the 3D photoelectrode, significantly increased photocurrent density was obtained with the photocatalysis of TiO_2 nanotubes in combination with enhanced electrical current path between conducting Ti substrate and the photocatalytic TiO_2. Such 3D straight fin array structures fabricated by a simple and versatile method can be useful for hydrogen generation by water splitting, CO oxidation and various other types of photocatalysts and photovoltaic cells.

Third, a novel X–Y matrix structured odor-releasing system with an elastomer-based device has been developed. Relatively low cost and compact design of the system may be achieved through the proposed switchable gas-release method. In addition, odor-release measurements with real time data-logging were also developed for model liquid/gas samples, such as ammonia, ethyl alcohol, and isopropyl alcohol, as well as two perfumes. The electrical actuation system enabled on–off switching of gas release.

Advanced photoelectrodes having nanostructured photocatalysts was investigated. In particular, photocatalytic electrodes have been developed on structures of substrate (microdimension) as well as photocatalyst (nanodimension). In the future, we would investigate nitrogen-doped TiO_2 electrodes consisting of extremely small

diameter nanotubes, which utilize a wider range of solar spectrum for energy harvesting. Then, these would be introduced to 3D photoanode structures for more efficient solar-to-chemical energy conversion.

Regarding X-Y matrix addressable PDMS odor releasing, we need further improvements in fabrication, the use of advanced materials, and device structures for storing a larger amount of odor. For practical applications of the synchronized odor-release for TVs and related electronic display devices, faster and longer-distance odor release system would also be desirable, and replaceable cartridge type odor-storage systems would be developed.

References

1. S. Solomon,G. K. Plattner, R. Knutti, P. Friedlingstein, *Irreversible climate change due to carbon dioxide emissions.* Proceedings of the National Academy of Sciences USA, 2009. **106**: p. 1704–1709.

2. R. D. Primio, B. Horsfield, M. A. Guzman-Vega, *Determining the temperature of petroleum formation from the kinetic properties of petroleum asphaltenes.* Nature, 2000. **406**: p. 173–176.

3. L. Chiari, Zecca, *Constraints of fossil fuels depletion on global warming projections*. Energy Policy, 2011. **39**: p. 5026–5034.

4. F. Dincer, *The analysis on wind energy electricity generation status, potential and policies in the world*. Renewable and Sustainable Energy Reviews, 2011. **15**: p. 5135–5142.

5. I. Yuksel, *Hydropower for sustainable water and energy development*. Renewable and Sustainable Energy Reviews, 2010. **14:** p. 462–469.

6. B. Parida, S. Iniyan, R. Goic, *A review of solar photovoltaic technologies.* Renewable and Sustainable Energy Reviews., 2011. **15**: p. 1625–1636.

7. W. T. Xie, Y. J. Dai, R. Z. Wang, K. Sumathy, *Concentrated solar energy applications using Fresnel lenses: A review.* Renewable and Sustainable Energy Reviews, 2011. **15**: p. 2588–2606.

8. E. Barbier, *Geothermal energy technology and current status: an overview*. Renewable & Sustainable Energy Reviews, 2002. **6**: p. 3–65.

9. E. Keidel, *Die Beeinflussung der Lichtechtheit von Teerfarblacken durch Titanweiss [Influence of titanium white on the fastness to light of coal-tar days]*. Farben-Zeitung. 1929 **34**: p. 1242-1243.

10. C. F. Doodeve and J. A. Kitchener, *The mechanism of photosensitisation by solids.* Transactions of the Faraday Society, 1938. **34**: p. 902-908.

11. K. Hashimoto, H. Irie, A. Fujishima *TiO_2 Photocatalysis: A Histori cal Overview and Future Prospects.* Japanese Journal of Applied Physics, 2005. **44**: p. 8269.

12. A. Fujishima and K. Honda, *Electrochemical Photolysis of Water at a Semiconductor Electrode.* Nature, 1972. **238**: p. 37.

13. T. Kawai, T. Sakata, *Photocatalytic hydrogen production from liquid methanol and water.* Journal of the Chemical Society, Chemical Communications, 1980. p. 694-695.

14. L. Kavan, M. Gra¨zel, S. E. Gilbert, C. Klemenz and H. J. Scheel, *Electrochemical and Photoelectrochemical Investigation of Single-Crystal Anatase*. Journal of the American Chemical Society, 1996. **118**: p. 6716-6723.

15. R. W. Matthews, *Photooxidation of organic impurities in water using thin films of titanium dioxide.* The Journal of Physical Chemistry, 1987. **91**: p. 3328- 3333.

16. O. Carp, C. L. Huisman, A. Reller, *Photoinduced reactivity of titanium dioxide.* Prog. Solid State Chem., 2004. **32**: p. 33–177.

17. M. D. Hernández-Alonso, F. Fresno, S. Suárez, J. M. Coronado, *Development of alternative photocatalysts to TiO_2: Challenges and Opportunities*. Energy and Environmental Science, 2009. **2**: p. 1231–1237.

18. A. Fujishima and X. T. Zhang, *Titanium dioxide photocatalysis: present situation and future approaches.* Comptes Rendus Chimie, 2006. **9**: p. 750-760.

19. A. A. Adesina, *Industrial exploitation of photocatalysis: progress, perspectives and prospects.* Catalysis Surveys from Asia, 2004, **8**(4): p. 265-273.

20. A. Mills and S.-K. Lee, *A web-based overview of semiconductor photochemistry-based current commercial applications*. Journal of Photochemistry and Photobiology A, 2002. **152**: p. 233-247.

21. M. Romero, J. Blanco, B. S_anchez, A. Vidal, S. Malato, A. Cardona and E. Garcı´a, *Solar Photocatalytic Degradation of Water and Air Pollutants: Challenges and Perspectives*. Solar Energy, 1999. **66**(2): p. 169-182.

22. J.-M. Herrmann, *Heterogeneous photocatalysis: fundamentals and applications to the removal of various types of aqueous pollutants*. Catalysis Today, 1999. **53**(1): p. 115-129.

23. N. Hosaka, T. Sekiya, C. Satoko, S. Kurita, *Optical properties of singlecrystal anatase TiO_2.* Journal of the Physical Society of Japan, 1997. **66**: p. 877–880.

24. R. G. Breckenridge, W. R. Hosler, *Electrical properties of titanium dioxide Semiconductors.* Physical Review, 1953. **91**(4**)**: p. 793–802.

25. N. Hosaka, T. Sekiya, M. Fujisawa, C. Satoko, S. Kurita, *UV reflection spectra of anatase TiO_2*. Journal of Electron Spectroscopy and Related Phenomena, 1996. **78**: 75–78.

26. T. Sekiya, K. Ichimura, M. Igarashi, S. Kurita, *Absorption spectra of anatase TiO_2 single crystals heat-treated under oxygen atmosphere*. Journal of Physics and Chemistry of Solids, 2000. **61**(8): p. 1237–1242.

27. V.E. Henrich, P. A. Cox, *The Surface Science of Metal Oxides*. Cambridge, UK: Cambridge University Press; 1994.

28. H. K. Ardakani, *Electrical and optical properties of in situ "hydrogenreduced" titanium dioxide thin films deposited by pulsed excimer laser ablation*. Thin Solid Films. 1994. **248**(2): p. 234–239.

29. A. T. Paxton, L. Thien-Nga, *Electronic structure of reduced titanium Dioxide*. Physical Review B, 1998. **57**(3): p. 1579–1584.

30. P. Kofstad, *Note on the defect structure of rutile (TiO_2)*. Journal of the Less Common Metals. 1967., **13**(6): p. 635–638.

31. P. Knauth, H. L. Tuller, *Electrical and defect thermodynamic properties of nanocrystalline titanium dioxide*. Journal of Applied Physics, 1999. **85**(2): p. 897–902.

32. H. P. R. Frederikse, *Recent studies on rutile (TiO_2)*. Journal of Applied Physics, 1961. **32**(10): p. 2211–2215.

33. K. Mizushima, M. Tanaka, A. Asai, S. Iida, G. B. Goodenough, *Impurity levels of iron-group ions in TiO_2(II)*. Journal of Physics and Chemistry of Solids. 1979. **40**(12): p. 1129–1140.

34. X. Chen, S. S. Mao. *Titanium dioxide nanomaterials: synthesis, properties, modifications, and applications*. Chemical Reviews, 2007. **107**(7): p. 2891–2959.

35. ''Mineral Commodities Summaries 2009'' US Geological Survey. http://minerals.usgs.gov/minerals/pubs/mcs/2009/mcs2009.pdf.

36. J. X. Wang, G. Q. Zhou, C. Y. Chen, H. W. Yu, T. C. Wang, Y. M. Ma, G. Jia, Y. X. Gao, B. Li, J. Sun, Y. F. Li, F. Jiao, Y. L. Zhao and Z. F. Chai ZF, *Acute toxicity and biodistribution of different sized titanium dioxide particles in mice after oral administration*. Toxicology Letters, 2007. **168**(2): p. 176-185.

37. A. L. Linsebigler, G. Lu and J. T. Yates, *Photocatalysis on TiO_2 Surfaces: Principles, Mechanisms, and Selected Results*. Chemical Reviews, 1995. **95**(3): p. 735–758.

38. T. L. Thompson and J. T. Yates, *Surface Science Studies of the Photoactivation of TiO_2 New Photochemical Processes.* Chemical Reviews, 2006, **106**: p. 4428–4453.

39. H. Z. Zhang and J. F. Banfield, *Understanding Polymorphic Phase Transformation Behavior during Growth of Nanocrystalline Aggregates: Insights from TiO_2.* The Journal of Physical Chemistry B, 2000. **104**: p. 3481–3487.

40. A. J. Maira, K. L. Yeung, C. Y. Lee, P. L. Yue and C. K. Chan, *Size Effects in Gas-Phase Photo-oxidation of Trichloroethylene Using Nanometer-Sized TiO_2 Catalysts*. Journal of Catalysis, 2000. **192(1)**: p. 185-196.

41. N. Serpone, D. Lawless and R. Khairutdinov, *Size Effects on the Photophysical Properties of Colloidal Anatase TiO_2 Particles: Size Quantization versus Direct Transitions in This Indirect Semiconductor?* The Journal of Physical Chemistry, 1995. **99**: p. 16646–16654.

42. C. Wang, J. Rabani, D. W. Bahnemann and J. K. Dohrmann, *Photonic efficiency and quantum yield of formaldehyde formation from methanol in the presence of various TiO_2 photocatalysts.* Journal of Photochemistry and Photobiology A: Chemistry, 2002. **148**: p. 169-176.

43. J. M. Coronado, B. Sanchez, R. Portela and S. Suarez, *Solar Photocatalysis for the Elimination of Trichloroethylene in the Gas Phase.* Journal of Solar Energy Engineering, 2008. **130**: p. 0110161.

44. V. Svrcek, A. Slaoui and J.-C. Muller, *Silicon nanocrystals as light converter for solar cells.* Thin Solid Films, 2004. 451–452: p. 384-388..

45. T. Lindgren, J. Lu, A. Hoel, C. G. Granqvist, G. R. Torres and S. E. Lindquist, *Photoelectrochemical study of sputtered nitrogen-doped titanium dioxide thin films in aqueous electrolyte.* Solar Energy Materials and Solar Cells, 2004. **84**: p. 145.

46. A. Fujishima, T. N. Rao, D. A. Tryk, *Titanium dioxide photocatalysis*. Journal of Photochemistry and Photobiology C: Photochemistry Reviews, 2000. 1: p. 11–21.

47. M. R. Hoffmann, S. T. Martin, W. Choi and D. W. Bahnemann, *Environmental Applications of Semiconductor Photocatalysis.* Chemical Reviews, 1995. **95**(1): p. 69–96.

48. R. I. Bickley, T. Gonzalez-Carreno, J. S. Lees, L. Palmisano and R. D. Tilley, *A structural investigation of titanium dioxide photocatalysts.* Journal of Solid State Chemistry, 1991. **92**: p. 178.

49. M. A. Henderson, *Structural Sensitivity in the Dissociation of Water on TiO_2 Single-Crystal Surfaces.* Langmuir, 1996. **12**: p. 5093.

50. W. C. Wu, C. C. Chuang and J. L. Lin, *Bonding Geometry and Reactivity of Methoxy and Ethoxy Groups Adsorbed on Powdered TiO_2.* J. Phys. Chem. B, 2000. **104**: p. 8719.

51. M. C. Lu, W. D. Roam, J. N. Chen and C.-P. Huan, *Adsorption characteristics of dichlorvos onto hydrous titanium dioxide surface.* Water Research, 1996. **30**(7): p. 1670.

52. J. Ryu and W. Choi, *Substrate-Specific Photocatalytic Activities of TiO_2 and Multiactivity Test for Water Treatment Application.* Environmental Science and Technology, 2008. **42**(1): p. 294.

53. J. Perkowski, S. Bzdon, A. Bulska, W. K. Józwiak, *Decomposition of detergents present in carwash sewage by titania photo-assisted oxidation*. Polish Journal of Environmental Studies, 2006. **15**: p. 457–465.

54. O. K. Varghese, D. Gong, M. Paulose, K.G. Ong, E.C. Dickey, C.A. Grimes *Extreme Changes in the Electrical Resistance of Titania Nanotubes with Hydrogen Exposure*. Advanced Materials, 2003. **15**: p. 624.

55. X. Peng and A. Chen, *Aligned TiO_2 nanorod arrays synthesized by oxidizing titanium with acetone.* Journal of Materials Chemistry, 2004. **14**: p. 2542.

56. J. Wu, H. C. Shih, W. Wu *Electron field emission from single crystalline TiO_2 nanowires prepared by thermal evaporation*. Chemical Physics Letters, 2005. **413**: p. 490.

57. T. Tachikawa, M. Fujitsuka, T. Majima, *Mechanistic insight into the TiO_2 photocatalytic reactions: design of new photocatalysts*. The Journal of Physical Chemistry C, 2007. **111**: p. 5259–5275.

58. K. Rajeshwar, C. R. Chenthamarakshan, S. Goeringer, M. Djukic, *Titania-based heterogeneous photocatalysis. Materials, mechanistic issues and implications*

for environmental remediation. Pure and Applied Chemistry. 2001. **73**: p. 1849–1860.

59. Z. Zhang, P. A. Maggard, *Investigation of photocatalytically-active hydrated forms of amorphous titania, $TiO_2 \cdot nH_2O$*. Journal of Photochemistry and Photobiology A, 2007. **186**: p. 8–13.

60. A. Kudo, Y. Miseki, *Heterogeneous photocatalyst materials for water splitting*. Chemical Society Reviews, 2009. **38:** p. 253–278.

61. M. Ni, M. K. H. Leung, D. Y. Leung, K. Sumathy, *A review and recent developments in photocatalytic water splitting using TiO_2 for hydrogen production*. Renewable and Sustainable Energy Reviews, 2007. **11**(3): p. 401–425.

62. G. K. Mor, O. K. Varghese, M. Paulose, K. Shankar, C. A. Grimes, *A review on highly ordered, vertically oriented TiO_2 nanotube-arrays: fabrication, material properties, and solar energy applications.* Solar Energy Mater Solar Cells. 2006. **90**(14): p. 2011–2075.

63. Y. Cong, F. Chen, J. Zhang, M. Anpo, *Carbon and nitrogen-codoped TiO2 with high visible light photocatalytic activity.* Chemistry Letters, 2006. **35**: p. 800.

64. R. Asahi, T. Morikawa, T. Ohwaki, K. Aoki, Y. Taga, *Visible-light photocatalysis in nitrogen-doped titanium oxides.* Science, 2001. **293**: p. 269–271.

65. N. Serpone, *Is the band gap of pristine TiO_2 narrowed by anion- and cation-doping of titanium dioxide in second-generation photocatalysts?* The Journal of Physical Chemistry B, 2006. **110**: p. 24287–24293.

66. Y. X. Li, G. X. Lu, S. B. Li, *Photocatalytic production of hydrogen in single component and mixture systems of electron donors and monitoring adsorption of donors by in situ infrared spectroscopy*. Chemosphere, 2003. **52**: p. 843–850.

67. K. Sayama, H. Arakawa, *Effect of carbonate salt addition on the photocatalytic decomposition of liquid water over Pt-TiO_2 catalyst*. Journal of the Chemical Society, Faraday Transactions, 1997. **93**: p. 1647–1654.

68. V. Subramanian, E. E. Wolf, P. V. Kamat, *Catalysis with TiO_2/gold nanocomposites. Effect of metal particle size on the Fermi level equilibration*. Journal of the American Chemical Society, 2004. **126**: p. 4943–4950.

69. G. R. Bamwenda, S. Tsubota, T. Nakamura, M. J. Haruta, *Photoassisted hydrogen production from a water-ethanol solution: a comparison of activities*

of Au-TiO2 and Pt-TiO_2. Photochemistry and Photobiology, 1995. **89**: p. 177–189.

70. M. Murdoch, G. I. N. Waterhouse, M. A. Nadeem, J. B. Metson, M. A. Keane, R. F. Howe, J. Llorca, H. Idriss, *The effect of gold loading and particle size on photocatalytic hydrogen production from ethanol over Au/TiO_2 nanoparticles.* Nature Chemistry, 2011. **3**: p. 489–492.

71. M. Anpo, M. Takeuchi, *The design and development of highly reactive titanium oxide photocatalysts operating under visible light irradiation*. Journal of Catalysis, 2003. **216**: p. 505–516.

72. A. Merlen, V. Gadenne, J. Romann, V. Chevallier, L. Patrone, J. C. Valmalette, *Surface enhanced Raman spectroscopy of organic molecules deposited on gold sputtered substrates.* Nanotechnology 2009, **20**(21): 215705.

73. A. Primo, A. Corma, H. Garcia, *Titania supported gold nanoparticles as photocatalyst.* Physical Chemistry Chemical Physics, 2011, **13**: p. 886–910.

74. K. Awazu, M. Fujimaki, C. Rockstuhl, J. Tominaga, H. Murakami, Y. Ohki, N. Yoshida, T. Watanabe, *A plasmonic photocatalyst consisting of sliver nanoparticles embedded in titanium Dioxide*. Journal of the American Chemical Society, 2008, **130**: p. 1676–1680.

75. E. Kowalska, R. Abe, B. Ohtani, *Visible light-induced photocatalytic reaction of gold-modified titanium(IV) oxide particles: Action spectrum analysis*. Chemical Communications, 2009, B815679D.

76. C. G. Silva, R. Juarez, T. Marino, R. Molinari, H. Garcia, *Influence of Excitation Wavelength (UV or Visible Light) on the Photocatalytic Activity of Titania Containing Gold Nanoparticles for the Generation of Hydrogen or Oxygen from Water.* Journal of the American Chemical Society, 2011. **133**: p. 595–602.

77. H. Kisch, L. Zang, C. Lange, W.F. Maier, C. Antonius, D. Meissner, *Modified, Amorphous Titania—A Hybrid Semiconductor for Detoxification and Current Generation by Visible Light.* Angewandte Chemie International Edition, 1998. **37**: p. 3034.

78. X. Li, C. Chen, J. Zhao, *Mechanism of Photodecomposition of H_2O_2 on TiO_2 Surfaces under Visible Light Irradiation*. Langmuir, 2001. **17**: p. 4118.

79. S. K. Kim, S. J. Hwang, W. Choi, *Visible Light Active Platinum-Ion-Doped TiO_2 Photocatalyst*. The Journal of Physical Chemistry B, 2005. **109**: p. 24260.

80. P. Ji, M. Takeuchi, T. Chuong, J. Zhang, M. Matsuoka, M Anpo, *Recent advances in visible light-responsive titanium oxide-based photocatalysts.* Research on Chemical Intermediates, 2010. **36**: p. 327-347

81. K. F. E. Schafhaul, Gelehrte Anzeigen Bayer, Akad, 1845. **20**: p. 557

82. P. Hoyer, *Formation of titanium oxide nanotube*. Langmuir, 1996. **12**: p. 1411–1413.

83. T. Kasuga, M. Hiramatsu, A. Hoson, T. Sekino, K. Niihara, *Formation of Titanium Oxide Nanotube.* Langmuir, 1998. **14**: p. 3160–3163.

84. V. Zwilling, M. Aucouturier, E. Darque-Ceretti, *Structure and physicochemistry of anodic oxide films on titanium and TA6V alloy*. Surface and Interface Analysis, 1999. **27:** p. 629–637.

85. T. Kasuga, M. Hiramatsu, A. Hoson, T. Sekino, K. Niihara, *Titania nanotubes prepared by chemical processing.* Advanced Materials, 1999. **11**: p. 1307–1311.

86. O. K. Varghese, D. Gong, M. Paulose, C. A. Grimes, E. C. Dickey, *Crystallization and high-temperature structural stability of titanium oxide nanotube arrays.* Journal of Materials Research, 2003. **18**: p. 156–165.

87. B. Poudel, W. Z. Wang, C. Dames, J.Y. Huang, S. Kunwar, D. Z. Wang, D. Banerjee, G. Chen, Z. F. Ren, *Formaiton of crystallized titania nanotubes and their transformation into nanowires*. Nanotechnology, 2005. **16:** P. 1935–1940.

88. B. O'Regan, M. Gr¨atzel, *A low-cost, high-efficiency solar cell based on dye sensitized colloidal TiO_2 films*. Nature, 1991. **6346**: p. 737-739.

89. J. Nowotny, T. Bak, M. K. Novotny, L. R. Sheppard, *Titanium dioxide for solar-hydrogen I. Functional properties.* International Journal of Hydrogen Energy, 2007. **32:** p. 2609-2629.

90. S. J. Limmer, T. P. Chou, G. Z. Cao, *A study on the growth of TiO_2 nanorods using sol electrophoresis.* Journal of Materials Science, 2004. **39:** p. 895-901.

91. B. Xiang, Y. Zhang, Z. Wang, X. H. Luo, Y. Zhu, H. Z. Zhang, D. P. Yu, *Field-emission properties of TiO_2 nanowire arrays*. Journal of Physics D: Applied Physics. 2005. **38:** p. 1152-1155.

92. M. Miyauchi, H. Tokudome, Y. Toda, T. Kamiya, H. Hosono, *Electron field emission from TiO_2 nanotube arrays synthesized by hydrothermal reaction.* Appl. Phys. Lett. 2006. **89:** p. 043114.

93. M. Miyauchi, H. Tokudome, *Super-hydrophilic and transparent thin films of TiO_2 nanotube arrays by a hydrothermal reaction*. Journal of Materials Chemistry, 2007. **17:** p. 2095-2100.

94. J. Yan, F. Zhou, *TiO_2 nanotubes: Structure optimization for solar cells*. Journal of Materials Chemistry, 2011. **21:** p. 9406-9418.

95. J. Lin, X. Liu, M. Guo, W. Lu, G. Zhang, L. Zhou, X. Chen, H. Huang, *A facile route to fabricate an anodic TiO_2 nanotube–nanoparticle hybrid structure for high efficiency dye-sensitized solar cells.* Nanoscale, 2012. **4:** p. 5148-5153.

96. J. H. Park, S. Kim, A. J. Bard, *Novel Carbon-Doped TiO_2 Nanotube Arrays with High Aspect Ratios for Efficient Solar Water Splitting*. Nano Letters, 2006. **6:** p. 24-28.

97. X. Chen, S. S. Mao, *Titanium Dioxide Nanomaterials: Synthesis, Properties, Modifications, and Applications*. Chemical.Reviews, 2007. **107:** p. 2891-2959.

98. A. V. Rupa, D. Divakarand, T. Sivakumar, *Titania and Noble Metals Deposited Titania Catalysts in the Photodegradation of Tartazine*. Catalysis Letters, 2009. **132:** p. 259-267.

99. F. Boccuzzi, A. Chiorino, M. Manzoli, *Au/TiO nanostructured catalyst: effects of gold particle sizes on CO oxidation at 90 K*. Materials Science and Engineering C, 2001. **15:** p. 215-217.

100. D. C. Meier, D. W. Goodman, *The Influence of Metal Cluster Size on Adsorption Energies:CO Adsorbed on Au Clusters Supported on TiO_2.* Journal of the American Chemical Society, 2004. **126**(6)**:** p. 1892-1899.

101. P. Konova, A. Naydenov, C. Venkov, D. Mehandjiev, D. Andreeva, T. J. Tabakova, *Activity and deactivation of Au/TiO_2 catalyst in CO oxidation.* Journal of Molecular Catalysis A: Chemical, 2004. **213:** p. 235-240.

102. J. D. Stiehl, T. S. Kim, S. M. McClure, C. B. Mullins, *Formation of Molecularly Chemisorbed Oxygen on TiO_2-Supported Gold Nanoclusters and Au(111) from Exposure to an Oxygen Plasma Jet*. The Journal of Physical Chemistry B, 2005. **109:** p. 6316-6322.

103. A. N. Grigorenko, A. K. Geim, H. F. Gleeson, Y. Zhang, A. A. Firsov, I. Y. Khrushchev, J. Petrovic, *Nanofabricated media with negative permeability at visible frequencies.* Nature, 2005. **438:** p. 335-358.

104. T. R. Jensen, M. D. Malinsky, C. L. Haynes, R. P. Van Duyne, *Nanosphere Lithography: Tunable Localized Surface Plasmon Resonance Spectra of Silver Nanoparticles.* The Journal of Physical Chemistry B, 2000. **104:** p. 10549-10556.

105. Y. Xiong, J. M. McLellan, J. Chen, Y. Yin, Z. Y. Li, Y. Xia, *Kinetically Controlled Synthesis of Triangular and Hexagonal Nanoplates of Palladium and Their SPR/SERS Properties.* Journal of the American Chemical Society, 2005. **127:** p. 17118-17127.

106. K. R. Catchpole, A. Polman, *Design principles for particle plasmon enhanced solar cells*. Applied Physics Letters, 2008. **93:** p. 191113.

107. S. Pillai, K.R. Catchpole, T. Trupke, M. A. Green, *Surface plasmon enhanced silicon solar cells*. Journal of Applied Physics, 2007. **101**: p. 093105.

108. R. Yoshida, Y. Suzuki, S. Yoshikawa, *Effects of synthetic conditions and heat-treatment on the structure of partially ion-exchanged titanate nanotubes.* Materials Chemistry and Physics, 2005. **91:** p. 409–416.

109. N. Nafarizal, N. Takada, K. Nakamura, Y. Sago, K. Sasaki, *Deposition profile of Ti film inside a trench and its correlation with gas-phase ionization in high-pressure magnetron sputtering.* Journal of Vacuum Science & Technology A, 2006. **24**(6)**:** p. 2206-2211.

110. K. Brammer, H. Kim, K. Noh, M. Loya, C. Frandsen, L. Conelly, L. Chen, S. Jin, *Highly Bioactive 8 nm Hydrothermal TiO_2 Nanotubes Elicit Enhanced Bone Cell Response.* Advanced Engineering Materials., 2011. **13:** B88.

111. D. Kim, A. L. Giermann, C. V. Thompson, *Solid-state dewetting of patterned thin films*. Applied Physics Letters, 2009. **95:** p. 251903.

112. A. L. Giermann, C. V. Thompson, *Solid-state dewetting for ordered arrays of crystallographically oriented metal particles.* Applied Physics Letters, 2005. **86:** p. 121903.

113. B. L. Zhu, Q. Guo, X. L. Huang, S. R. Wang, S. M. Zhang, S. H. Wu, W. P. Huang, *Characterization and catalytic performance of TiO_2 nanotubes-supported gold and copper particles.* Journal of Molecular Catalysis A: Chemical, 2006. **249:** p. 211-217.

114. R. Z. Ma, T. Sasaki, Y. Bando, *Layer-by-Layer Assembled Multilayer Films of Titanate Nanotubes, Ag- or Au-Loaded Nanotubes, and Nanotubes/Nanosheets with Polycations.* Journal of the American Chemical Society, 2004. **126:** p. 10382-10388.

115. X. Z. Li, F. B. Li, *Surface characterization and photocatalytic reactivity of innovative Ti/TiO_2 and Ti/Pt–TiO_2 mesh photoelectrodes*. Journal of Applied Electrochemistry, 2002. **32:** p. 203-210.

116. B. H. Erne, D. Vanmackelbergh, J. J. Kelly, *Morphology and Strongly Enhanced Photoresponse of GaP Electrodes Made Porous by Anodic Etching.* Journal of the Electrochemical Society, 1996. **143**(1)**:** p. 305-314.

117. X. Quan, S. Yang, X. Ruan, H. Zhao, *Preparation of Titania Nanotubes and Their Environmental Applications as Electrode.* Environmental Science and Technology, 2005. **39:** p. 3770-3775.

118. N. Chandrasekharan, P. V. Kamat, *Improving the Photoelectrochemical Performance of Nanostructured TiO_2 Films by Adsorption of Gold Nanoparticles.* The Journal of Physical Chemistry B, 2000. **104**(46): p. 10851-10857.

119. T. L. Villarreal, R. Gomez, *Interfacial electron transfer at TiO_2 nanostructured electrodes modified with capped gold nanoparticles: The photoelectrochemistry of water oxidation.* Electrochemistry Communications, 2005. **7:** p. 1218-1224.

120. Y. Nakato, K. Ueda, H. Yano, H. Tsubomura, *Effect of Microscopic Discontinuity of Metal Overlayers on the Photovoltages in Metal-Coated Semiconductor-Liquid Junction Photoelectrochemical Cells for Efficient Solar Energy Conversion.* The Journal of Physical Chemistry, 1988. **92:** p. 2316-2324.

121. G. R. Bamwenda, S. Tsubota, T. Nakamura, M. Haruta, *The influence of the preparation methods on the catalytic activity of platinum and gold supported on TiO_2 for CO oxidation* Catalysis Letters, 1997. **44:** p. 83-87.

122. S. Sakthivel, M. V. Shankar, M. Palanichamy, B. Arabindoo, D. W. Bahnemann, V. Murugesan, *Enhancement of photocatalytic activity by metal deposition: characterisation and photonic efficiency of Pt, Au and Pd deposited on TiO_2 catalyst.* Water Research , 2004. **38**: p. 3001-3008.

123. Y. Mizukoshi, Y. Makise, T. Shuto, J. W. Hu, A. Tominaga, S. Shironita, S. Tanabe, *Immobilization of noble metal nanoparticles on the surface of TiO_2 by the sonochemical method: Photocatalytic production of hydrogen from an aqueous solution of ethanol.* Ultrasonics Sonochemistry, 2007. **14**, 387-392.

124. V. Iliev, D. Tomova, L. Bilyarska, G. Tyuliev, *Influence of the size of gold nanoparticles deposited on TiO_2 upon the photocatalytic destruction of oxalic acid.* Journal of Molecular Catalysis A: Chemical, 2007. **263:** p. 32-38.

125. J. Xu, Y. Sun, Y. M. Zhao, J. J. Huang, C. M. Chen, Z. Y. Jiang, *Photocatalytic Inactivation Effect of Gold-Doped TiO_2 (Au/TiO_2) Nanocomposites on Human Colon Carcinoma LoVo Cells.* International Journal of Photoenergy, 2007. **1**: p. 97308.

126. H. Zhu, X. Chen, Z. Zheng, X. Ke, E. Jaatinen, J. Zhao, C. Guo, T. Xie, D. Wang, *Mechanism of supported gold nanoparticles as photocatalysts under ultraviolet and visible light irradiation.* Chemical Communications, 2009. P. 7524–7526.

127. B. Balamurugan, T. Maruyama, *Evidence of an enhanced interband absorption in Au nanoparticles: Size-dependent electronic structure and optical properties*. Applied Physics Letters, 2005 **87**: 143105.

128. Y. Tian, T. Tatsuma, *Mechanisms and Applications of Plasmon-Induced Charge Separation at TiO_2 Films Loaded with Gold Nanoparticles*. Journal of the American Chemical Society, 2005 **127**(19), 7632-7637.

129. S. Mekhilef, R. Saidur, A. Safari, *A review on solar energy use in industries*. Renewable and Sustainable Energy Reviews, 2011. **15**: p. 1777–90.

130. H. Schnitzer, C. Brunner, G. Gwehenberger *Minimizing greenhouse gas emissions through the application of solar thermal energy in industrial processes.* Journal of Cleaner Production , 2007. **15**: p. 1271-1286.

131. K. Christopher, R. Dimitrios, *A review on exergy comparison of hydrogen production methods from renewable energy sources*. Environmental Science, 2012. **5**: p. 6640-6651.

132. A. Currao, *Photoelectrochemical Water Splitting*. Chimia, 2007. **61**(12): p. 815–819.

133. K. Maeda, *Photocatalytic water splitting using semiconductor particles: History and recent developments.* Journal of Photochemistry and Photobiology C: Photochemistry Reviews, 2011. **12**: p. 237– 268.

134. A. Fujishima, T. N. Rao, D. A. Tryk, *Titanium dioxide photocatalysis*. Journal of Photochemistry and Photobiology C: Photochemistry Reviews, 2000. **1**: p. 11–21.

135. X. Peng, A. Chen *Aligned TiO_2 nanorod arrays synthesized by oxidizing titanium with acetone*. Journal of Materials Chemistry, 2004. **14**: p. 2542-2548.

136. J. Wu, H. C. Shih, W. Wu, *Electron field emission from single crystalline TiO_2 nanowires prepared by thermal evaporation.* Chemical Physics Letters, 2005: **413**: p. 490-494.

137. D. Wang, T. Hu, L. Hu, B. Yu, Y. Xia, F. Zhou, W. Liu, *Microstructured Arrays of TiO_2 Nanotubes for Improved Photo-Electrocatalysis and Mechanical Stability.* Advanced Functional Materials, 2009. **19**: p. 1930–1938.

138. R. F. Pease, S. Y. Chou, *Lithography and Other Patterning Techniques for Future Electronics*. Proceedings of the IEEE, 2008. **96**: p. 248–270.

139. N. Kahraman, *The influence of welding parameters on the joint strength of resistance spot-welded titanium sheets.* Materials and Design, 2007. **28**: p. 420-427.

140. M. Jou, *Real time monitoring weld quality of resistance spot welding for the fabrication of sheet metal assemblies.* Journal of Materials Processing Technology, 2003. **132**: p. 102-113.

141. Y. Kaya, N. Kahraman, *The effects of electrode force, welding current and welding time on the resistance spot weldability of pure titanium*. International Journal of Advanced Manufacturing Technology, 2012. **60**: p. 127–134.

142. T. Tachikawa, S. Tojo, M. Fujitsuka, T. Sekino, T. Majima, *Photoinduced Charge Separation in Titania Nanotubes*. The Journal of Physical Chemistry B, 2006. **110**(29): p. 14055-14059.

143. D. V. Bavykin, A. A. Lapkin, P. K. Plucinski, J. M. Friedrich, F. C. Walsh, *Reversible Storage of Molecular Hydrogen by Sorption into Multilayered TiO2 Nanotubes*. The Journal of Physical Chemistry B, 2005. **109**: p. 19422-194227.

144. M. Zyda, From *Visual Simulation to Virtual Reality to Games*. IEEE Computer Society, 2005. **38**: p. 25–32.

145 L. Sastry, D. R. S. Boyd, *Virtual Environments for Engineering Applications.* Virtual Reality, 1998. **3**: p. 235–244.

146. R. McCloy, R. Stone, *Science, medicine, and the future Virtual reality in surgery.* British medical journal , 2001. **323**: p. 912 – 915.

147. L. Nehaoua, H. Mohellebi, A. Amouri, H. Arioui, S. Espie, A. Kheddar, *Design and Control of a Small-Clearance Driving Simulator.* IEEE Transactions on vehicular technology, 2008. **57**(2): p. 736– 46.

148. T. Yamada, S. Yokoyama, T. Tanikawa, K. Hirota, M. Hirose, *Wearable Olfactory Display: Using Odor in Outdoor Environment*. IEEE Virtual Reality, 2006. p. 199–206.

149. M. Heilig in Digital Illusion (Ed.: C. Dodsworth, Jr.) ACM Press, New York, 1998. p. 343–351.

150. J. P. Cater, *Smell/Taste: Odors in Virtual Reality*. IEEE International Conference on Systems, Man, and Cybernetics, 1994. p. 1781.

151. R. Tortell, D. Luigi, A. Dozois, S. Bouchard, J. Morie, D. Ilan, *The effects of scent and game play experience on memory of a virtual environment*. Virtual Reality, 2007. **11**: p. 61 – 68.

152. T. Hoare, J. Santamaria, G. F. Goya, S. Irusta, D. Lin, S. Lau, R. Padera, R, Langer, D. S. Kohane, *A Magnetically Triggered Composite Membrane for On-Demand Drug Delivery*. Nano Letters, 2009. **9**(10): p. 3651–3657.

153. J. D. Ehrick, S. K. Deo, T.W. Browning, L. G. Bachas, M. J. Madou, S. Daunert, *Genetically engineered protein in hydrogels tailors stimuli-responsive characteristics.* Nature Materials, 2005. **4**: p. 298–302.

154. T. Okano, Y. H. Bae, H. Jacobs, S. W. Kim, *Thermally on-off switching polymers for permeation and release.* Journal of Controlled Release, 1990. **11**: p. 255–265.

155. Dow Corning 2005 Product information sheet of Sylgard 184.

156. S. A. Visser, R.W. Hergenrother, S. L. *Cooper in Biomaterials Science* (Eds.: B. D. Ratner, A. S. Hoffman, F. J. Schoen, J. E. Lemons), Academic Press, 1996. p. 50–60.

157. J. N. Lee, C. Park, G. M. Whitesides, *Solvent Compatibility of Poly(dimethylsiloxane)-Based Microfluidic Devices*. Analytical Chemistry, 2003. **75**: p. 6544–6554.

158. A. L. Andrady, M. D. Sefcik, *Transport of hydrogen and carbon monoxide in highly crosslinked poly(propylene glycol) networks*. Journal of Polymer Science Part B, 1984. **22**: p. 237–243.

159. I. De Bo, H. Van Langenhove, P. Pruuost, J. De Neve, J. Pieters, I. F. J. Vankelecom, E. Dick, *Investigation of the permeability and selectivity of gases and volatile organic compounds for polydimethylsiloxane membranes*. Journal of Membrane Science, 2003. **215**: p. 303–319.

160 F. Schneider, T. Fellner, J. Wilde, and U. Wallrabe, *Mechanical properties of silicones for MEMS*. Journal of Micromechanics and Microengineering, 2008. **18**: 065008.

161. B. Esser, T. M. Swager, *Detection of Ethylene Gas by Fluorescence Turn-On of a Conjugated Polymer*. Angewandte Chemie International Edition, 2010. **49**: p. 8872–8875.

162. F. Feigl, V. Anger, *Spot Tests in Organic Chemistry*. 7th ed., Elsevier, Amsterdam, 1966. p. 43–48.

163. N. A. Rakow, K. S. Suslick, *A colorimetric sensor array for odour visualization*. Nature, 2000. **406**: p. 710–713.

164. Q. Zhou, T. M. Swager, *Fluorescent Chemosensors Based on Energy Migration in Conjugated Polymers: The Molecular Wire Approach to Increased Sensitivity*. Journal of the American Chemical Society, 1995. **117**: p. 12593–12602.

165. T. Mayr, G. Liebsch, I. Klimant, O. S. Wolfbeis, *Multi-ion imaging using fluorescent sensors in a microtiterplate array format*. Analyst, 2002. **127**: p. 201–203.